Master's thesis

NTNU
Norwegian University of Science and Technology
Faculty of Natural Sciences
Department of Materials Science and Engineering

Caroline Sindland

Production Rate of SiO Gas from Industrial Quartz and Silicon

Master's thesis in Materials Science and Engineering
Supervisor: Merete Tangstad
June 2020

NTNU
Norwegian University of
Science and Technology

Caroline Sindland

Production Rate of SiO Gas from Industrial Quartz and Silicon

Master's thesis in Materials Science and Engineering
Supervisor: Merete Tangstad
June 2020

Norwegian University of Science and Technology
Faculty of Natural Sciences
Department of Materials Science and Engineering

NTNU
Norwegian University of
Science and Technology

Preface

The work in this report is done as part of the master thesis TMT4950, at the department of Materials Science and Engineering at the Norwegian University of Science and Technology, during the spring of 2020. The work is part of the project Controlled Tapping, a collaboration between multiple companies within metal production in Norway and it is supported by the Norwegian Research Council.

I am very thankful for being able to work on this project, with Merete Tangstad as my supervisor. She has provided me with excellent guidance and feedback whenever it was needed. The university and our laboratories was shut down for almost two months due to COVID-19 this spring but most of my experiments were done before that and I am grateful to be able to deliver on time. I think a good supervisor as well as planning and excellent training from technical staff making experiments run smooth is the main reasons for this. A few tasks were remaining the day school shut down, but thanks to help from Julian Richard Tolchard and Martin Syvertsen, two research Scientist at SINTEF I got to finish the XRD analysis and wettability measurements that I had started within reasonable time.

I would also like to thank the other students in my program, especially the one in our reading room at the 2nd floor of Bergbygget. They have been taking part in interesting discussions and made sure we had enough coffee in the beginning of this semester. Unfortunately we did not get to complain about long days at school at the end of this semester. Instead, we ended up missing our reading area and being able to spend time together during these months where social distancing occupied everyone's mind. But I am still looking back at five years that have been way more and better than expected. It has been five years filled with good friends, long days at school and even longer days in the mountains.

Trondheim, June 2020

Caroline Sindland

Abstract

The production rate of SiO gas from industrial quartz and silicon has been investigated by isothermal heat treatment experiments at elevated temperatures. Mixtures of silicon and different quartz samples has been heated to temperatures ranging from 1650 to 1950°C and held for 30 to 120 minutes before cooling. The weight loss of each sample has been correlated to degree of reaction and a model for the reaction rate of Si + SiO_2 has been developed based on these values. Five different types of industrial quartz were used in the experiments and there was not found any significant difference between their reaction rate, even though there is a significant difference between the content of impurity, melting rate, decrepitation and phase transformation rate of each sample. It is therefore shown that the reaction rate of silicon mixed with various types of quartz can be described by one Arrhenius equation, given by Equation 1. A reaction constant (k_0) equal to $6.25 \cdot 10^8 s^{-1} m^{-2} g$ and an activation energy (Q) equal to $557 kJ mol^{-1}$ were obtained by an Arrhenius plot of the experimental data. The degree of reaction (α) is increasing with an increasing available reaction area (A), temperature and time.

$$\frac{d\alpha}{dt} = 9.81 \cdot 10^7 \cdot A \cdot exp(-\frac{557 \cdot 10^3}{RT}) \tag{1}$$

The main goal of this project is a better understanding of the overall $SiO_{(g)}$ loss in silicon furnaces. The obtained reaction rate for the Si + SiO_2 reaction has therefore been compared to reaction rate of the other $SiO_{(g)}$ producing reaction in a silicon furnace, reaction between silicon carbide and silica. It is shown that their rate is within the same range as long as their available reaction area is within the same range, the reaction rate of both reactions increases with temperature and available reaction area. The production rate of SiO gas in a silicon furnace is therefore highly dependent on the distribution of silicon, silica and silicon carbide in the hot temperature zone of the furnace.

Sammendrag

Reaksjonshastigheten til den SiO produserende reaksjonen, reaksjon mellom silisium og silika er undersøkt ved isoterm varmebehandling. Flere blandinger av silisium og silika har blitt varmet opp til temperaturer fra 1650 til 1950°C og holdt i 30 til 120 minutter før de har blitt avkjølt. Vekttapet til hver prøve har blitt knyttet opp mot reaksjonsgrad og en modell for Si + SiO_2 reaksjonen har blitt utviklet basert på disse verdiene. Fem ulike typer kvarts har blitt brukt i forsøkene og det er ikke funnet noen signifikant forskjell mellom deres reaksjonshastighet, til tross for varierende smeltehastighet, hastighet for fasetransformsjon, dekrepitering og innhold av urenheter. Reaktiviteten til silisium blandet med ulike typer industriell kvarts kan derfor beskrives av en likning, gitt av likning 1. Reaksjonsgraden (α) øker med økende reaksjonsareal, temperatur og tid.

$$\frac{d\alpha}{dt} = 9.81 \cdot 10^7 \cdot A \cdot exp(-\frac{557 \cdot 10^3}{RT}) \tag{1}$$

En bedre forståelse av $SiO_{(g)}$ tap på silisiums ovner er hovedmålet for denne oppgaven. Reaksjonshastigheten for Si + SiO_2 reaksjonen har derfor blitt sammenliknet med reaksjonshastigheten for den andre $SiO_{(g)}$ produserende reaksjonen, reaksjon mellom silika og silisium karbid. Det er vist at deres reaksjonshastighet er relativt lik, så lenge de har et relativt likt reaksjonsareal tilgjengelig og begges reaksjonshastighet øker med temperatur og tilgengelig areal. Mengden SiO gas produsert i en silisiums ovn er dermed hovedsakelig avhengig av fordeling av silisium, silika og silisium karbid i den delen av oven med høy temperatur.

Contents

1 Introduction

Silicon is produced in Norway by the use of submerged arch furnaces (SAF) with coal, charcoal, woodchips, quartz and electricity as input and silicon, $CO_{(g)}$ and $SiO_{(g)}$ as output. The total ideal reaction is presented in Equation 2 and one of the intermediate reactions, reaction between silicon and silica is the main focus of this work. The work presented in this report is done as part of NTNUs participation in the project Controlled Tapping, supported by the Norwegian Research Council (running from 2017-2021). Its overall goal is to maximize metal yield, maximize operation load and minimize hazardous tapping conditions within silicon production and other metallurgical industry [26].

$$SiO_2 + 2C = Si + 2CO \tag{2}$$

The production of silicon is far more complicated than the equation above. Reduction of quartz to form silicon happens in several intermediate steps and there are silicon losses in form of $SiO_{(g)}$ escaping through the exhaust, SiC build up and silicon metal lost during tapping. Industrial measurements shows that there is a relation between an increased $SiO_{(g)}$ loss and bad tapping of metal, the reason for this is not agreed upon. One suggestion is that the untapped silicon reacts with SiO_2 in the furnace to form $SiO_{(g)}$. An increased amount of $SiO_{(g)}$ in the furnace is further on related to increased losses. The goal of this project is hence to investigate the reactivity of silicon and silica mixtures, described by Equation 3, to get a better understanding on its affect on $SiO_{(g)}$ loss. The reactivity will further on be compared with literature on the reactivity of SiC and silica mixtures, representing the other $SiO_{(g)}$ producing reaction in a silicon furnace.

$$SiO_2 + Si = 2SiO \tag{3}$$

There is two SiO forming reactions within a silicon furnace, the reaction between SiC and silica and the reaction between silicon and silica. The first reaction has been investigated by Tangstad et al. (2019) [39] and they have developed a model for the reactivity, including a reaction constant and activation energy. The other reaction has been investigated and there is some literature available on the topic, but no model had been developed until last fall. Development of a model was therefor of high interest, to be able to compare the two SiO forming reactions. The development of a model was therefor started by Sindland as part of a specialisation project last fall (2019) [35], where one type of quartz mixed with silicon was heated and hold at different temperatures. The goal of this master thesis is to further develop and improve the model, as well as including multiple industrial types of quartz. Five different types of quartz will be mixed with silicon, in a 1:1molar ratio, heated and hold at given temperatures for a given time. The weight loss of the samples will further on be correlated to formation of SiO gas and reactivity. 13 experiments were performed during the fall of 2019 and another 17 experiments are planned for this master thesis, giving a total of 30 data point for the model of silicon/silica reactivity.

The over all goal is to get a better understanding of silicon and silica reactivity, as function of temperature, time, available reaction area and quartz quality, all giving a better understanding og SiO losses in a silicon furnace.

1.1 Metallurgical production of high silicon alloys

Silicon is produced by carbothermic reduction of silica (silicon dioxide). Silica and carbon are added to the top of the furnace, molten silicon are tapped at the bottom of the furnace and a mixture of CO and SiO gas escapes at the top of the furnace. The simple and idealised version of silicon production is summarised by Equation 2 and does not include losses in form of SiO gas and SiC build up in the furnace.

The silicon furnace is normally divided in two zones, a cold upper zone with temperatures ranging from 700 - 1300 °C, Tangstad [38] and a hot lower zone close to 2000 °C. Production of silicon happens in multiple steps in these two zones, schematically described in Figure 1.

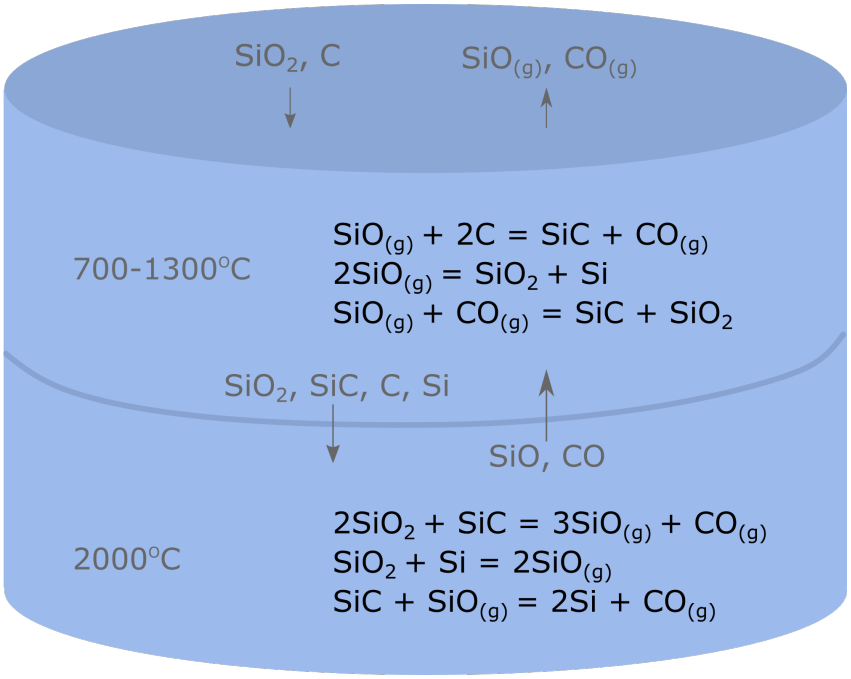

Figure 1: A simple sketch including reactions, material flow and temperature in a silicon furnace. The figure is inspired by figure 5-9 in Metal production in Norway by Tangstad (2013) [38].

Carbon will react in the cold temperature zone according to equation 4 and silicon and silica will be formed from the condensation reaction given by the reverse of equation 3. The inputs in the hot zone is therefor SiO_2, C, SiC and Si. The main silicon producing reaction is happening within the hot zone and it is given by Equation 5. The source of SiO gas is reaction between silicon and silica as well as silica and silicon carbide, according to equation 3 and 6. The CO gas formed in the hot temperature zone and any SiO that does not react according to Equation 5 will rise to the low temperature zone. Some of the rising SiO gas will condensate according

to the reverse of equation 3, while the rest will rise further and oxidise before it leaves the furnace as SiO_2 in the exhaust system. The silica can be collected from the off gas and sold as a valuable product to the concrete industry. Regardless of its value it is wanted to be able to control the amount of silica in the off gas and investigation of the SiO producing reactions is one step towards a more controlled SiO loss.

$$SiO_{(g)} + 2C_{(s)} = SiC_{(s)} + CO_{(g)} \tag{4}$$

$$SiC_{(s)} + SiO_{(g)} = 2Si_{(l)} + CO_{(g)} \tag{5}$$

$$2SiO_{2(s,l)} + SiC_{(s)} = 3SiO_{(g)} + CO_{(g)} \tag{6}$$

2 Theory

Thermodynamic relations and properties within the silicon, oxygen and carbon system will be discussed in this section. Isothermal heating of silicon and silica in a graphite crucible is the main experiments in this thesis and equilibrium with carbon is therefor considered, in addition to equilibrium between silicon and silica them self. There is two SiO forming reactions in a silicon furnace, the one investigated in this thesis and the reaction between silica and silicon carbide. The SiC + SiO_2 reaction is a reference to the Si + SiO_2 reaction and relevant literature on both reactions is therefor presented towards the end of this chapter.

A review of relevant theory and literature on reactivity of silicon and silica was carried out by the author in a specialisation project preceding this thesis, Sindland [35]. Some of the sections below are therefor containing content from the specialisation project in addition to discussion of papers that have been studied this spring.

2.1 Silicon

Silicon has a melting temperature in the range of 1400-1420°C, depending on the reference [32, p. 21] [6] and a density of $2.3 g/cm^{-3}$ at room temperature [6]. The viscosity of silicon as function of temperature is presented in Figure 2 [31]. It can be speculated if the higher viscosity values in the figure, measured by Glasov, Kakimoto and Sasaki is due to particles in the alloy and hence that the true viscosity is close to the lowest measurements. Excluding the high measurements in the figure and including values obtained by Nishimurab et al. [23] gives a viscosity in the range of $5 - 9 \cdot 10^{-3}$ Poise from 1420°C to 1650°C.

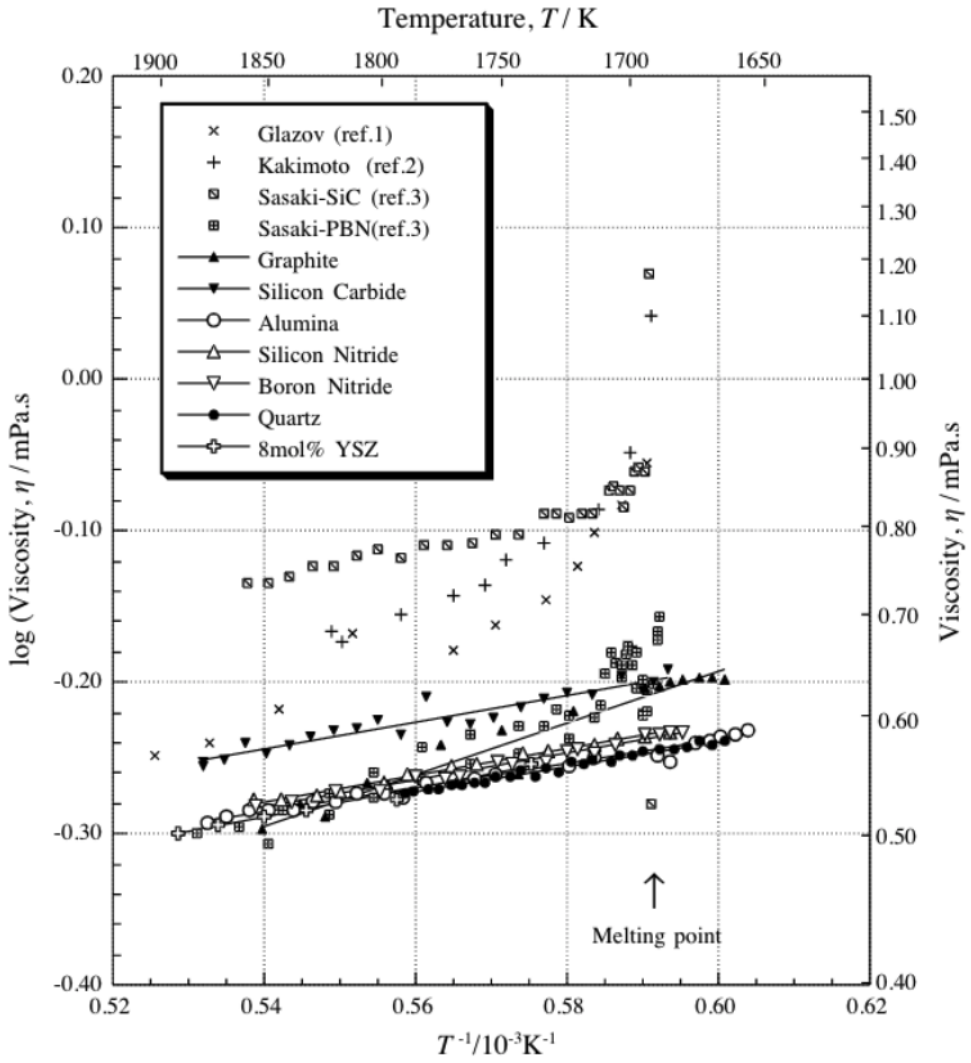

Figure 2: Viscosity of molten silicon obtained for various materials of crucibles with literature values obtained by Y. Sato et al. [31].

2.2 The Si-O system

A mixture of silica and silicon will be solid up to the melting point of silicon at 1405°C, according to the phase diagram in Figure 3. Liquid silicon will be present along with solid silica up to its melting point around 1700°C. Silicon and silica are both present as liquid at higher temperatures and the two liquids will stay separated. Liquid silica tends to be present as a layer on top of molten silicon due to density differences. It should be noted that the presence of tridymite in pure silica as shown in the phase diagram in Figure 3 is debated. This is further discussed in section 2.3.1.

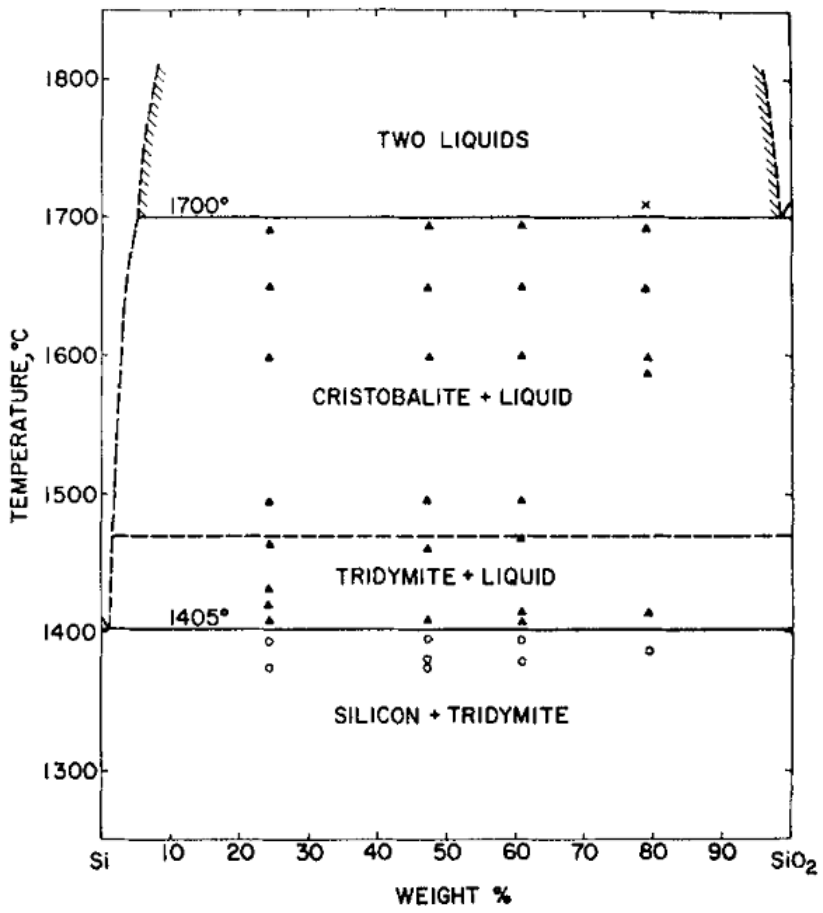

Figure 3: Phase relations in the Si-O system as determined by Johnson and Muan [16]. Dashed lines represent boundary curves whose existence is inferred and the phase diagram should only be used for qualitative information.

Silicon and silica in solid and/or liquid phase will be in equilibrium with $SiO_{(g)}$ gas [7]. This gas is stable at higher temperatures and will condense when temperature is decreased. Brewer and Edwards [7] claim that SiO exists as a meta stable phase at higher temperatures, but it will be converted to SiO_2 and Si at lower temperatures and SiO is not stable at room temperature. Literature studies and experiments done by Schnurre et al. [33] points out that amorphous silicon mono oxide $SiO_{(am)}$ can exist at room temperature, only showing an inhomogeneity at nano scale. Condensed SiO is however not easily found and it is a common belief that the condensed SiO will be mainly a mixture of Si and SiO2.

2.3 Quartz

Quartz is a crystalline mineral where silicon-oxygen (SiO_4^{4-}) tetrahedrons are arrayed in a regular and ordered manner, giving it the chemical formula SiO_2 and a density of 2.65 g/cm^2 at room temperature. The mineral is abundant in the earths crust and can be found with a low impurity content, which is beneficial for the production of high purity silicon. Quartz is a low temperature polymorph and the phase transformations happening within quartz at higher temperatures is

discussed in the next section. Melting, softening and viscosity of quartz as well as decrepitation are factors that affect the flow of silica and gas in a silicon furnace as well as reactivity of the material. Available literature on these topics have therefor been studied as well.

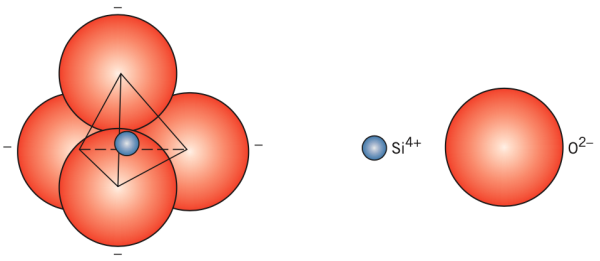

Figure 4: A silicon-oxygen (SiO_4^{4-}) tetrahedron [8].

2.3.1 Phase transformation in quartz

Quartz goes through multiple phase transitions when heated from room temperature to 1800°C. The stable phase at room temperature is α - quartz which will transform into β - Quartz at 573°C. Transition into HP-Trydimite occur at 870°C before it is transformed into β - Christobalite at 1470°C and melting occur at 1728°C, according to Klein and Hulbert [22, p. 530]. Melting occur at 1713°C according to SI-chemical data [6]. The transformation to tridymite as described by Klein and Hulbert [22, p. 530] is debated [36] [18] [21]. It is shown that tridymite is an impurity derived structure and not stable in pure silica. Transition from quartz to cristobalite seems to occur via a non-crystalline transition phase and can be described by Reaction 7.

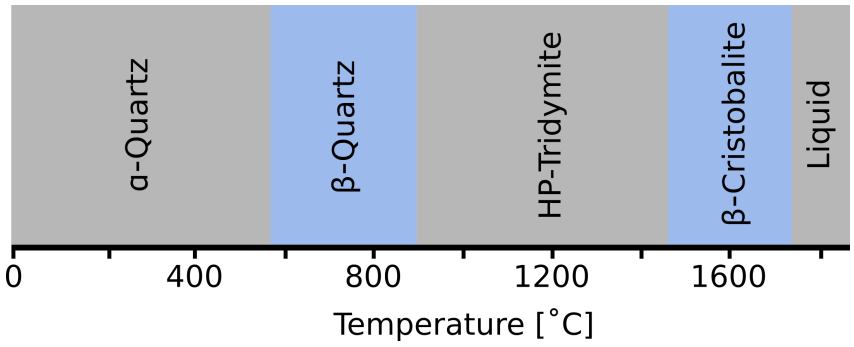

Figure 5: The different polymorphs of silica (SiO_2) as function of temperature at 1 atm. The figure is adapted from the phase diagram by Klein and Hulbut [22, p. 527].

$$Quartz \rightarrow Amorphousphase \rightarrow cristobalite \tag{7}$$

Phase transformation in industrial quartz has been investigated by Jusnes and some of the results are presented in an unpublished article [18]. Additional results have been obtained and will be included in her PhD monograph [17]. Multiple figures have been made available for this

report and the most relevant figures are included below. The three quartz called A, D and F in her work have been used in this master thesis as well but with different labels. Figure 6 shows the phase distribution in four different samples before heating while Figure 7 shows the phase distribution after heating to 1600°C and held from 0 to 120 minutes before cooling.

There is no significant different between the phase composition of the various quartz types before any heating and after heating for 120 minutes at 1600°C. During heating there is however a significant difference in the transformation of each quartz. The transformation rate of quartz F is higher than quartz D which is again higher than quartz A. The samples have to be heated and held at 1600°C for 0, 20 and $\sim$ 120 minutes for quartz F, D and A respectively to reach a content of less than 10% quartz.

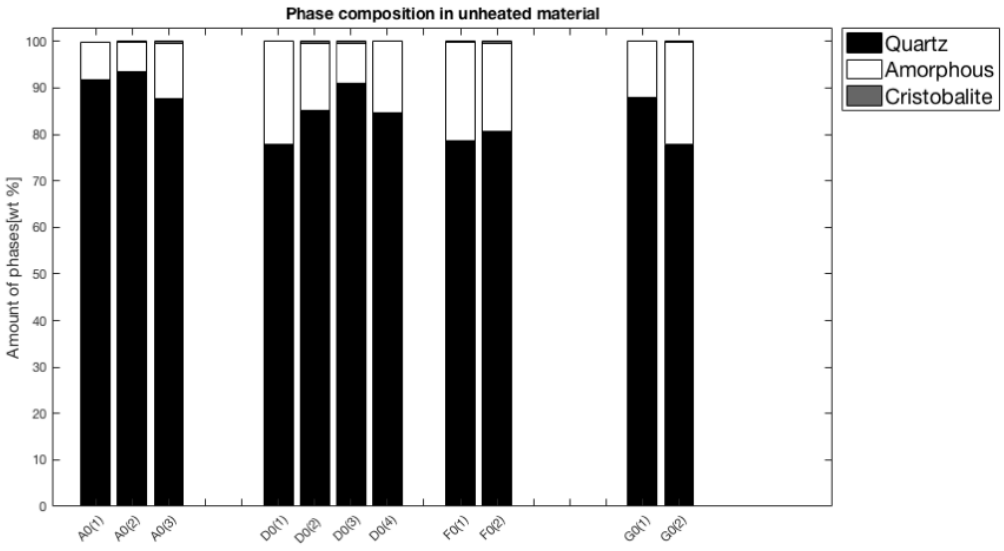

Figure 6: Phase composition of different industrial quartz before any heating. Results obtained by Jusnes [18].

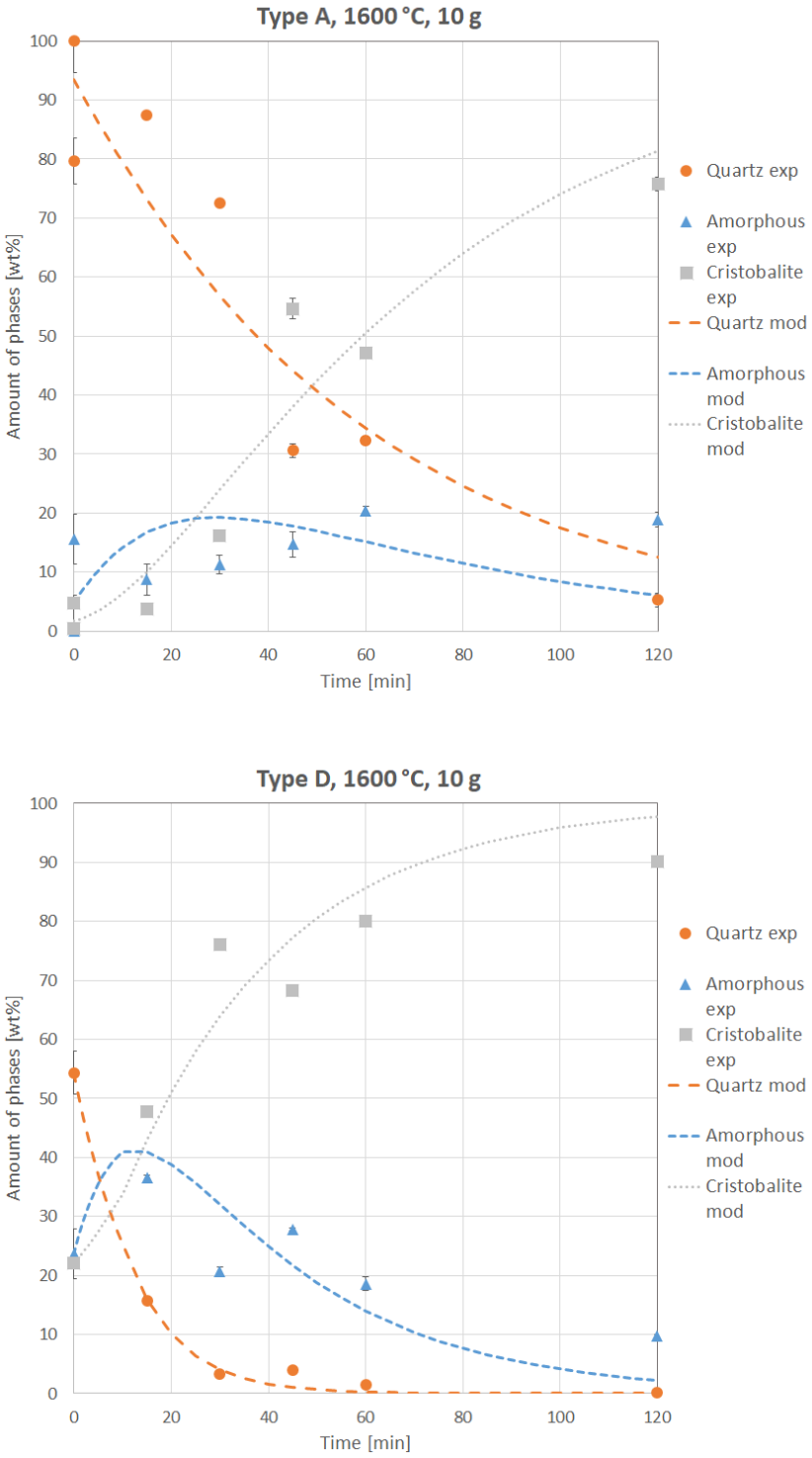

Figure 7: The phase composition of quartz after heating to 1600°C and held for 0 to 120 minutes. The results are obtained by Jusnes [17].

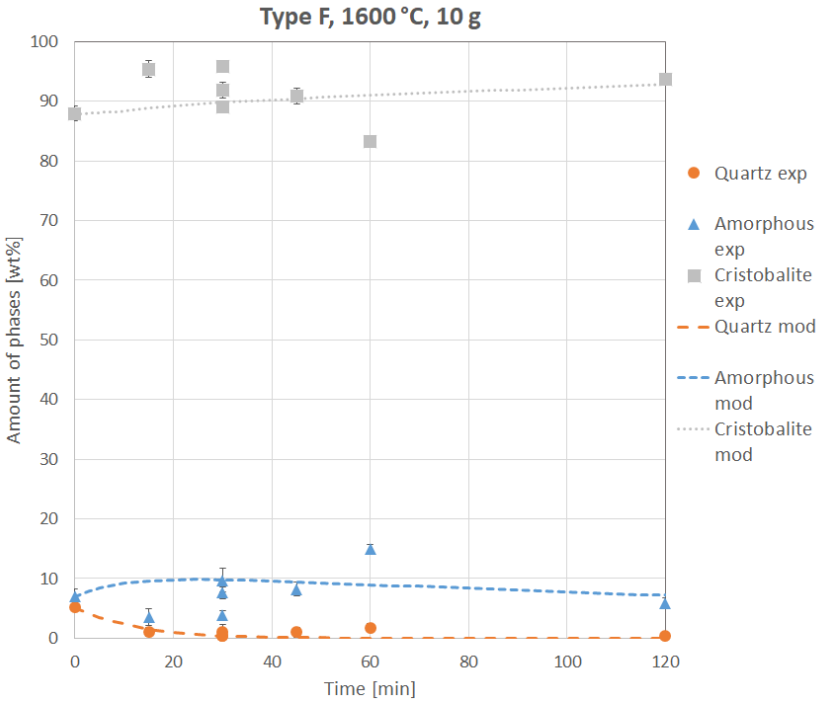

Figure 8: The phase composition of quartz after heating to 1600°C and held for 0 to 120 minutes. The results are obtained by Jusnes [17].

2.3.2 Melting and softening of quartz

The softening and melting of quartz used in industry have been investigated by Nordnes in her specialisation project [24] and master thesis [25]. Figure 9 shows the melting and softening point of four types of quartz heated at a rate of 5°C/min before isothermal heat treatment at different temperatures. Nordnes report a melting temperature of quartz in the range of 1730-1850°C. Softening is reported to occur before melting, at temperatures in the range of 1690-1740°C. Samples heated to temperatures above 1800 °C melted before isothermal temperature was reached while heating to temperatures below 1800°C required some holding time to reach complete melting. Figure 10 shows melting rate at different holding temperatures below 1800 °C. The results from the work done by Nordnes indicates that quartz has a slow melting rate that increases with increasing holding temperature as well as amount of impurities. There was not found any correlation between phase composition after heat treatment to 1650°C and melting rate. Modelling performed by Nordnes indicated that heat transfer is negligible when it comes to melting rate in the experiments. It should be noted that Jusnes and Nordnes used different letters to label the same type of quartz samples, quartz A presented in the work done by Jusnes is not the same as quartz A investigated by Nordnes.

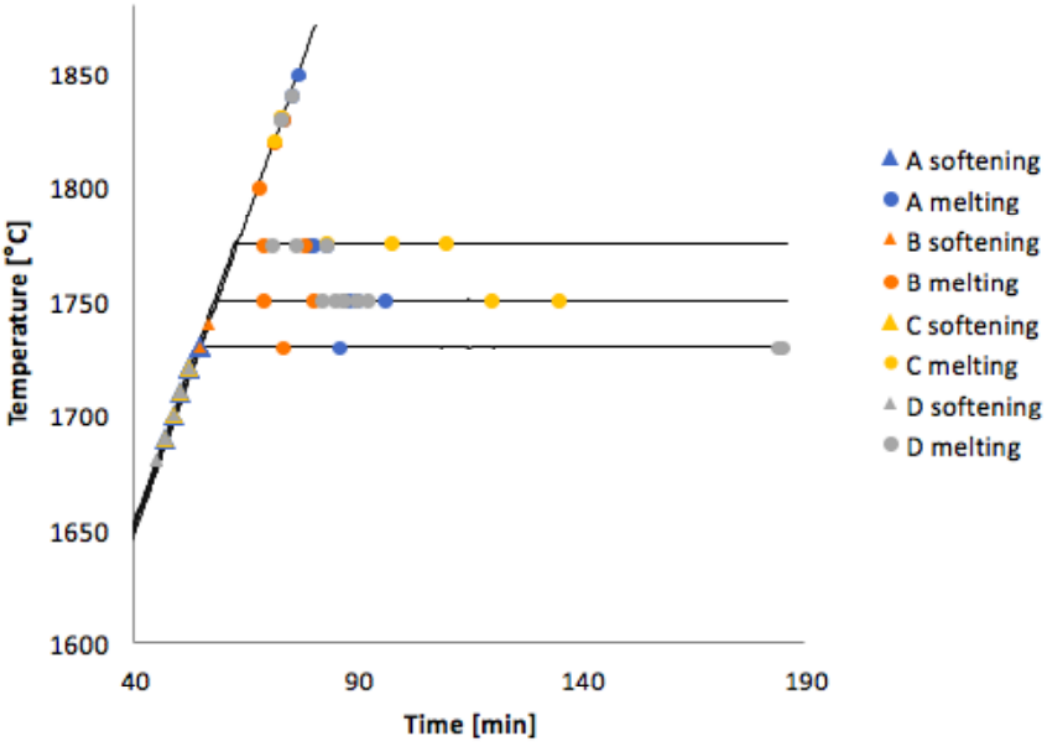

Figure 9: Heat treatment of four different types of quartz in argon atmosphere done by Nordnes [25]. The letters in the legends indicate the different types of quartz and three of them are used in this thesis.

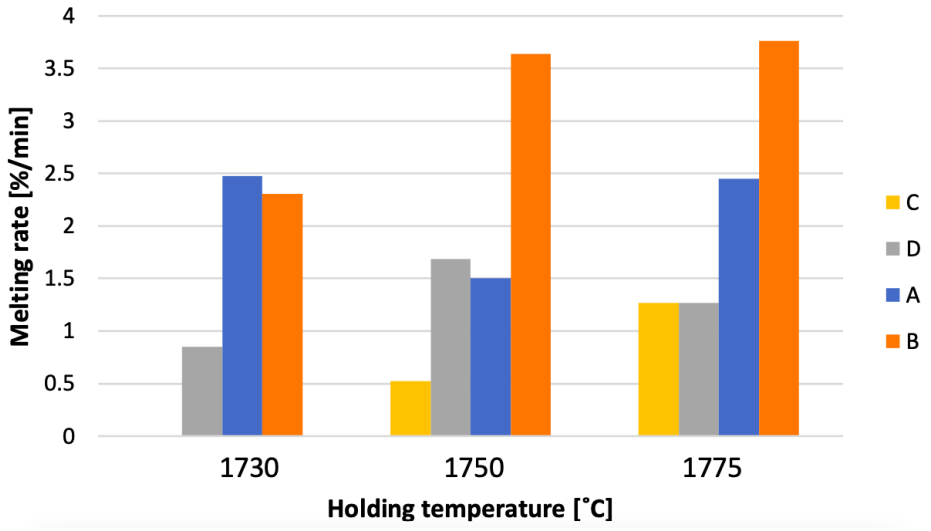

Figure 10: Average melting rate at holding temperature for four different quartz types, measured by Nordnes [25]. The letters in the legends indicate the different types of quartz and three of them are used in this thesis.

The viscosity of silica is calculated to be $2 \cdot 10^7$ Poise at the melting temperature [29] and its behaviour is close to a solid until the temperature is increased further. The viscosity is above

$2 \cdot 10^6$ Poise up to temperature of about 1875°C and decreases drastically at higher temperatures [29]. It should be noted that the viscosity of silica is significant higher than the viscosity of silicon.

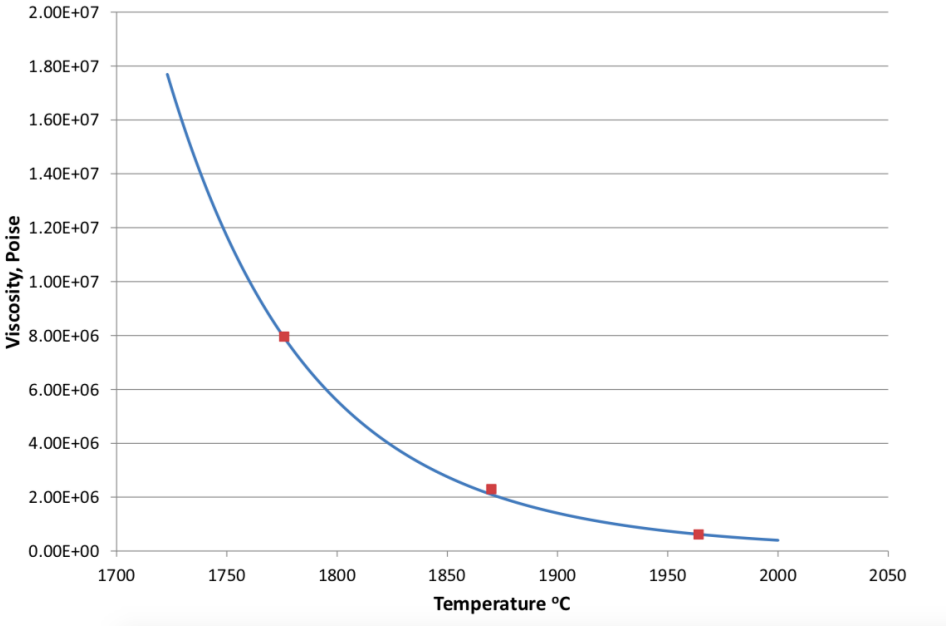

Figure 11: The viscosity of silica as function of temperature calculated by the use of FactSage by Halvor Dalaker and Kai Tang, Sintef [29].

2.3.3 Decrepitation of quartz

Shock heating of quartz will lead to decrepitation, the sample dissintegrate into smaller particles. Decrepitation of industrial quartz has been investigated by multiple people and some of the work has been summarised by Jusnes [19], presented in Figure 12. Jusnes found that disintegration after shock heating to 1500°C varies more between different types of quartz than between the parallels for each sample. The amount of particles smaller than 10mm after shock heating varies from 5% for the most stable sample to 75% for the most fragile sample. Decrepitation of quartz will increase the amount of fines in the furnace and further reduce the gas permeability of the charge. It will also increase the available reaction area for formation of SiO gas in a silicon furnace due to higher surface area per mass unit, and this might lead to SiO formation higher up in the furnace. Both cases are unwanted.

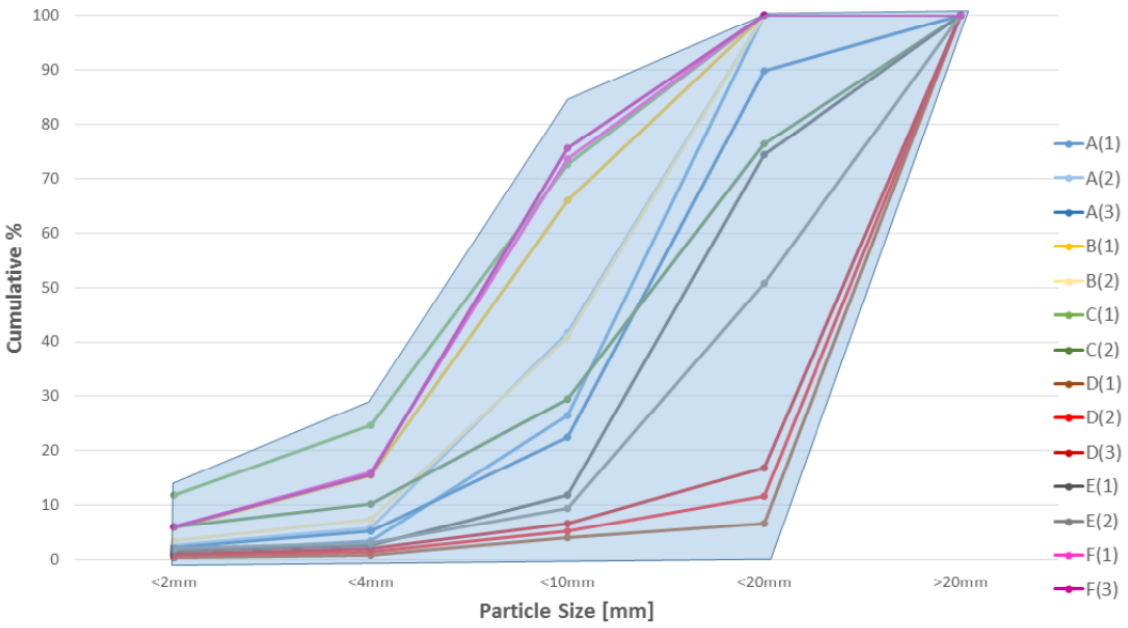

Figure 12: Cumulative representation of different quartz samples after shock heating to 1500°C by Jusnes [19]. The interval which most of earlier results by Ringdalen [27] and Paulsen and Bakken [3] fall into, are shown as a shaded area. The letters in the legends indicate the different types of quartz where three of them is used in this thesis as well with different labels.

2.4 The Si-C system

Silicon will react with carbon to form SiC at temperatures below 2800°C, as seen in Figure 13. This means that there will be formed SiC at a graphite/silicon interface. It can also be seen that the solubility of carbon in liquid silicon increase with temperature. This means that silicon carbide will be precipitated during cooling liquid silicon that has been in contact with carbon at high temperatures.

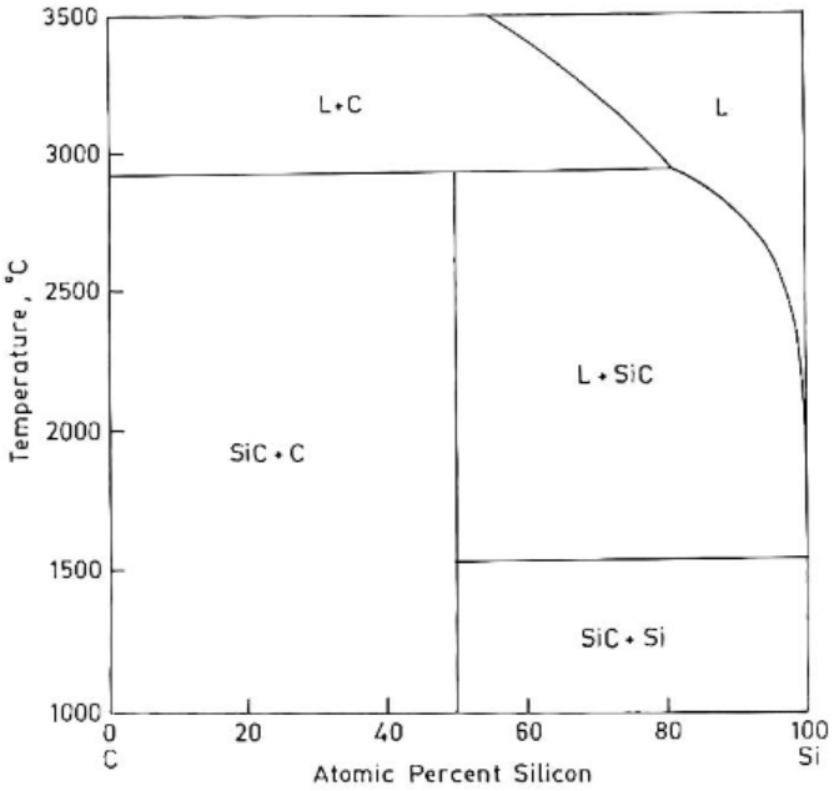

Figure 13: Phase relations in the Si-C system by Bandyopadhyay [4].

2.5 The Si-O-C system

There are multiple possible reactions in a Si-O-C system, all of them represented in the equations below. The stability of each reaction is plotted as function of temperature and SiO pressure in Figure 14 [32, p. 29]. The total pressure of the system is assumed to be $1bar = P_{SiO} + P_{CO}$. A red line is added to Figure 14 to highlight the reaction investigated in this report. Silicon and silica react to form SiO gas at SiO pressures below 0.1 bar when the temperature is 1600 °C, at pressures below 0.6 bar when the temperature is 1800 °C and at any pressure when temperature is increased above 1850°C.

$$SiO_2(s,l) + 2C(s) = SiO(g) + CO(g) \tag{8}$$

$$2SiO_2(s,l) + SiC(s) = 3SiO(g) + CO(g) \tag{6}$$

$$SiO_2(s,l) + Si(s,l) = 2SiO(g) \tag{3}$$

$$SiO(g) + 2C(s) = SiC(s) + CO(g) \tag{4}$$

$$SiO(g) + SiC(s) = 2Si(s,l) + CO(g) \tag{5}$$

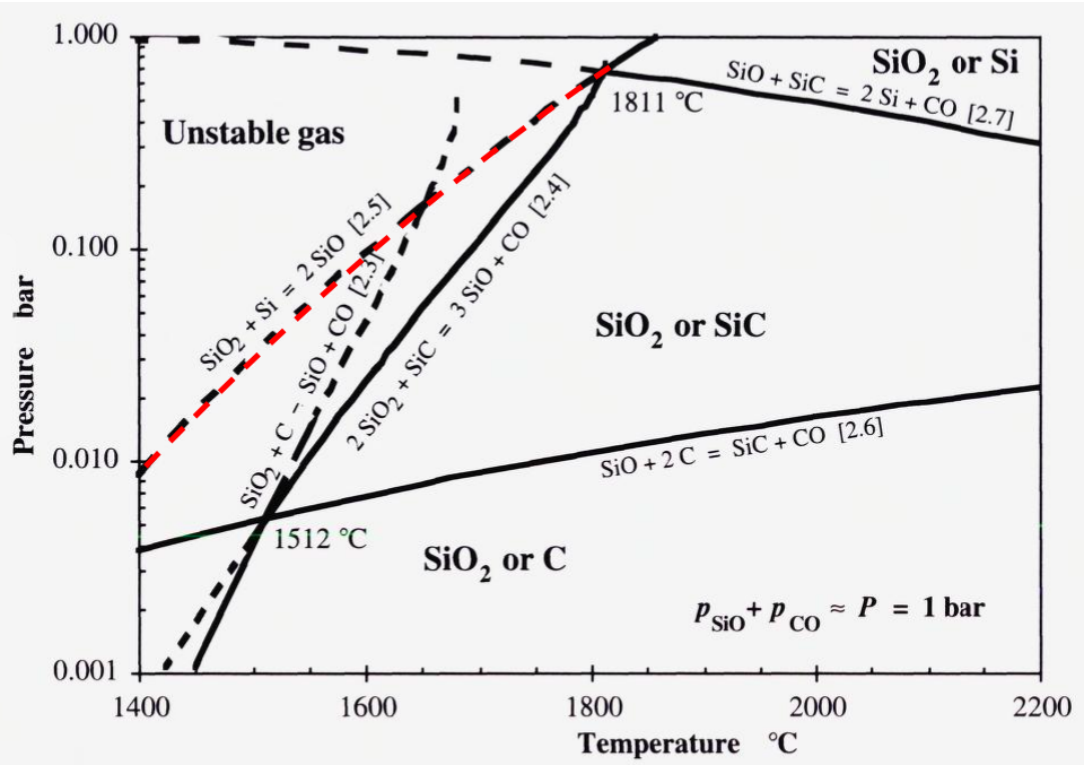

Figure 14: Stability diagram of the Si-O-C system by Schei et al. [32, p. 29], calculated from the JANAF Thermochemical Tables. The red line is added by the author of this report. Broken lines indicate that the gas composition lies in an unstable area.

2.5.1 Wetting in the Si-C-O system

The wettability of a phase towards another phase is defined by the contact angle between the two phases, noted as Θ_γ in Figure 15. A liquid droplet shows wetting behaviour towards a substrate if the contact angle is less than 90°and a non-wetting behaviour if the contact angle is more than 90°.

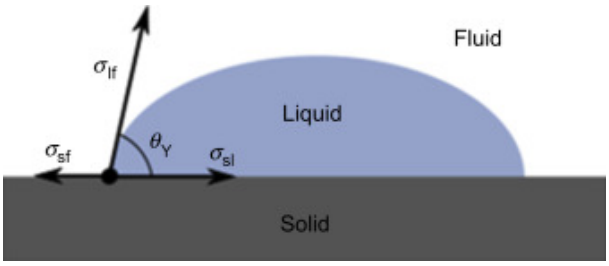

Figure 15: Measurement of the contact angle of a three-phase system [13].

Silicon on graphite has an initial contact angle of about 120 °, but liquid silicon will eventually wet the substrate due to formation of a SiC layer at the interface. The equilibrium contact

angle of silicon on a graphite substrate is reported to be 3-40°by the use of sessile drop technique [10][11]. The finale angle is depending on the surface roughness and is obtained after 5-10 min of heating [10].

According to Alphei et. al [1] silicon has a contact angle of 90°on solid silica substrates. They observed that silicon droplets vibrate on silica substrates, resulting in an oscillating contact angle and further on spreading due to changes in the solid liquid surface tension, as shown in Figure 16. An apparent average wetting angle between 90° and 95° is reported by other sources that also observed vibration of the silicon droplet[20][14], where experiments were performed in 1 atm Ar atmosphere. Formation and release of $SiO_{(g)}$ is a suggested cause of vibration and no secondary phase was found on the silicon/silica interface [20]. Leakage paths like dimples and grooves are found to reduce the amount of vibration and a more constant wetting angle was observed in this case compared to heating on a smooth substrate [20].

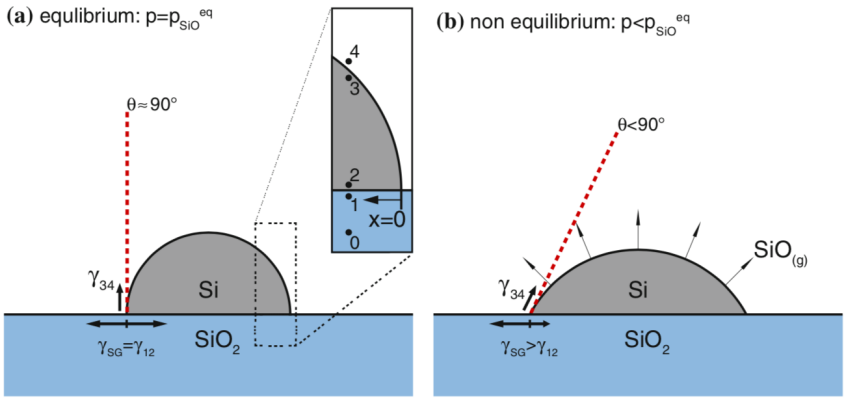

Figure 16: Schematic model of the droplet in it's **a** equilibrium and **b** non equilibrium state. Due to changes in the solid liquid surface tension the droplet starts spreading[1]

Heating of brown condensate in a sessile drop furnace has been performed by Vangskaasen [40]. The condensate consisted mostly of silicon and silica, products from the condensation of $SiO_{(g)}$, represented by the reaction in Equation 3 reversed. The silicon in the brown condensate melted away from the surrounding SiO_2 at temperatures above 1395°C. The separation of silicon happened most rapidly above 1700°C. The remaining amorphous SiO_2 retained its shape up to the maximum temperature of the furnace at about 1850°C and showed no signs of melting. The two phases, silicon and silica did not wet each other.

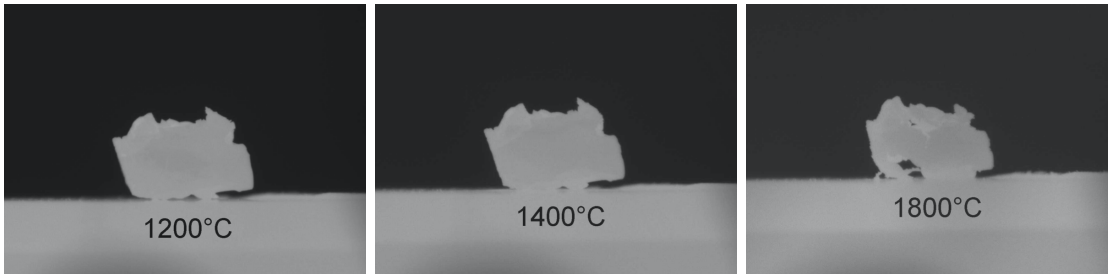

Figure 17: Heating of brown condensate in a sessile drop furnace was performed by Vangskaasen [40]. The silicon was melted and separated from the SiO_2 matrix during heating of the condensate.

There is not much literature on the wetting of silica on graphite substrates but melting and softening experiments were performed with silica on a graphite substrate in a sessile drop furnace by Nordnes [25] as mentioned earlier. The images of completely melted samples show a contact angle above 90°C, and show that the silica does not wet the graphite substrate.

Boron nitride (BN) is one of the very few materials that are non-wetted by liquid silicon [12]. The contact angle between the two materials has been reported to be somewhere between 105°and 145°[12][42][9], all within the non-wetting area ($\theta > 90°$).

2.6 The reactivity of silicon and silica mixtures

The rate of reaction between silicon and silica in pellets, described by Equation 3, increase from 1550°C to its maximum at 1820°C, according to Bao et al. [5]. The reaction rate decrease at higher temperatures and two possible reasons are given: the reaction between silica and silicon are exothermic and the Si vapour increases at higher temperatures, leaving a very low reduction area between Si02 and Si. The reactivity of silicon/silica pellets was calculated to be higher than the one of silica/SiC pellets at temperatures below 1820°C and the opposite was measured for temperatures above 1820°C. The difference at high temperatures was assumed to be due to a low silicon/silica reactivity.

Andersen [2] reported an exponential increase of reaction rate from 1450°C to 1723°C, a reduced reaction rate from 1723°C to 1860°C and finally a significant increase of reaction rate at 1910°C. Bubbeling in the mixture was observed during heating of silicon and silica pellets between 1750°C and 1869°C in a wettability furnace, indicating formation of SiO gas at the silicon/silica interface. The drop in reactivity at these temperatures was therefor related to a high viscosity of the liquid silica and a low gas removal rate. The equilibrium pressure of SiO gas exceeds 1 bar around 1860°C and this is pointed out as a possible reason for increasing reactivity at high temperatures. An activation energy between 438 kJ/mole and 528 kJ/mole is reported by Andersen [2].

Experiments on silicon and silica reactivity of particles were conducted by Sindland in the summer and fall of 2019 [35][34]. It was shown that the reactivity increases with time and temperature and can be described by Equation 9. The model is based on isothermal heat treatment experiments, performed at temperatures from 1650°C to 1950°C, in two different furnaces. 20g of raw materials was either layered or mixed in a graphite crucible and no significant difference between the two methods were discovered. The weight loss as function of time can be found in Figure 19 along with lines indicating the modelled weight loss. It was observed that silicon and silica agglomerate at temperatures above the melting point of silica, as seen in Figure 18. The two phases seems to agglomerate and separate from each other when both phases are liquid, which reduces the available reaction area significantly. One experiment was performed with a boron nitride (BN) crucible and the silicon and silica agglomerated in this case as well and the silicon did not drain, it stayed on top of the silica phase. It was therefor concluded that the agglomeration was due to silicon/silica interaction and not due to silicon wetting the graphite crucible.

$$\frac{d\alpha}{dt} = 1,01 \cdot 10^8 \cdot A_0 \cdot (1-\alpha) \cdot exp(-\frac{552 \cdot 10^3}{RT}) \tag{9}$$

Where α is the degree of reaction [ ], t is the time [s], k_0 is the reaction constant $[s^{-1} \cdot cm^{-2}]$, A_0 is the initial reaction area $[cm^2]$, Q is the activation energy [J/mol], R is the gas constant and T is the temperature [K]. It should be noted that Sindland used an initial area with units of cm^2 (instead of $cm^2 \cdot g^{-1}$) making the model specific to a set-up of 20g sample.

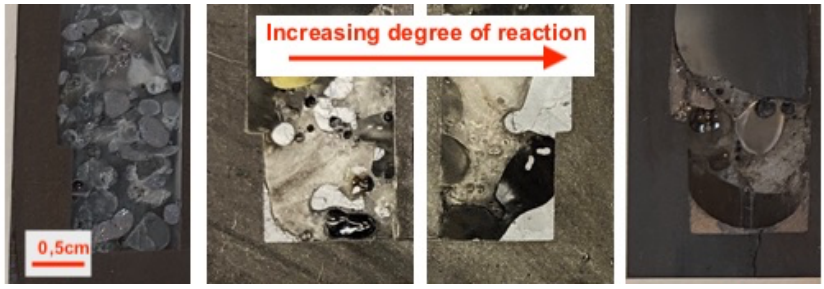

Figure 18: Phase distribution in silicon/silica samples heated by Sindland [35]. The Figure show distribution in graphite crucibles for increasing degree of reaction. The first crucible shows an experiment that was terminated before isothermal heat treatment was started. The other crucibles shows samples heated at an increasing time and temperature. The silicon and silica seems to agglomerate during isothermal heat treatment and the reaction area decrease drastically.

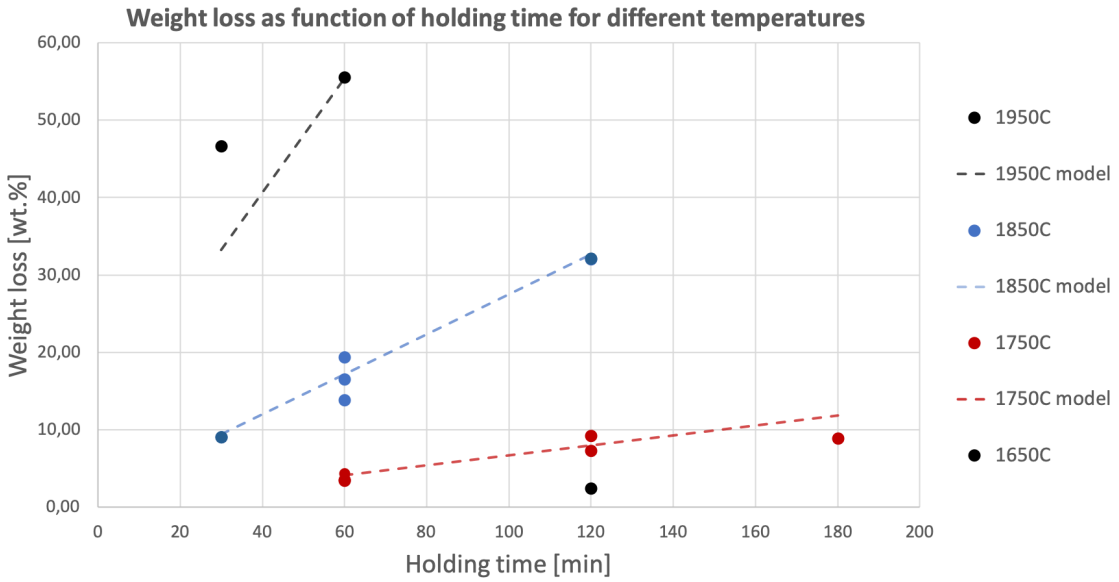

Figure 19: Weight loss as function of holding time for different temperatures. The points are experimental values for weight loss while the dotted lines are weight loss predicted by the model developed by Sindland [35].

Sindland observed that a stable SiC layer was formed after heating for short time at a low temperature and no correlation between thickness of the layer, time and temperature was observed. Weather the weight loss due to SiC formation was significant was therefor dependent on the over all weight loss. Weight loss due to interaction with crucible and formation of CO gas was calculated to be 20 to 50% of the total weight loss of samples heated to 1650°C for 120 minutes. But the weight loss due to SiC formation was found to be less than 10% of the overall weight loss for samples hated to 1850°C for 60 minutes. The weight loss was found to be significant at low temperatures but it was neglected for the entire temperature range.

The rate of a heterogeneous reaction is dependent on the steps listed below [30]:

1. Supply of the reactant in the direction of fluid flow
2. Diffusion of reactant to the interface
3. Interface reaction
4. Diffusion of products from the interface
5. Removal of products in the direction of fluid flow

Depending on the system, the rate can be significantly slower for one of the steps, making that step rate determining. Reaction between silicon and silica will result in formation of SiO gas which does not react with either silicon or silica. Contact between silicon and silica is therefor required for any reaction to happen, and the produced gas is not diffusing through any liquid of solid. Diffusion is therefor not a limiting step as long as we are talking about relatively pure

reactants and step 1 and 3 will therefor determine the rate of reaction. It should however be noted that step 2, diffusion of reactants to the interface can be a limiting factor is we are talking about reaction between silicon and a slag containing silica. The activity of SiO_2 in bulk will affect the concentration gradient between bulk and reaction interface and therefor affect the diffusion of SiO_2 to the interface, described by step 2.

The reaction rate of the silicon/silica reaction is highly dependent on the available reaction area, as descried by step 1, supply of reactants. The available reaction area will be dependent on the melting point, viscosity and wettability of both phases. The second rate determining step for the silicon/silica reactivity, interface reaction, is dependent on temperature. The over all reaction rate of a silicon/silica mixture is therefor determined by the available reaction area and the interface reaction, where the interface reaction rate is increasing with temperature.

2.7 The reactivity of silica and silicon carbide mixtures

The second reaction producing SiO gas in the silicon furnace (in addition to Si/SiO_2 reaction) is Reaction 6 where SiO_2 reacts with SiC to SiO and CO gas. It is interesting to look at litterature regarding the reactivity of this reaction, to be able to compare the two $SiO_{(g)}$ producing reactions and further on comment their impact on SiO losses in industrial furnaces. The reaction rate of the reaction between SiC and silica has been measured by Tangstad et al. [39] and they found it to be described by Equation 10, under the assumption that the surface area of SiO_2 is rate limiting. Their obtained values for reaction constant and activation energy is presented in Table 1. The measurements were done on pellets which gives a high reaction area.

$$\frac{d\alpha}{dt} = k_0 \cdot A_0 \cdot (1-\alpha) \cdot exp(\frac{-Q}{RT}) \tag{10}$$

Where α is the degree of reaction [ ], t is the time [s], k_0 is the reaction constant $[s^{-1} \cdot cm^{-2}g]$, A_0 is the initial reaction area $[cm^2 \cdot g^{-1}]$, Q is the activation energy [J/mol], R is the gas constant and T is the temperature [K].

Table 1: Reaction constant and activation energy for $2SiO_2 + SiC = 3SiO + CO$, measured in pellets [39], k_0 is for the case where the surface area of SiO_2 is limiting.

k_0 $[s^{-1} \cdot cm^{-2}g]$	Q [kJ/mol]
$1,9 \cdot 10^5$	424-464

Tangstad et al. [39] found that the difference in reaction rate is insignificant between pellets of quartz and SiC compared to pellets of cristobalite and SiC, as seen in Figure 20. It was believed that the cristobalite would have a higher reaction rate due to a lower density and hence a higher volume, in addition to a higher surface area as it will crack in the transformation from quartz

to cristobalite. This was however not the case as seen in Figure 20, where the quartz is on the top of the curve, with insignificantly higher conversion.

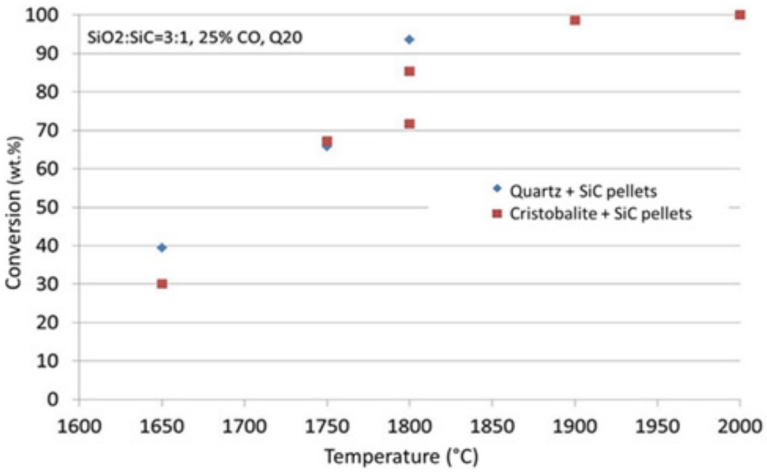

Figure 20: Conversion (wt.%) after 60 minutes at different temperatures (°C). Quartz and cristobalite are used as raw materials. [39]

The reactivity of silica and SiC pellets has also been investigated by Bao et al. [5]. They heated pellets of silica and SiC at 1550, 1730 and 1820°C at a heating rate of 15°C/min and held it for a given time. They found that the reaction rate is almost constant at 1550°C and then increases exponentially to 1730 and 1820°C, until the samples are almost consumed. Temperature accelerates the reaction substantially. Andersen [2] found that the reaction rate increase exponentially from 1450°C to about 1700 °C, it had a constant or reduced rate during melting and a rapid increase from 1770°C.

3 Experimental

This chapter describes the experimental procedures, raw materials and apparatus. The main experiments have been isothermal heat treatment of 1:1 molar mixtures of silicon and silica in graphite crucibles. 17 experiments have been performed at temperatures between 1650 and 1950°C, at holding times between 30 and 120 minutes and with a heating rate of 50K/min until isothermal temperature was reached. The weight loss of each sample has been measured and correlated to formation of SiO gas and reaction rate. Macro, SEM and LOM images have been taken of the heat treated samples and a chemical analysis of the raw materials have been performed. Further analysis of the different quartz samples have been performed to distinguish them and their properties. The wettability of silicon on the different quartz samples has been measured in a sessile drop furnace and the phase composition after heat treatment of the quartz samples has been measured by XRD.

Five different quartz samples have been investigated this spring, where one of them is the same as the one used by Sindland in previous work on silicon/silica reactivity in 2019 [35][34]. Only one type of silicon has been used, a silicon of metallurgical grade. Most of the experiments were performed with particles of size fraction 1-2mm, except the experiments with quartz A which had a size fraction equal to the one used in previous work done by Sindland (2-4.7mm). In addition to this, three experiments with quartz of higher fraction (2-5 and 5-8mm) have been performed, to investigate the affect of particle size on reactivity.

3.1 Raw materials

Chemical composition and particle size of the silicon and quartz used in the experiments is presented in Table 2. The silicon is the same as the one used by Sindland [35] in earlier experiments, four different size fractions have been used. The first four experiments done as part of this master thesis (the experiments with quartz A) were from the exact same batch as the one used by Sindland in the fall and the rest of the experiments used silicon of same quality but from a different batch and size fractions. The first four experiments were run with the same quartz as the one used by Sindland in the fall, and the rest of the experiments were run with different industrial quartz qualities of a 1-2mm size fraction, in addition to three experiment with larger size fractions of quartz E. The method used for chemical analysis of silicon is unknown and the quartz was analysed by XRF, except quartz A which was analysed by ICP-OES.

Table 2: Composition and size of the raw materials.

a) Silicon

Particle size mm	Si wt%	Fe wt%	Ca wt%	Ti ppmw	P ppmw
1-2, 2-4.7, 2-5 and 5-8	Min 99.0	Max 0.40	Max 0.10	200-300	20-40

b) Quartz. The rest is assumed to be SiO_2. *Above calibration limit and must be seen as guidance.

Name	Particle size mm	Al wt%	Fe wt%	K wt%	Ca wt%	Ti wt%	Mg wt%	Na wt%	P wt%
A	2-4.75	0.031	0.012	0.009	0.0046	0.002	0.0017	0.001	0.0003
B	1-2	0.006	0.006	0.002	<0.0011	<0,001	0.0005	<0.0011	<0,0004
C	1-2	0.211	0.192	0.063	0.0026	0.017	<0.0005	0.0022	0.0016
D	1-2	0.038	0.010	0.017	0.0415	0.001	<0.0005	0.0125	<0.0004
E	1-2, 2-5, 5-8	0.505	0.111	0.126	0.0324	0.016	0.0071	0.027*	0.0016

The theoretical product of the investigated reaction is $SiO_{(g)}$ and it was therefor aimed for a 1:1 molar ratio between oxygen and silicon in the samples. A total weight of 20g silicon and quartz was prepared for each sample. The weight ratio between the raw material is presented in Table 3 and calculated as described by Sindland in the spesialization project report [35].

Table 3: The weight of each raw materials in a sample of 20g

Material	Weight	mole of Si
Si	6.37g	0.227
SiO_2	13.63g	0.227

3.2 Furnace and experimental set up for isothermal heat treatment

Mixtures of silicon and silica have been heated in an induction heat furnace called ReSiNa, to measure weight loss as function of time and temperature, which has been correlated to reactivity. For each experiment, 20 grams of SiO_2 and Si (1:1 molar ratio) was mixed and placed in a small graphite crucible ($d_{inner} = 32mm$, $h_{inner} = 61mm$). This mixture was heated in an Ar atmosphere to given temperature at a heating rate of 50 K/min and held for a given time before cooling. The weight of the crucible was measured before and after heating.

3.2.1 The ReSiNa furnace

The furnace used in the isothermal heat treatment experiments is a resistance heating furnace called ReSiNa. Figure 21 shows the set up of the furnace, with the sample inside. The sample (silicon and silica) is placed in a small graphite crucible inside a reaction chamber filled with argon. A condensation chamber filled with silicon carbide is placed above the reaction chamber, which causes any SiO formed in the reaction chamber to condense on the silicon carbide, due to a temperature gradient. The temperature of the sample is monitored by a C-type thermocouple placed in the bottom of the crucible. The bottom part of the thermocouple is covered by graphite while the upper part is covered by alumina, which allows process gas (argon in this case) to flow down to the reaction chamber through the alumina cover. Any gas going through and escaping the condensation chamber will be filtered and sent to an exhaust system. The experiments were run with a small flow of argon, only to maintain a constant pressure of about 1.5atm inside the reaction chamber. The gas was entering the reaction chamber above the crucible containing the sample and is assumed to not interfere with the reaction rate. It should also be noted that Helium was used as inert gas for the two experiments where temperatures above 1900°C were reached, to prevent ionisation of the argon gas and make sure the temperature could be held constant.

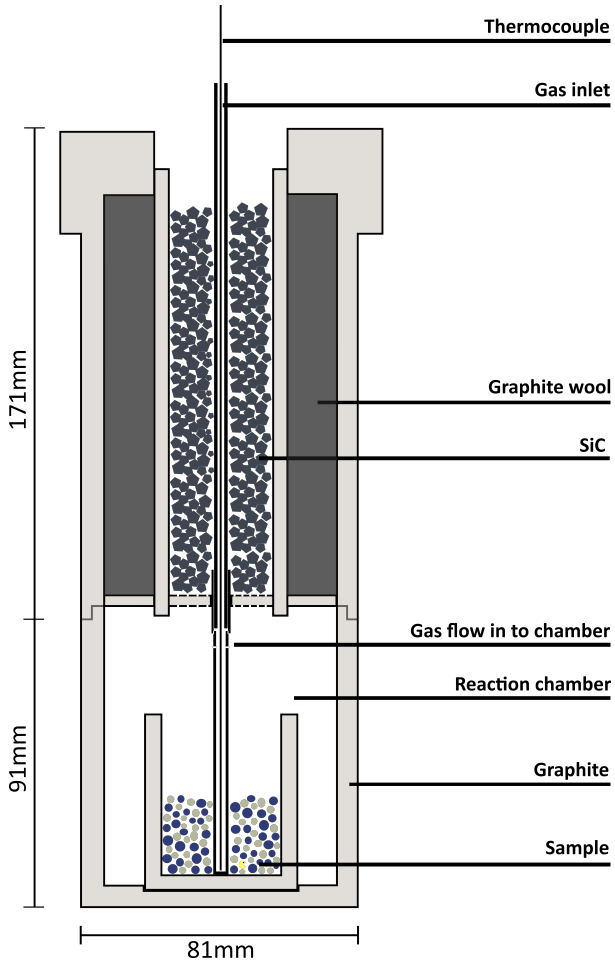

Figure 21: Experimental setup, ReSiNa furnace

The temperature gradient inside the reaction chamber was measured during one of the experiments at 1950°C and the results are presented in Figure 22. The temperature decrease about 15°C per centimetre in the beginning before it decreases even more rapidly. This means that it is very important to measure the temperature at the same height in each experiment. It also means that the temperature inside the condensation chamber should be low enough to ensure condensation of the $SiO_{(g)}$.

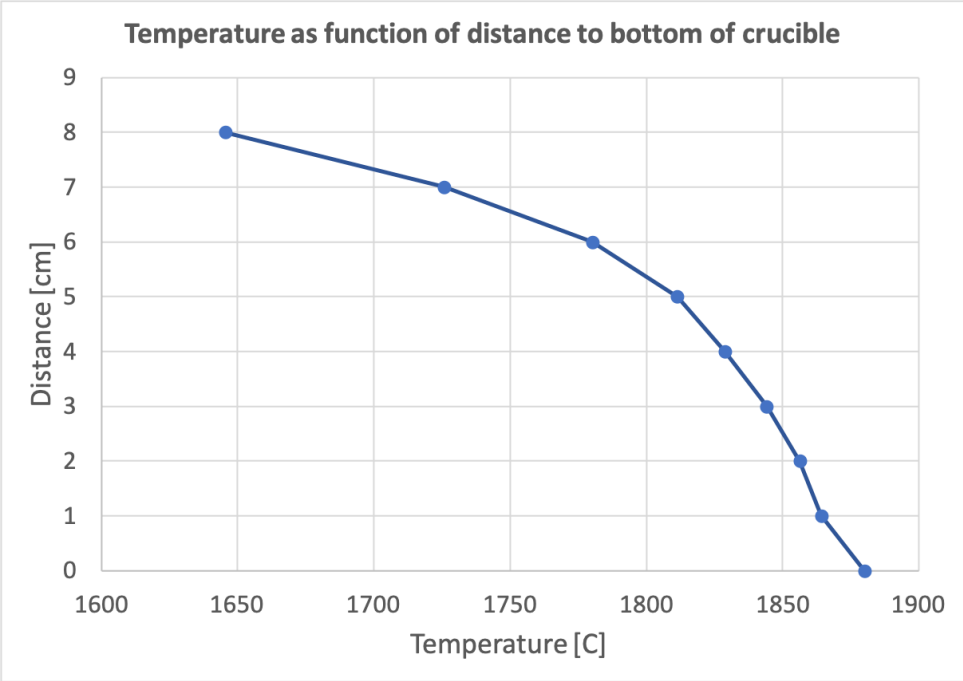

Figure 22: Temperature gradient in the ReSiNa furnace measured 04.02.2020. Temperature is plotted as function of distance from bottom of crucible.

3.2.2 Temperature control

Two temperatures were measured throughout each experiment, the temperature of the sample (which is used in modelling of the results) and the temperature of the furnace (measured outside the reaction chamber). The first one is used in modelling of the results and the last one is used to control the power during operation of the furnace. The set point for experiments where samples were heated to 1650 and 1750°C for 120 minutes and 1850 and 1950°C for 60 min is presented in Figure 23. All of the samples were heated at a rate of 50 K/min up to 25K under isothermal temperature. From this temperature and up to isothermal temperature the heating rate was 5 K/min. The slow heating was programmed to ensure that the actual temperature did not rise high above the maximum set point.

The temperature of each sample was measured and logged through all of the experiments, except experiment M6 where the thermocouple failed. The temperature of the sample in M6 could however be calculated based on the furnace temperature and previous difference between furnace and crucible temperature.

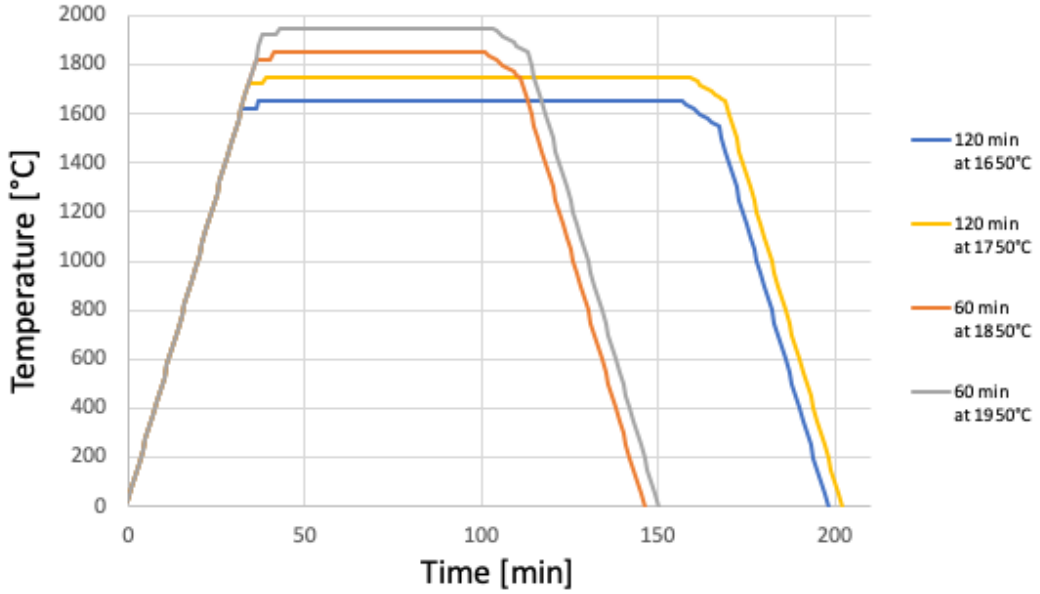

Figure 23: Temperature program for samples heated at 1650 and 1750°C for 120 minutes and 1850 and 1950°C for 60 minutes.

3.2.3 Crucible material

Most parts used in the experimental set-up, the outer crucible, inner crucible and thermocouple cover in the reaction chamber was made of graphite. The properties of the graphite used for crucibles is presented in Table 4.

Table 4: Properties of the graphite crucibles, quality IG-15. Values given by Toyo Tanso CO., LTD

Bulk Density	Cumulative Pore Volume	Open Porosity	Radius of Average Open Porosity
Mg/m^3	m^3/g	%	µm
1.90	0.052	10	1.4

3.2.4 Experimental log

An experimental log is presented in Table 5. The temperatures listed in Table 5 is the furnace set point and the actual temperature measured inside the crucible. The difference between those two temperatures varied from 10°C lower to 10 °C higher, except for M1 to M4 where the temperature inside the crucible was 20 to 40°C higher than the set point. The actual isothermal temperature ($T_{crucible}$) was used in the modelling of reaction rate.

Table 5: Experimental log including set point and actual temperatures inside crucible (the last one used in modelling of data). The silicon and silica had the same particle size in each individual experiment and the value for particle size/size fraction are listed in the table.

Quartz type	T_{SP} [°C]	$T_{crucible}$ [°C]	Holding time [min]	Exp. number	Particle size
A	1650	1660	120	M2	2-4,7mm
A	1750	1775	120	M1	2-4,7mm
A	1850	1880	60	M3	2-4,7mm
A	1950	1980	60	M4	2-4,7mm
B	1650	1636	120	M5	1-2mm
B	1850	1833	60	M7	1-2mm
C	1650	1644	120	M14	1-2mm
C	1750	1746	120	M12	1-2mm
C	1850	1854	60	M8	1-2mm
C	1950	1946	30	M13	1-2mm
D	1650	1644	120	M9	1-2mm
D	1850	1856	60	M10	1-2mm
E	1650	1658*	120	M6	1-2mm
E	1850	1853	60	M11	1-2mm
E	1850	1855	60	M17	2-5mm
E	1650	1645	120	M15	5-8mm
E	1850	1840	60	M16	5-8mm

*The thermocouple inside crucible failed and $T_{crucible}$ was calculated based on $T_{furnace}$.

3.3 Characterisation

The main experimental result in this report is the weight loss of each sample after isothermal heat treatment. This was measured by weighing the crucible, thermocouple cover and samples individually before heating and weighing of crucible with sample and thermocouple cover after heating. The weight loss of each sample was assumed to be equal to the total weight loss of sample, crucible and cover described by Equation 11. This means that weight loss of the graphite parts was neglected.

$$Wt.loss = \frac{(crucible,\ sample\ and\ cover)_{before} - (crucible,\ sample\ and\ cover)_{after}}{sample\ weight\ before} \tag{11}$$

The next step in characterisation was investigation of the phase distribution of each sample. Two different methods were used for cutting, the method in Figure 24 gives macro images showing the radial distribution in additional to vertical distribution. Each crucible was filled with epoxy and cut according to Figure 24 a or Figure 25 a, before macro images were obtained. The

samples cut according to Figure 25 were further on cut according to 25b before another macro image was obtained. The samples were then cut according to Figure 24 b and c and Figure 25 c to prepare for microscope investigation. The samples were moulded in epoxy and polished before LOM investigation. It was wrapped in aluminium and carbon coated to ensure sufficient conductivity before investigation in SEM.

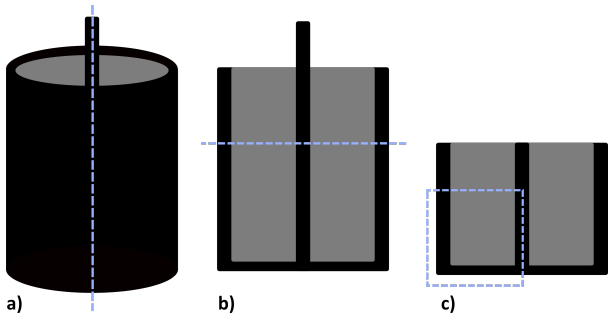

Figure 24: Sample M1 to M8 were cut according to the blue line in a) before macro investigation and according to the blue lines in b) and c) before investigation in microscope.

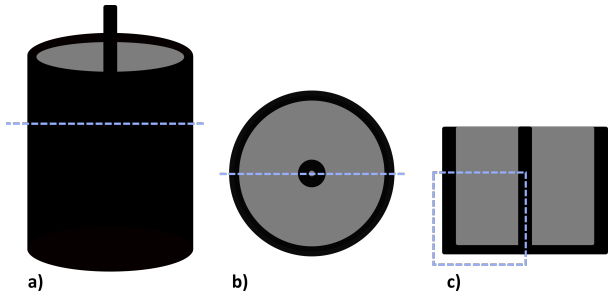

Figure 25: Sample M9 to M17 were cut according to the blue lines in a) and b) before macro investigation and according to the blue line before investigation in microscope.

3.3.1 SEM - BSE pictures and EDS

Each sample was characterised with back scattered electrons (BSE) in SEM and an EDS analysis was performed at different spots. An example on how the samples were wrapped and coated to ensure good conductivity is presented in Figure 26. Zeiss Ultra, a field emission SEM located at Bergbygget, NTNU was used for the analysis.

Figure 26: Sample ready for SEM.

The area investigated by SEM are hit by a thin and focused electron beam, scanning the surface of the sample. The incoming beam results in multiple outgoing signals as secondary electrons, back scattered electrons and characteristic x-ray radiation that can be detected [15, p. 2]. The back scatter signal was used to take images of each sample in this report. The intensity of the back scatter signals is dependent on the average atomic number

in the point where the electron beam hits the sample. The intensity of the BSE signal increase with increasing atomic number, giving contrast to the images. A graphite crucible will for example be darker than silica which again will be darker than silicon in a given image. EDS on the other hand is based on the characteristic X-ray radiation of each element. Each element in the periodic table will emit a characteristic X-ray radiation when it is hit by an electron beam. The intensity of the characteristic signal is dependent on the concentration of the given element. An approximate phase composition can therefor be determined in given point by the use of EDS analysis [15, p. 46]. The intensity of X-ray signals decrease with decreasing atomic number and it is therefor difficult to detect elements with a low atomic number as carbon, nitrogen and boron. They can usually be identified but an exact molar fraction is not possible to detect by EDS.

3.4 Heat treatment and X-ray diffraction (XRD) of quartz

The phase composition of the five different quartz samples after heat treatment at 1650°C was determined by XRD. The different types of quartz were heated in Nabertherm LHT 04/18, a high temperature furnace to 1650°C and held for 120min, following the same program as the samples heated in ReSiNa. The samples were first cooled for some time in the furnace before they were cooled on a brick to room temperature.

The samples were then prepared for XRD analysis by milling of the sample, drying and mixing with a spike. The samples were milled in a tungsten carbide chamber at 700rpm for 20 seconds before they were dried at 150°C over night. Approximate 0.7g sample and 0.17g spike (Al_2O_3), both weighted to an exact amount, was then mixed by the use of acetone and a mortar and the mixture was analysed by XRD. Three parallels of each sample were analysed, to highlight any weighing error and such.

X-ray diffraction is used for crustal structure and interplanar spacing determinations[8]. The sample are grind to powder and pressed before it is exposed to a monochromatic x-radiation, ensuring a random distribution of crystalline orientation of each particle. The incoming x-rays are scattered by the atoms in the powder. This means that the outgoing beam will have an intensity varying as a function of the incoming beams angle, giving a diffraction pattern where the intensity is plotted as function of 2θ. The variation of the intensity of the outgoing beam are due to scattering causing interfering between the waves. The incoming waves will remain in phase after scattering if Bragg's law given by Equation 12 is fulfilled, giving an outgoing beam of high intensity. Analysing the intensity of the beam after scattering will therefore make it possible to determine the interplanar spacing and phase composition of a material. The amount of amorphous phase in a sample can be determined by addition of a spike. The intensity of the peaks in a diffraction pattern indicating the amount of spike can be compared to the the peaks indicating the samples crystalline phases. The amount of crystalline phase can be determined because the amount of spike is known, and the rest of the sample $(1 - x_{cryst.})$ is assumed to be

amorphous.

$$n\lambda = 2d_{hkl}sin\theta \tag{12}$$

Where n is the order of reflection (any integer), λ is the wave length, d is the interplanar spacing and θ is the angle of the incoming beam.

3.5 Sessile drop durnace - Wettability

There is two different sessile drop furnaces in Alfred Getz' vei 2 (NTNU, Gløshaugen). The main difference between the two furnaces are the vacuum level that can be reached. Furnace 2 can reach a higher vacuum than Furnace 1, and Furnace 2 is therefor proffered for heating of samples subjected to oxidation. This is therefor the preferred furnace for silicon. Both of the sessile drop furnaces were used to investigate the wettability of the different types of quartz and silicon. One experiment, heating of quartz C was done by Sindland in the sessile drop furnace called furnace 2 in Alfred Getz vei 2 (NTNU, Gløshaugen) but problems with the vacuum and lack of people who could fix it this spring prevented any further experiments. Measures against the COVID-19 virus prevented the master students from working in the labs for a few weeks and did not allow any new training after that. All of the samples were therefor heated in sessile drop furnace 1 by Syvertsen (SINTEF) in the end.

Wettability of a sample is measured in the sessile drop furnace by heating of a sample on a given substrate, while images of the sample is taken thought the entire experiment. The images is then analysed and a wetting angle was obtained for each sample by the used of ImageJ. A silica substrate was prepared from each sample by cutting of disks from core samples, this was done by Edvardsen (SINTEF). The discs were grinded by SiC paper to make sure the bottom and top of the disks was parallel, preventing the droplet from rolling during heating. Silicon particles of about 100mg were placed on top of the substrate and the samples were heated in argon atmosphere. The sample was set to be heated to 900°C within 3 minutes before it was heated to 1350°C at a heating rate of 50 K/min and finally at a rate of 5 K/min to 1450°C, except the one experiment in Furnace 2 where the sample was heated at a rate of 10K/min in the last step to 1450°C. It was then set to be held at 1450°C for 120 minutes before cooling. Pictures were taken throughout the entire experiment with 1 image/K (2 images per K during heating from 900 to 1450°C).

The temperature of the furnace is monitored by a thermocouple that is ageing over time, it is therefor common to run a calibration test before any series of samples. The calibration was done by calculating the difference between the measured melting point of silicon on a graphite substrate and the theoretical melting point (1414°C). All of the samples in that sequence were then corrected accordingly to that difference. The experiments in Furnace 1 was conducted within 2 following days and the calibration test was performed at the first day of experiments. The

thermocouple of Furnace 1 showed a temperature that was 73°lower than the actual temperature and the samples were therefor held at 1523°C instead of the set point temperature of 1450°C. The temperature in furnace 2 was calibrated the same day as the experiment was run.

3.6 Modelling

The degree of reaction (α) of a silicon and silica mixture is equal to the sample weight loss described by Equation 11, if all of the weight loss is due to the investigated reaction. Values for weight loss as function of time and temperature (obtained by experiments) can therefor be used to model the reactivity of a silicon and silica mixture. An Arrhenius relation has been used to model the reactivity and the final equation is including the reaction area in addition to the reaction constant and activation energy, as presented in Equation 13. The available reaction area was assumed to be described by the initial area multiplied with the fraction unreacted sample and an agglomeration factor, presented by Equation 14. The surface area of silicon was used as initial reaction area due to the fact that initial surface area of silicon was lower than initial surface area of silica. The agglomeration factor was included to take into account that the reaction area decreases significantly when both phases are liquid, due to agglomeration. The factor (F) is set to be equal to 1 below the melting point of quartz, and equal to 0.5 above it, as described by Equation 15.

$$\frac{d\alpha}{dt} = k_0 \cdot A \cdot exp(-\frac{Q}{RT}) \tag{13}$$

$$A = A_{0,Si} \cdot (1-\alpha) \cdot F \tag{14}$$

$$T < T_{m,QZ} \Longrightarrow F = 1 \qquad T > T_{m,QZ} \longrightarrow F = 0.5 \tag{15}$$

Where α is the degree of reaction [ ], t is the time [s], k_0 is the reaction constant $[s^{-1} \cdot cm^{-2}g]$, A is the available reaction area, $A_{0,Si}$ is the initial reaction area $[cm^2 \cdot g^{-1}]$, F is the agglomeration factor, Q is the activation energy [J/mol], R is the gas constant and T is the temperature [K].

The reaction constant and activation energy were obtained from experimental data by the use of an Arrhenius plot and linear regression. Equation 16 was obtained by integration of Equation 13, as described in Appendix I. The left side of the equation can be plotted based on experimental values, towards corresponding 1/T on the x-axis. This was done and a linear regression was used to find an equation that fits the points. The reaction constant is then equal to the exponential of the regression intersection with 1/T = 0 and the activation energy is equal to the slope of the regression multiplied by -R.

$$ln(-ln(1-\alpha)) - ln(A_{0,Si} \cdot F) - ln(t) = ln(k_0) - \frac{Q}{RT} \tag{16}$$

3.6.1 Probability and Statistics

Linear regression is used to fit the experimental data in an Arrhenius plot. The regression is based on minimisation of the sum of square errors and the coefficient of determination (R^2) is used as a measure of quality. One should be aware of the fact that R^2 can be made artificially high by an unwise practice of overfitting[41]. Additional terms in the model should only be added it if it can be justified by an observed phenomena (eg. agglomeration of phases leading to a significant decrease in reaction area above melting point of quartz) and should not be added with the main goal of increasing the coefficient of determination.

A 95% prediction interval described by Equation 17 is used in this report to determine whether multiple types of quartz can be fitted to the same model. A group of 17 result (both from this master thesis and the specialisation project delivered by Sindland) from different experiments with one type of quartz (quartz A) was used to develop a linear regression and a prediction interval based on this population can than be created. It can be justified to include the future measurements in the same model, regardless of the raw materials used, if 95% of the new results lay within the prediction interval. In that case, where 95% of the new measurements lay within the prediction interval, a new regression can be obtained based on all of the data. One can say that there is a high probability that all of the raw materials have the same true linear regression. This will be the method of determining whether reactivity of silicon and silica mixtures depend on the type of quartz used or not.

$$\hat{y}_0 - t_{\alpha/2} s \sqrt{1 + \frac{1}{n} + \frac{(x_0 - \bar{x})^2}{S_{xx}}} < y_0 < \hat{y}_0 + t_{\alpha/2} s \sqrt{1 + \frac{1}{n} + \frac{(x_0 - \bar{x})^2}{S_{xx}}} \tag{17}$$

4 Results

The weight loss of different silicon and quartz mixtures after isothermal heat treatment can be correlated to the rate of the $Si + SiO_2$ reaction and it is therefor the most important result of this report. SEM and macro images have been obtained from each sample after heating, to investigate the phase distribution and any reaction that might affect the correlation between weight loss and reactivity. Additional investigation of each quartz sample have been performed to be able to correlate any difference between them to difference in reactivity. That includes investigation of phase distribution after heating at 1650°C for 120 minutes and wettability of silicon on substrates made of each quarts type.

4.1 Weight loss

17 isothermal heat treatment experiments were performed as part of this thesis and the weight loss after heating is listed in Table 6 and shown in Figure 27. The weight loss increase exponentially with increasing temperature, even though the holding temperature has been decreased for experiments at higher temperatures. Five different types of quartz have been used in the experiments and the different types of quartz are indicated in Figure 28. There is no significant difference between the weight loss of the different quart samples.

Table 6: Quartz type, fraction, crucible temperature and holding time for each experiment is listed as well as sample weight loss after heating. Each sample was weighted to 20,0g prior to heating with a Si:SiO_2 molar ratio of 1:1. The weight loss increase with temperature.

Quartz	Fraction [mm]	T [°C]	t_{hold} [min]	Weight loss [wt.%]	Exp. Nr.
A	2-4,7	1670	120	3,25	M2
A	2-4,7	1775	120	12,65	M1
A	2-4,7	1880	60	22,00	M3
A	2-4,7	1985	60	71,80	M4
B	1-2	1636	120	4,40	M5
B	1-2	1833	60	20,56	M7
C	1-2	1644	120	5,10	M14
C	1-2	1746	120	11,83	M12
C	1-2	1854	60	26,45	M8
C	1-2	1946	30	47,35	M13
D	1-2	1644	120	5,66	M9
D	1-2	1856	60	23,20	M10
E	1-2	1658	120	4,45	M6
E	1-2	1853	60	22,57	M11
E	2-5	1855	60	17,85	M17
E	5-8	1645	120	2,60	M15
E	5-8	1840	60	13,54	M16

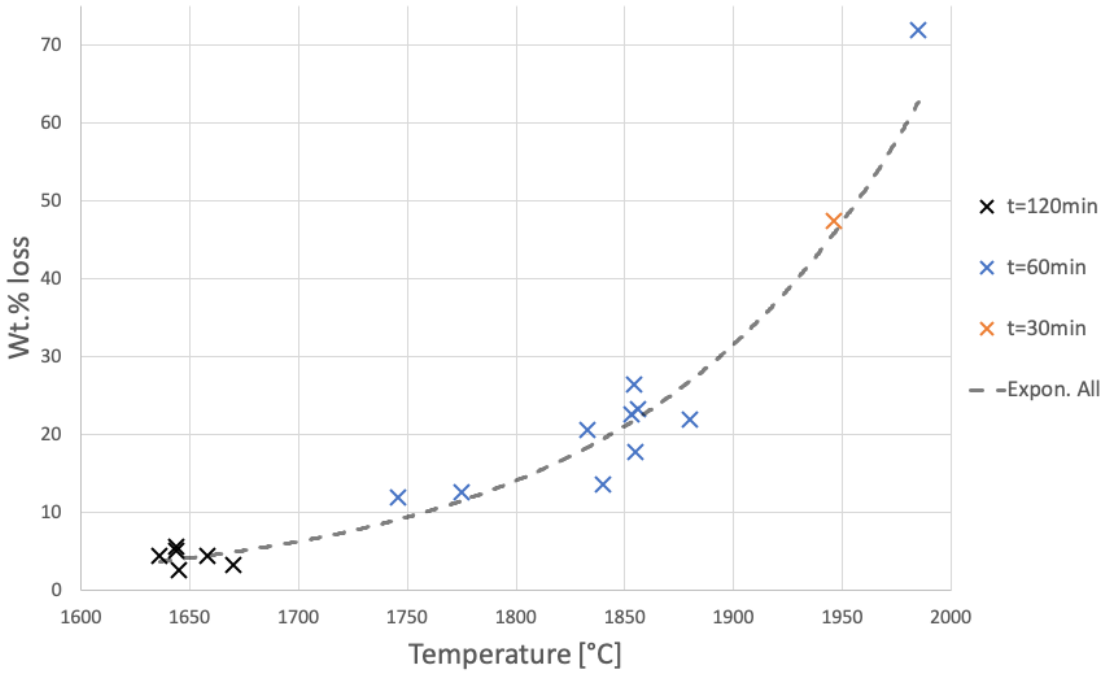

Figure 27: The weight loss after heating samples of quartz A to E mixed with silicon. The colour indicate the isothermal holding time. The dashed line is a regression based on all of the results.

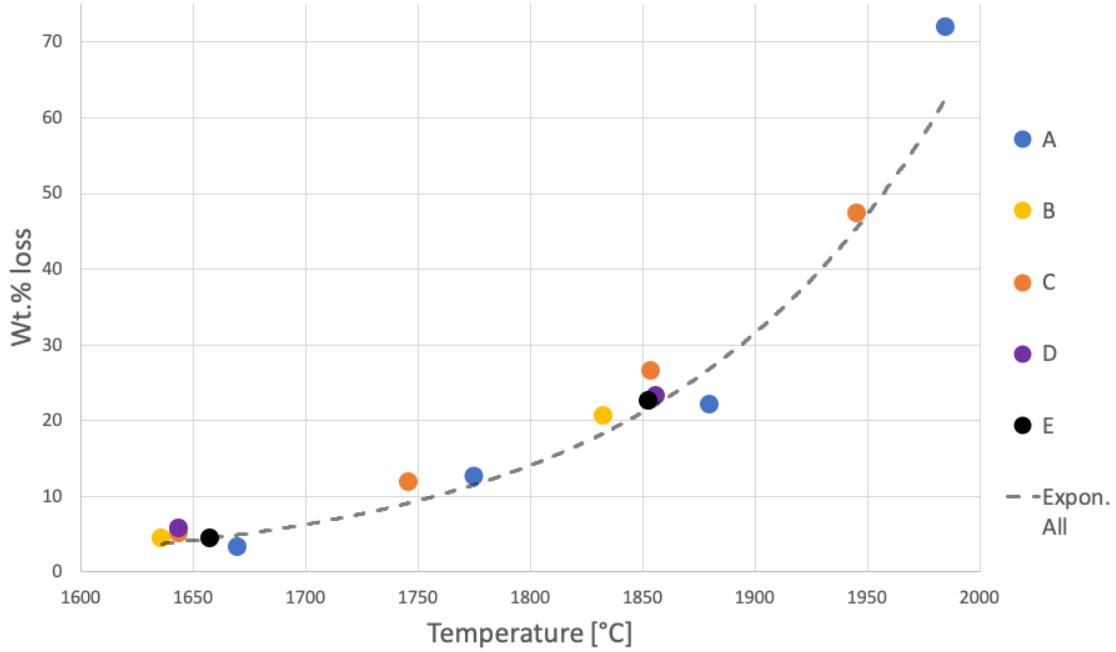

Figure 28: The weight loss after heating samples of quartz A to E mixed with silicon. The colour indicate the type of quartz used in each experiment. The dashed line is a regression based on all of the results.

4.2 A model for reactivity - Arrhenius plot

A model has been chosen for reactivity of silicon and silica mixtures, as described in the experimental section. The reaction rate is described by Equation 13, where Equation 14 describes the available reaction area. The left side of Equation 16 is plotted against -1/T in an Arrhenius plot, to evaluate the fit of the data to the model and further on be able to extract values for reaction constant and activation energy. The value for initial reaction area (A_0) varies for the different experiments due to use of different particle sizes as noted in Table 5. The initial reaction area are given by the initial area of silicon in the experiments of this report because the surface area of silicon is less than silica in a 1:1 molar mixture of particles with similar size fraction. The initial reaction area are given by Equation 18 and the calculated values for each size fraction of sample are listed in Table 7. The temperature used in the Arrhenius plot is the measured crucible temperature, also listed in Table 5.

$$\frac{d\alpha}{dt} = k_0 \cdot A \cdot exp(-\frac{Q}{RT}) \tag{13}$$

$$A = A_{0,Si} \cdot (1-\alpha) \cdot F \tag{14}$$

Where α is the degree of reaction [ ], t is the time [s], k_0 is the reaction constant $[s^{-1} \cdot cm^{-2}g]$, A is the available reaction area $[cm^2g^{-1}]$, $A_{0,Si}$ is the initial reaction area $[cm^2 \cdot g^{-1}]$, F is the agglomeration factor, Q is the activation energy [J/mol], R is the gas constant and T is the temperature [K].

$$ln(-ln(1-\alpha)) - ln(A_{0,Si} \cdot F) - ln(t) = ln(k_0) - \frac{Q}{RT} \tag{16}$$

$$A_{0,Si} = \frac{1}{\rho_{Si}} \cdot \frac{S_{part.}}{V_{part.}} \tag{18}$$

Where ρ_{Si} is the density of silicon, $S_{part.}$ is the surface area of one particle and $V_{part.}$ is the volume of one particle.

Table 7: Calculation of available reaction area per gram silicon for different size fractions.

Fraction [mm]	1-2	2-4,7	2-5	5-8
Average particle diameter [mm]	1,5	3,35	3,5	6,5
Average particle radius [cm]	0,075	0,1675	0,175	0,325
Volume of one particle, $V_{part.}$ $[cm^3]$	0,002	0,020	0,022	0,114
Surface of one particle, $S_{part.}$ $[cm^2]$	0,071	0,352	0,385	1,327
Surface per gram of Si particles, A_0 $[cm^2g^{-1}]$	17,39	7,79	7,45	4,01

All of the results presented in Figure 27 have been plotted in an Arrhenius plot as described above and the result is presented in Figure 29. A linear regression was obtained based on the data points and the regression with corresponding equation and R^2 value is included in the figure.

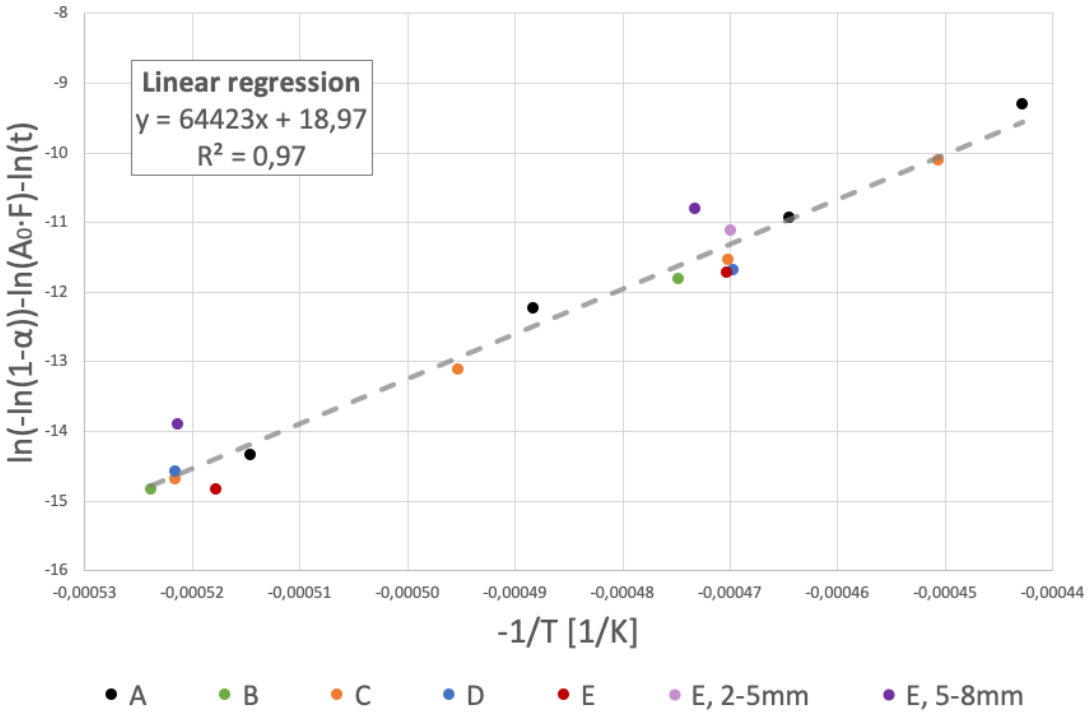

Figure 29: An Arrhenius plot of the degree of reaction obtained after isothermal heat treatment of quartz A to E. The actual crucible temperature for each experiment has been used, as well as initial reaction area (A_0) based on the particle size used in the different experiment. The different colours indicate the different types of quartz and the fraction of the raw materials in the case where different fractions were used for the same type of quartz.

4.3 Macro observations

Most of the crucibles cracked during heating or cooling. No leak of materials was observed due to cracking and hence it is believed that the cracking happened during cooling due volume expansion of the silicon phase. All of the crucibles were filled with epoxy after the experiment and further on cut in half for macro imaging. A complete collection of those macro images, similar to Figure 30 showing one of the samples, can be found in appendix II. A small part of each sample was polished and prepared for SEM analysis and a collection of macro images taken of those samples are presented below.

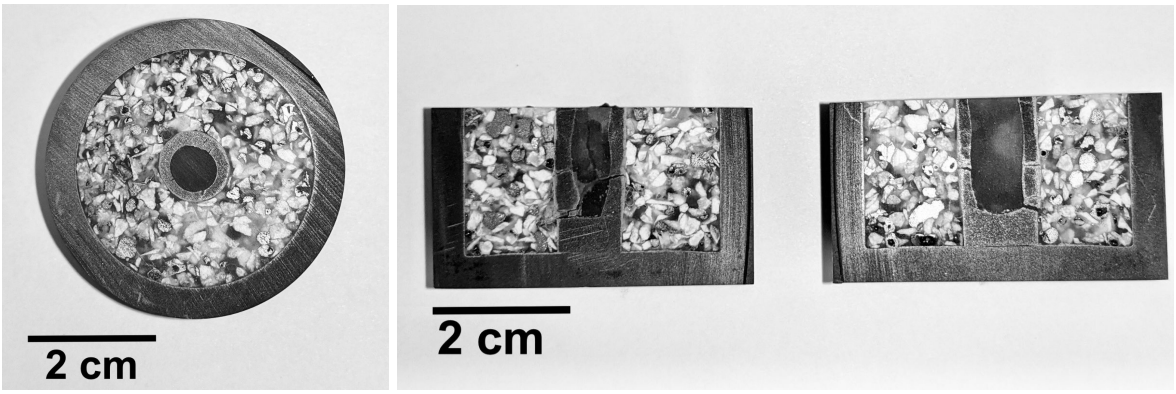

Figure 30: Crucible after the first cutting, from experiment M9 where quartz D was heated to 1650 °C for for 120 min.

Figure 31 shows macro images of quartz A (size fraction 2-4,7mm) after heating at temperatures ranging from 1650°C to 1950°C. Quartz A shows a high degree of agglomeration already at 1750°C, and the two phases are completely separated after heating to 1850°C and 1950°C. The silicon are melted and agglomerated at 1650°C but the silica particles does not show any sign of softening.

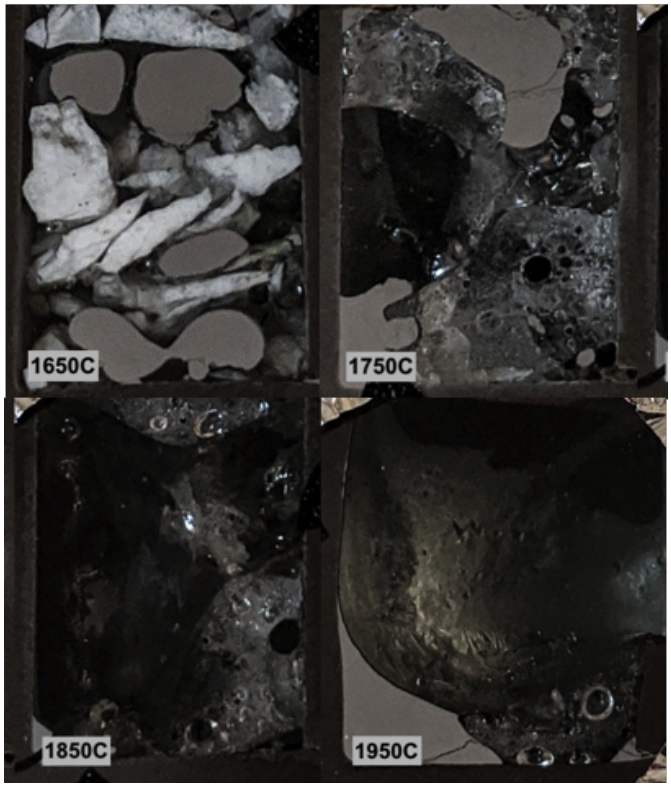

Figure 31: Macro images of quartz A heated to 1650, 1750, 1850 and 1950°C for 120, 120, 60 and 60 minutes respectively. The isothermal temperature for each experiment is indicated in the images.

Figure 32 shows macro images if quartz C (size fraction 1-2mm) after heating at temperatures ranging from 1650°C to 1950°C. Quartz C shows a lower degree of agglomeration at 1750°C and 1850°C than quartz A, but both types of quartz shows significant agglomeration and separation of the two phases at 1950°C. The silicon are melted and agglomerated at 1650°C in this case as well as for quartz A, and the silica show signs of softening and/or sintering. The different quartz particles can not be distinguished from each other.

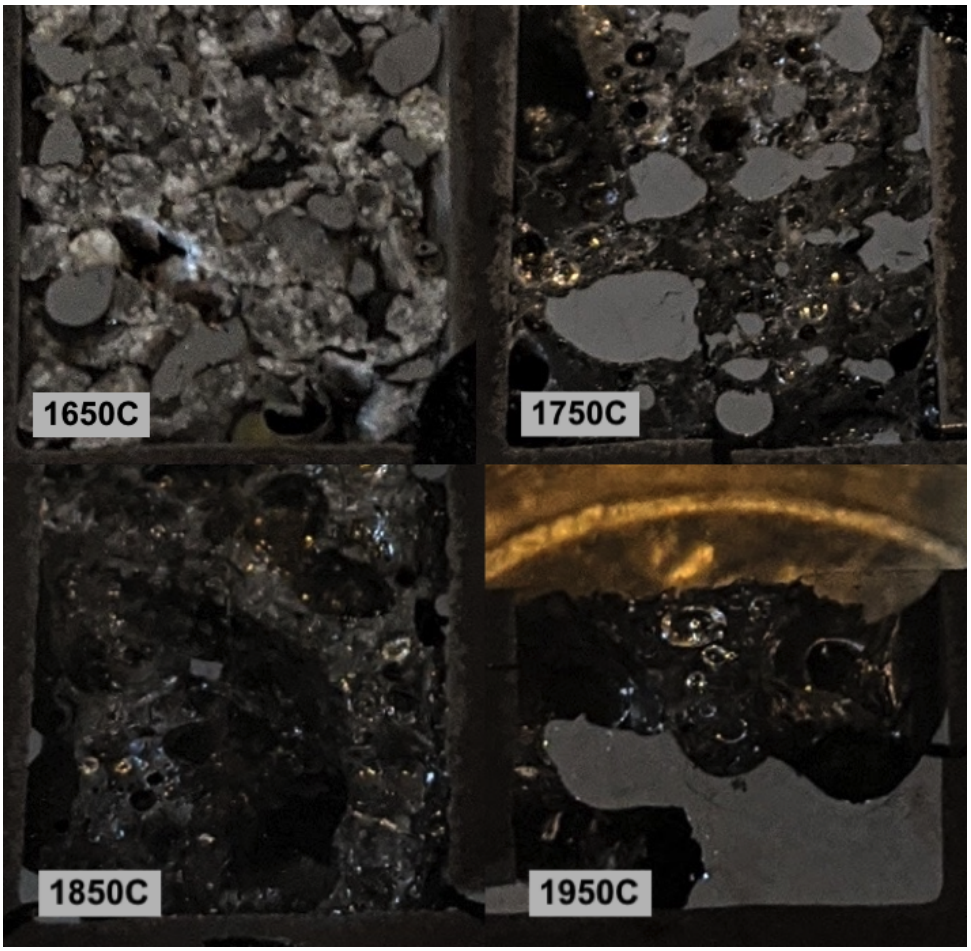

Figure 32: Macro images of quartz C heated to 1650, 1750, 1850 and 1950°C held for 120, 120, 60 and 30 minutes respectively. The isothermal temperature for each experiment is indicated in the images.

Figure 33 shows macro images of all of the samples heated to 1650°C. The experiments with quartz A were performed with quartz and silicon of a bigger fraction than the other samples, which gives a significant difference in available reaction area. The silicon has been melted in all cases and seems to agglomerate into bigger droplets/particles. The silica has remained solid or partly solid in all cases. The samples with quartz C and E shows signs of softening and/or sintering. There is no significant difference between the samples other than that.

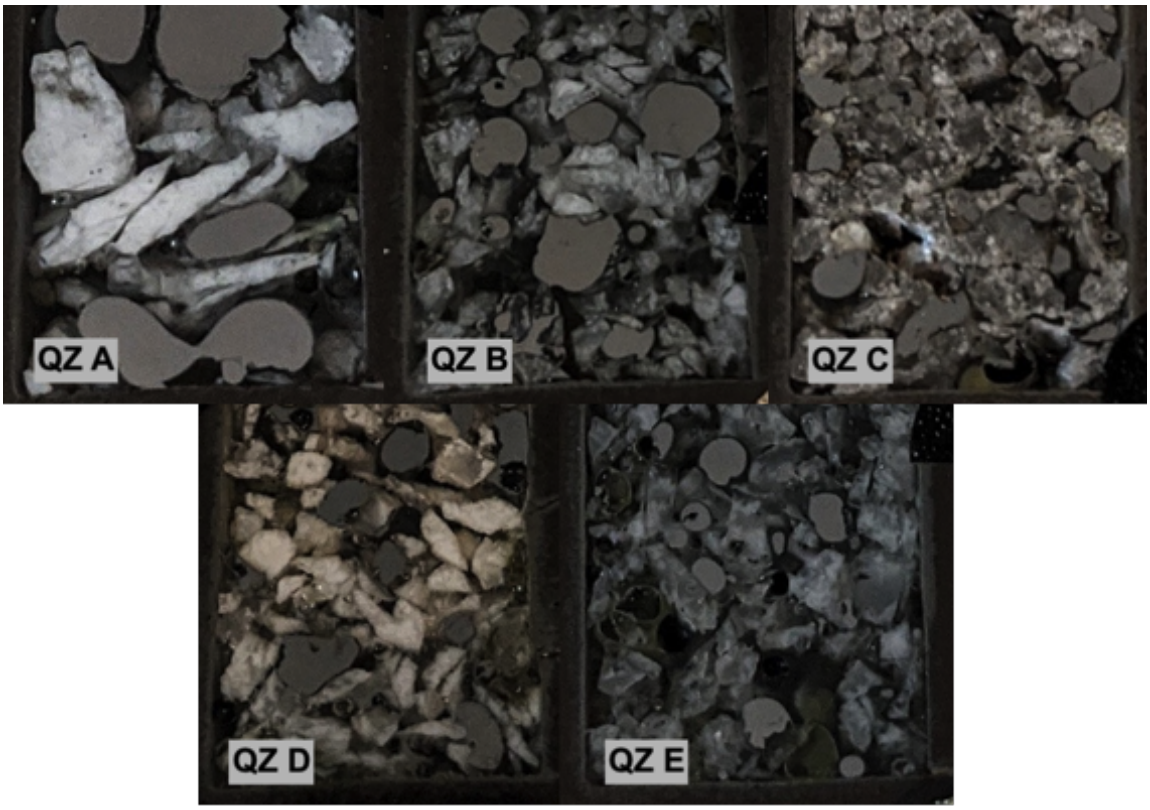

Figure 33: Macro images of quartz A to E heated to 1650°C and held for 120minutes. The quartz used in each experiment is indicated in the images.

Figure 34 shows macro images of all of the samples heated to 1850°C. Air gaps or bubbles indicates that there have been gas formation in all of the samples. All of the samples show a high degree of agglomeration, the silicon and silica tends to separate. However, the silicon does not seem to drain to the bottom of the crucible as one would expect by looking at the density difference of the two phases. There is no significant difference between the samples other than the amount of air gaps.

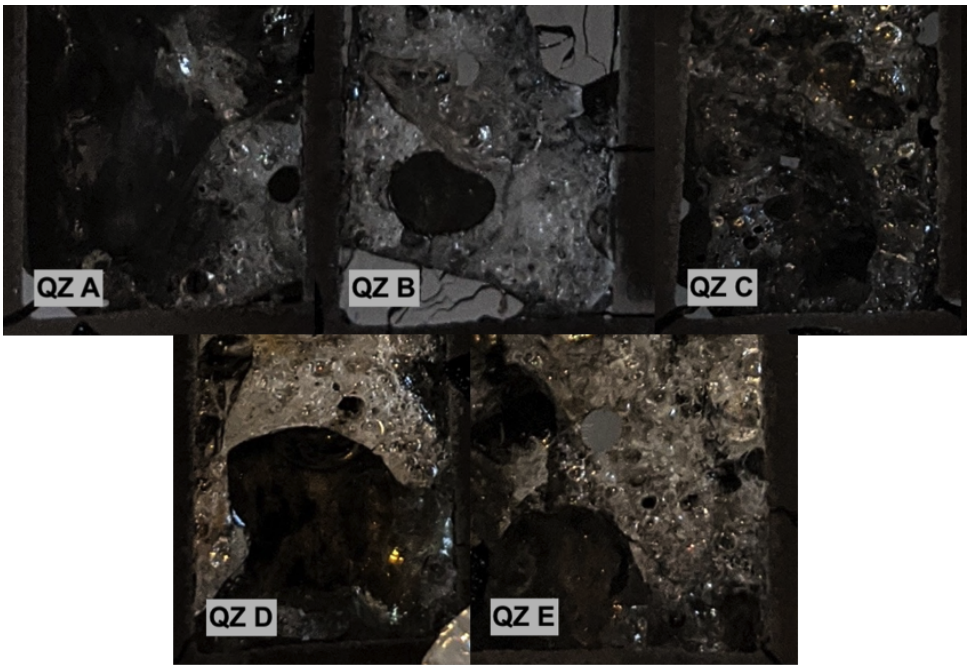

Figure 34: Macro images of quartz A to E heated to 1850°C and held for 60minutes. The quartz used in each experiment is indicated in the images.

Different size fractions of quartz E were heated to 1850°C and macro images of the tree fractions are included in Figure 35 for comparison. The available reaction area is significantly reduced with increasing size fraction and the silicon has drained to the bottom of the crucibles for the samples with particles above 2mm, this is not the case for the sample of 1-2mm fraction.

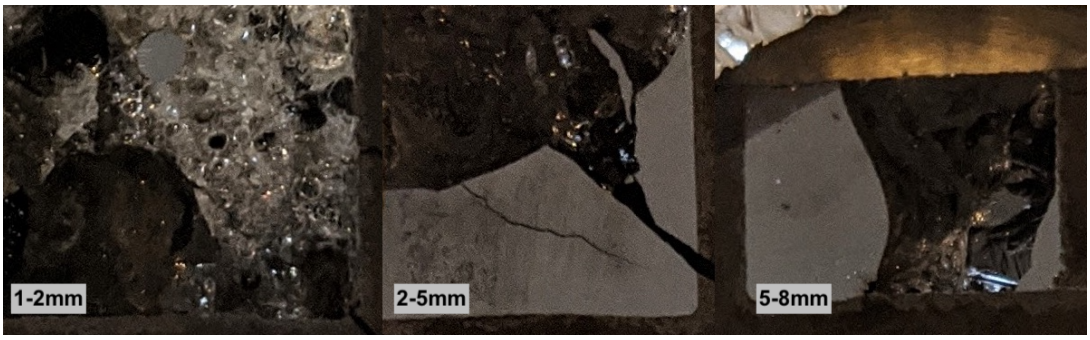

Figure 35: Macro images of different size fractions (1-2, 2-5 and 5-8mm) of quartz E heated to 1850°C and held for 120minutes.

4.4 Microscopy

Investigation of the samples in light optical microscopy (LOM) was done to get an overview of the phase distribution and interaction with crucible before analysis by scanning electron microscope (SEM). The SEM images give more detailed information than the images taken by LOM and the LOM images is therefor not included here, but they can be found in Appendix III. All of the samples were investigated in scanning electron microscopy (SEM) and analysed by energy dispersive X-ray spectroscopy (EDX) to determine approximate phase compositions. Back scatter electron (BSE) images from all of the samples are included in Figure 36 to 52. Elements with a low atom number is difficult to detect by EDS due to a low signal, but carbon was present in high concentrations and C (graphite) and SiC is therefor indicated as the present phase in multiple figures.

A SiC layer has been formed at the crucible interface on all of the samples as shown in Figure 36 to 52. This could be a result of reaction between silicon and graphite as well as silica and graphite. It was not observed any correlation between time, temperature and thickness of the SiC layer. Silicon and silica were also found in all of the samples, in addition to impurities precipitated at silicon grain boundaries, as seen in Figure 36b and 39a, among others. Formation of this phase is most likely due to segregation of impurities during solidification. Silicon has a low solubility of elements like iron and aluminium and the last solidified silicon will therefor have a higher content of these elements.

All of the samples heated to 1650 and 1750°C had a SiC layer on the surface of the silicon droplets in addition to the SiC layer at the crucible, as seen in Figure 36 and 46, among others. This was not found in any of the samples heated to 1850 and 1950°C. Silicon carbide at the surface of a particle could be due to the fact that liquid silicon has a high solubility of carbon compared to solid silicon. Carbon can therefor dissolve in the liquid silicon before it is precipitated at lower temperatures. This is however not assumed to be the case for these samples because this would have caused formation of silicon carbide at the surface of particles heated above 1800°C as well. It is therefor more likely that the particles reacted with carbon during heating, causing formation of silicon carbide at the surface of each particle which again started to react at temperatures above 1800°C. A droplet with a silicon carbide layer, a "shell" of silicon carbide partly filled with silicon and an empty silicon carbide shell can be seen in Figure 46a. These three stages were observed in multiple samples and it can be assumed that the silicon reacts more rapidly at lower temperatures than the silicon carbide, leaving an empty SiC shell.

An eutectic phase was found on one sample where quartz E was heated to 1853°C, as seen in Figure 49b. The eutectic phase identified at the edge of a silicon droplet and it looks like it is a result of solidification of silicon with a reduced solubility of impurities compared to the liquid. The solubility of impurities in silicon is reduced from liquid to solid state and the silicon that solidifies in the end will therefor have a high content of impurities and an eutectic phase could be formed as seen in this sample. The eutectic phase was only identified in one sample (quartz

E heated to 1853°C for 60 minutes), but this could have been overseen in other samples due to its small amount. It should also be noted that quartz E is the sample with the highest content of impurities and the metallic silicon could reduce some of the impurities in the quartz, giving a higher concentration of impurities in the silicon droplet.

The expected phases: silicon, silica, graphite and silicon carbide at crucible interface were found in all of the samples in addition to impurities at the silicon grain boundaries. Silicon carbide was found at the surface of the silicon particles for samples heated to less than 1800°C and an eutectic phase was found in one sample. All of the samples shows similar behaviour other than that.

4.4.1 Quartz A

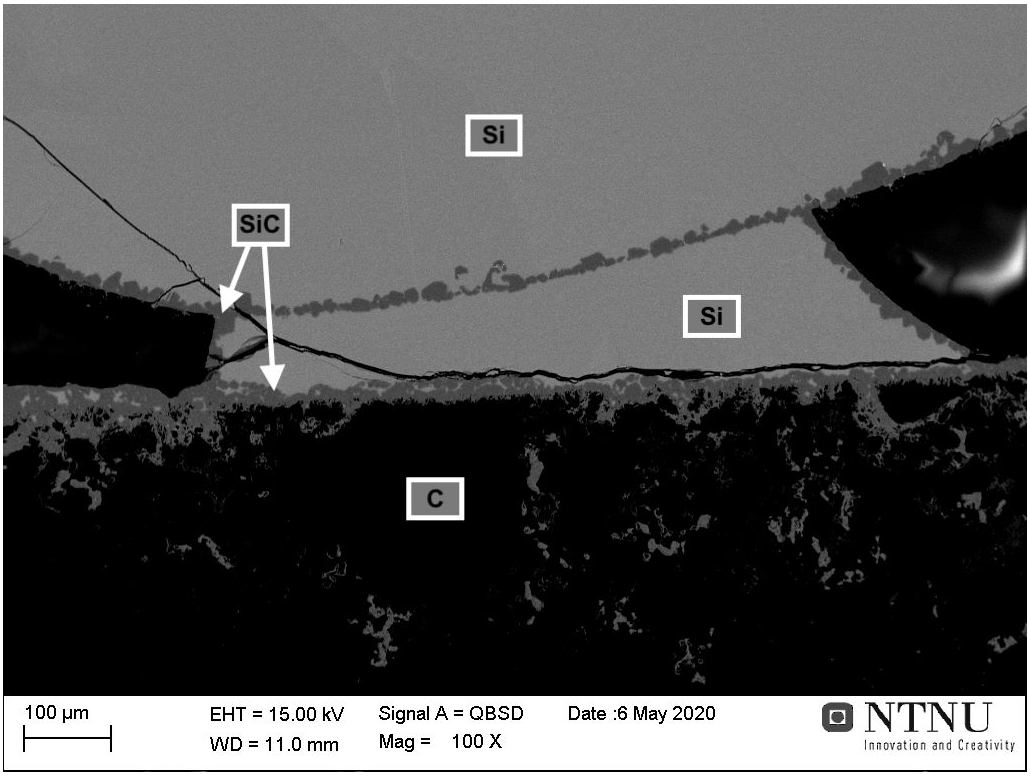

(a) An image showing a silicon droplet and the graphite crucible, both covered in a layer of silicon carbide.

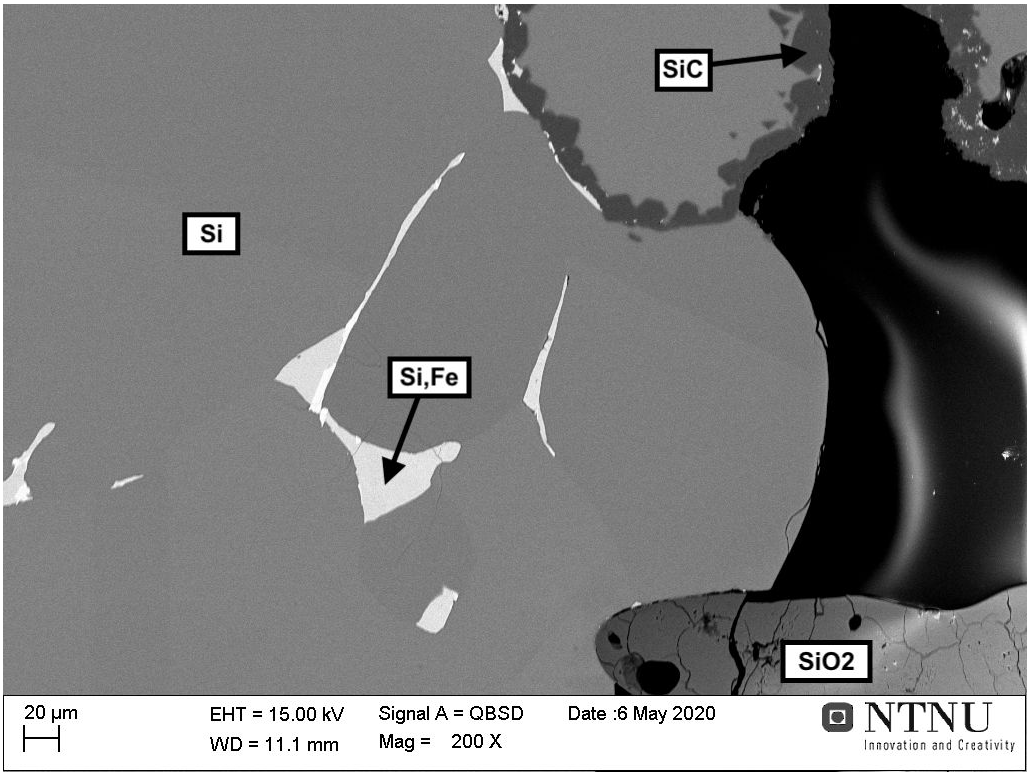

(b) Impurities are precipitated at the silicon grain boundaries.

Figure 36: SEM images taken of quartz A heated to 1670°C for 120 minutes, experiment M2.

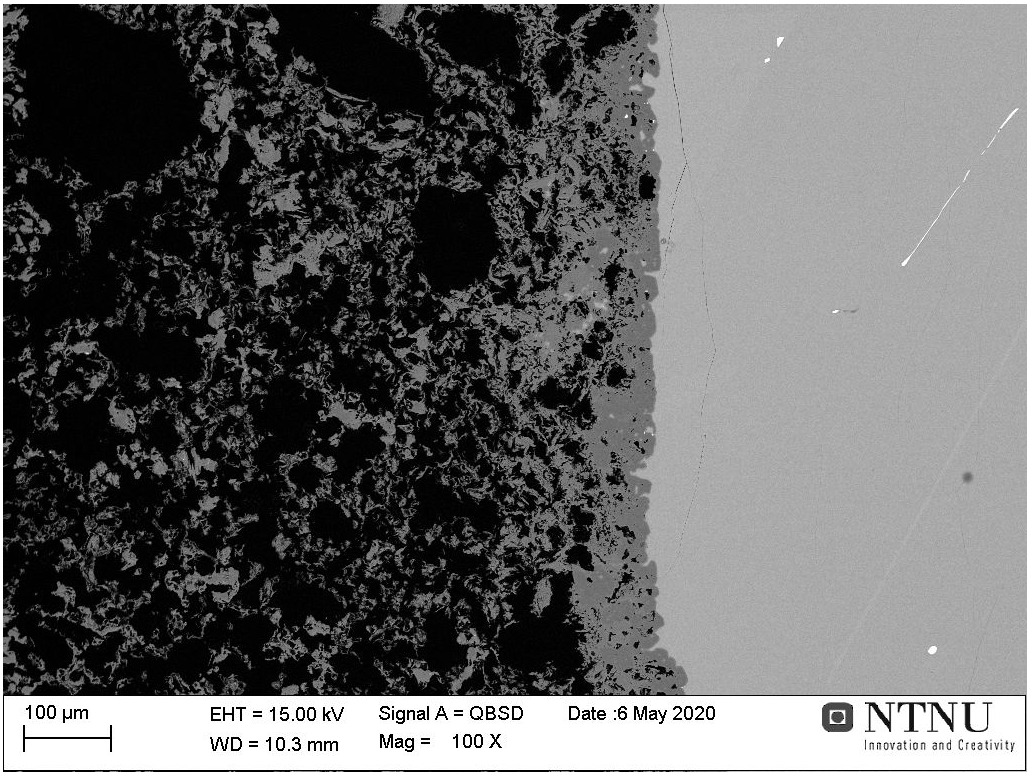

(a) Silicon carbide is found at the crucible interface and impurities are precipitated at the silicon grain boundaries.

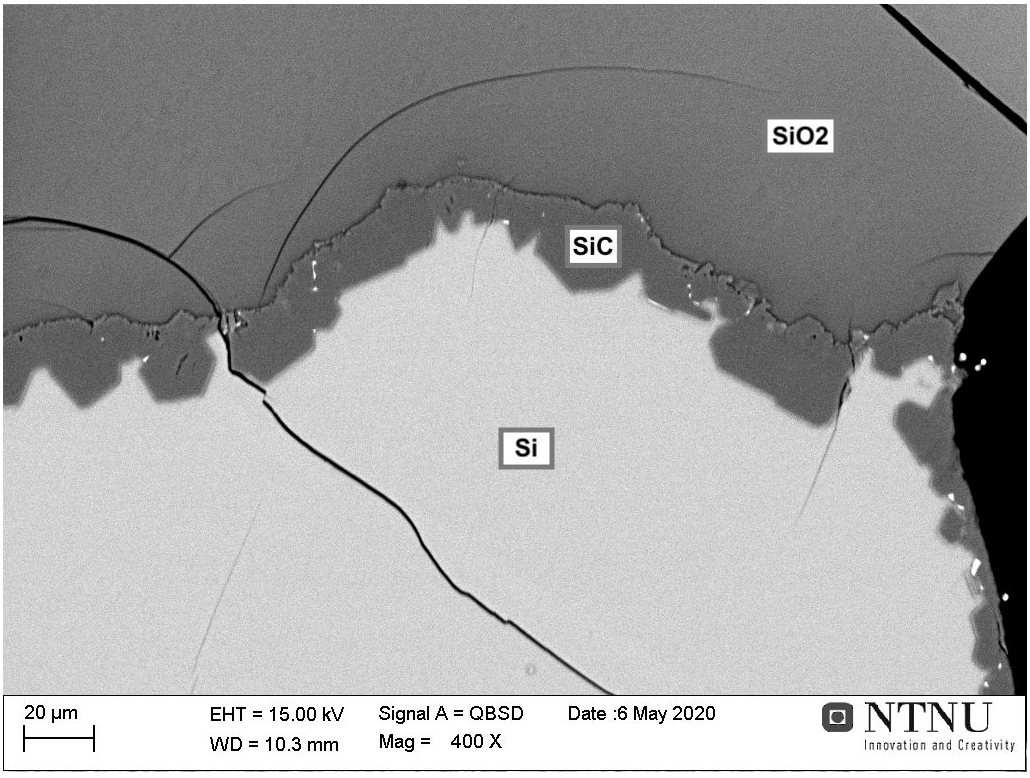

(b) The interface between silicon and silica, with a layer of silicon carbide in between the two phases.

Figure 37: SEM images taken of quartz A heated to 1775°C for 120 minutes, experiment M1.

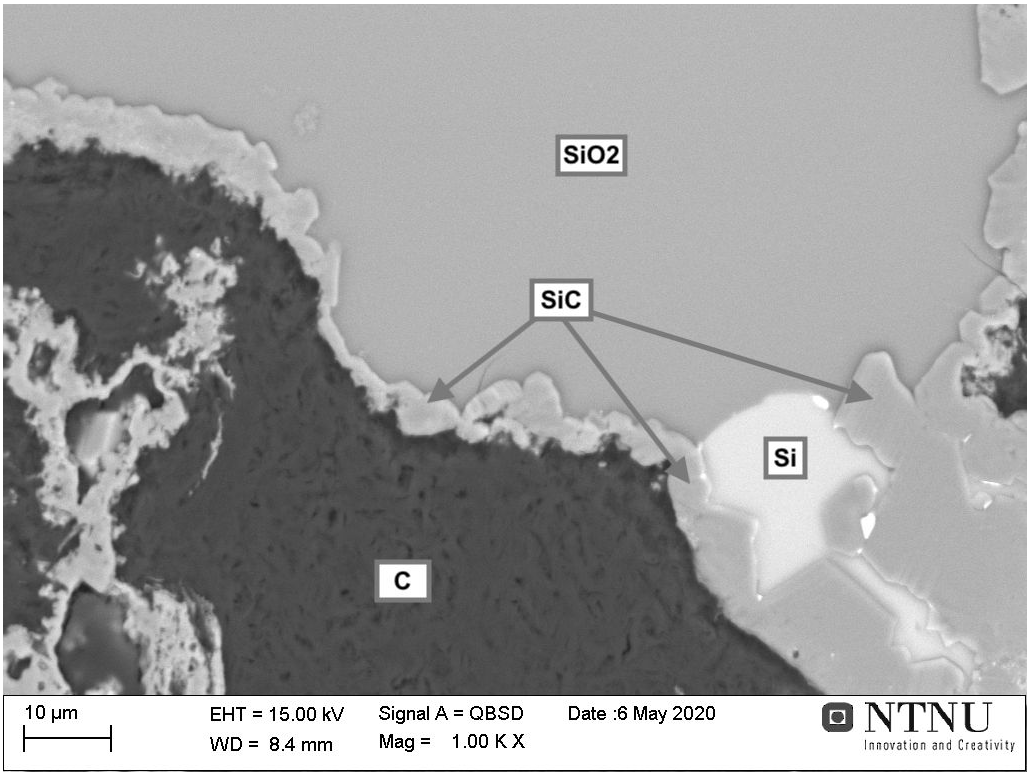

(a)

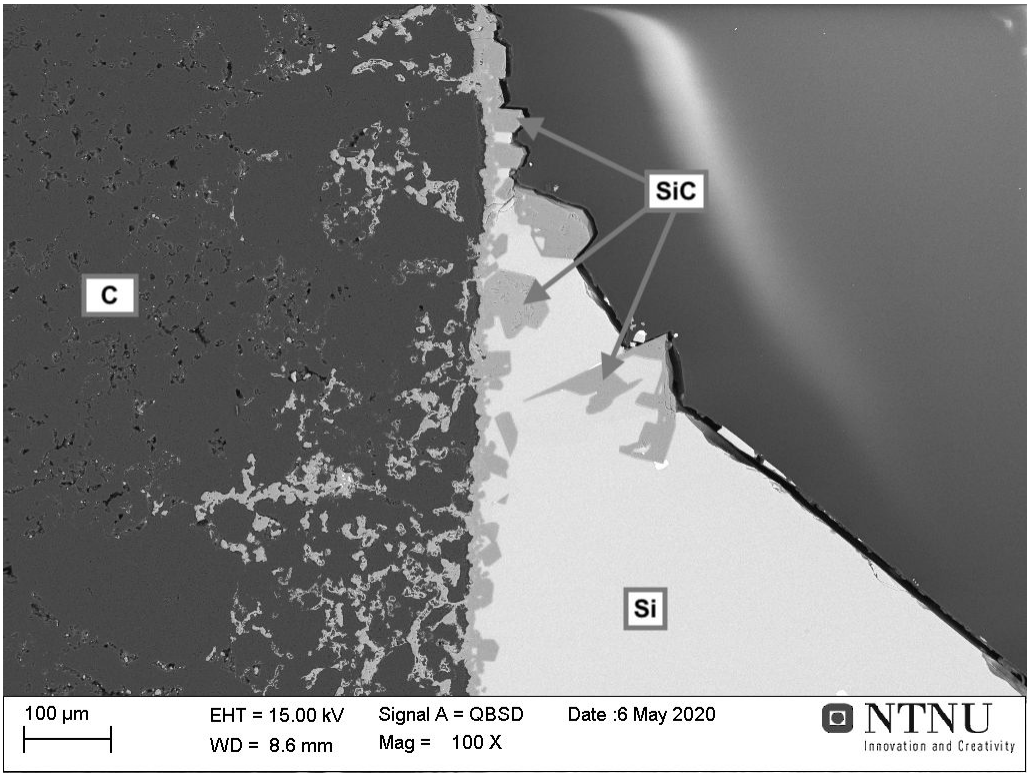

(b)

Figure 38: SEM images taken of quartz A heated to 1880°C for 60 minutes, experiment M3. Both images show formation of a SiC layer at the crucible interface.

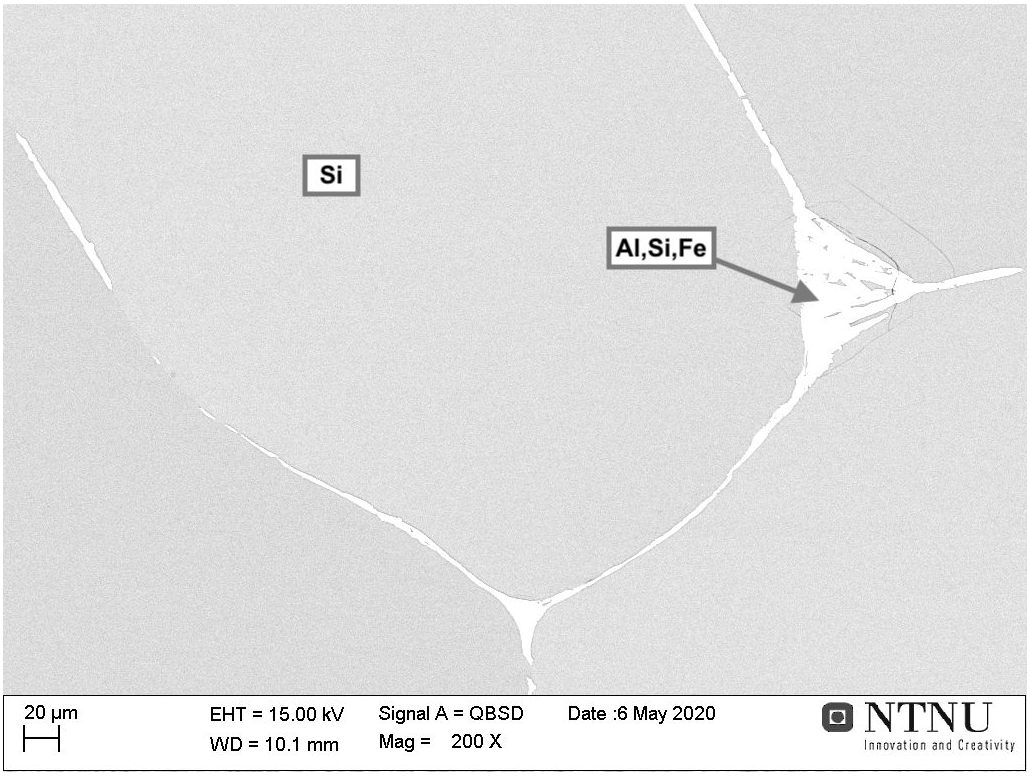

(a) Precipitation of impurities at the silicon grain boundaries.

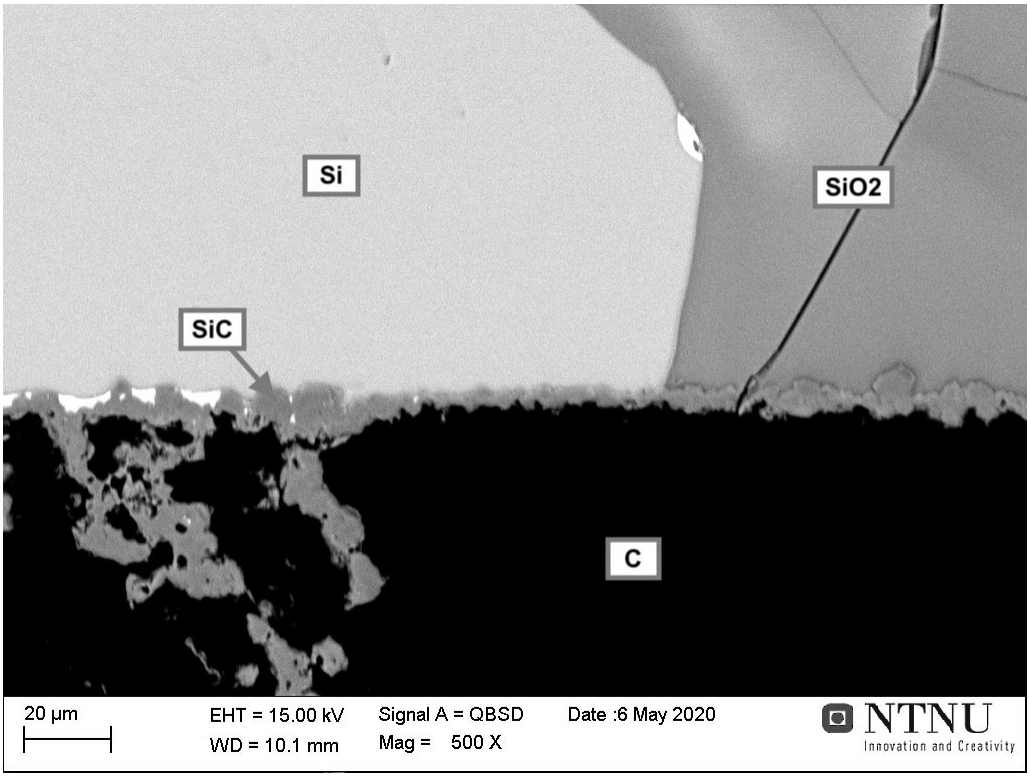

(b) Silicon and silica at the bottom of the crucible which is covered by a layer of silicon carbide.

Figure 39: SEM images taken of quartz A heated to 1980°C for 60 minutes, experiment M4.

4.4.2 Quartz B

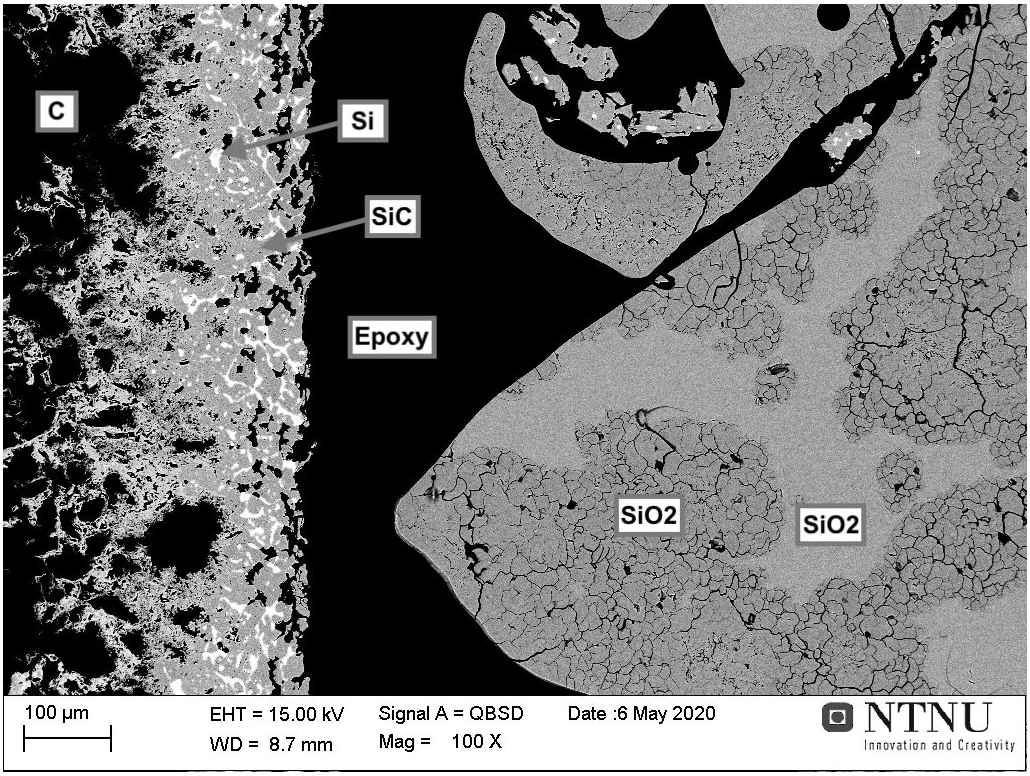

(a) Silica present close to the crucible which is covered in a layer of silicon carbide and traces of silicon.

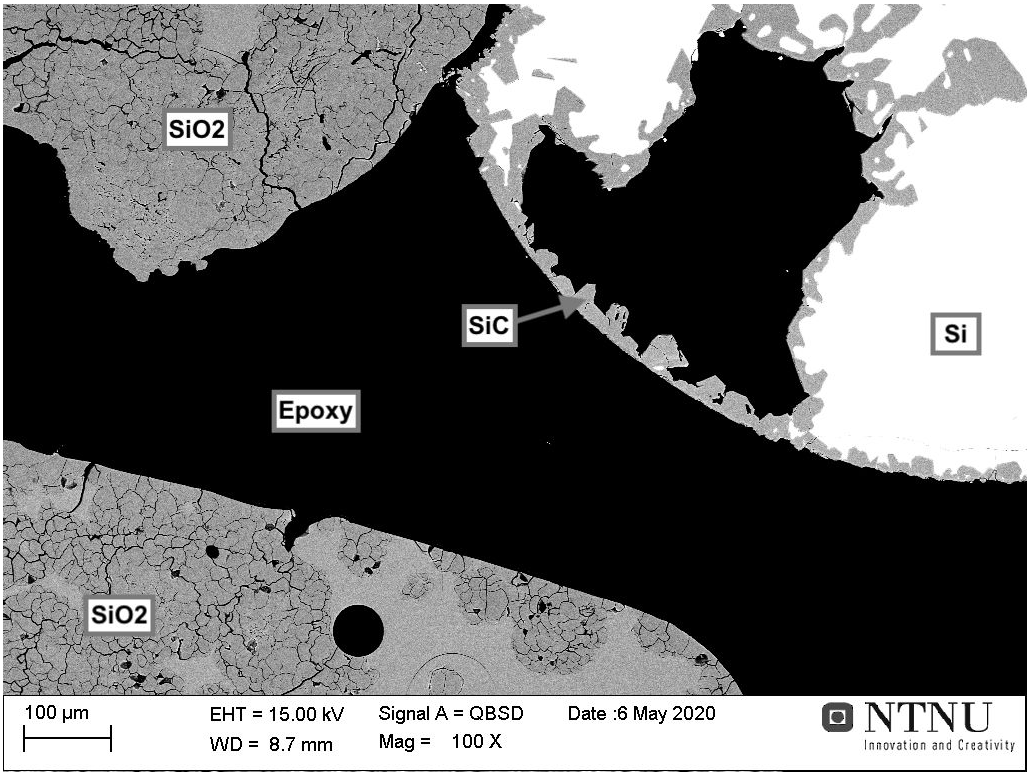

(b) Silicon and silica particles, the silicon is covered by a layer of silicon carbide.

Figure 40: SEM images taken of quartz B heated to 1636°C for 120 minutes, experiment M5.

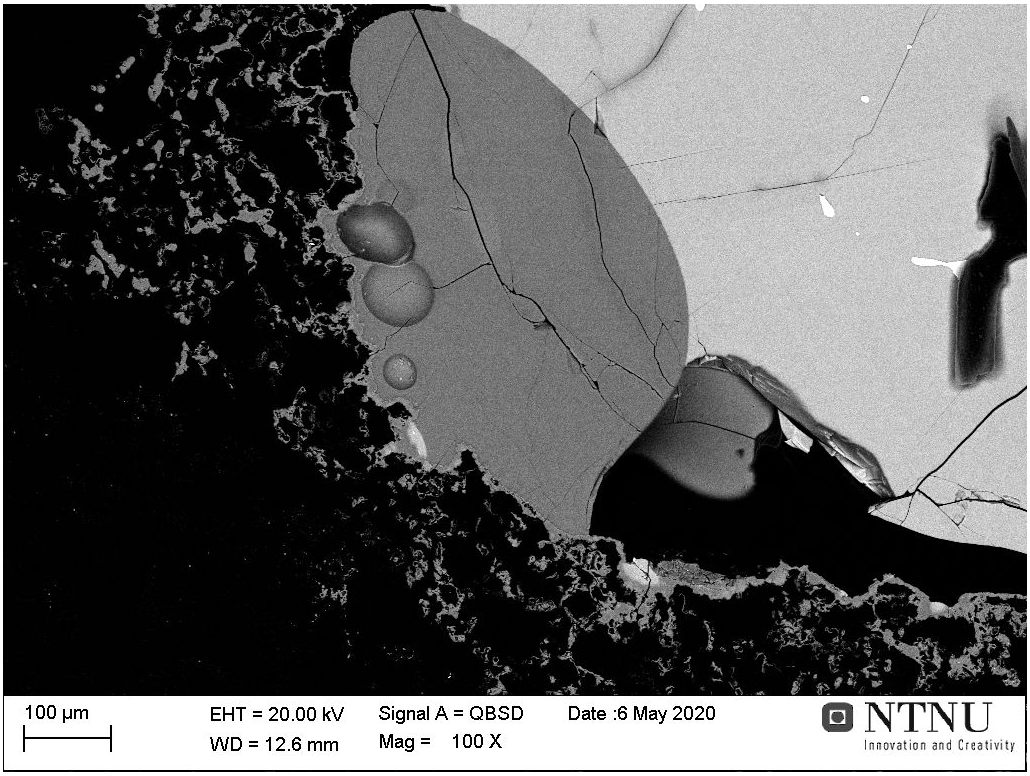

(a)

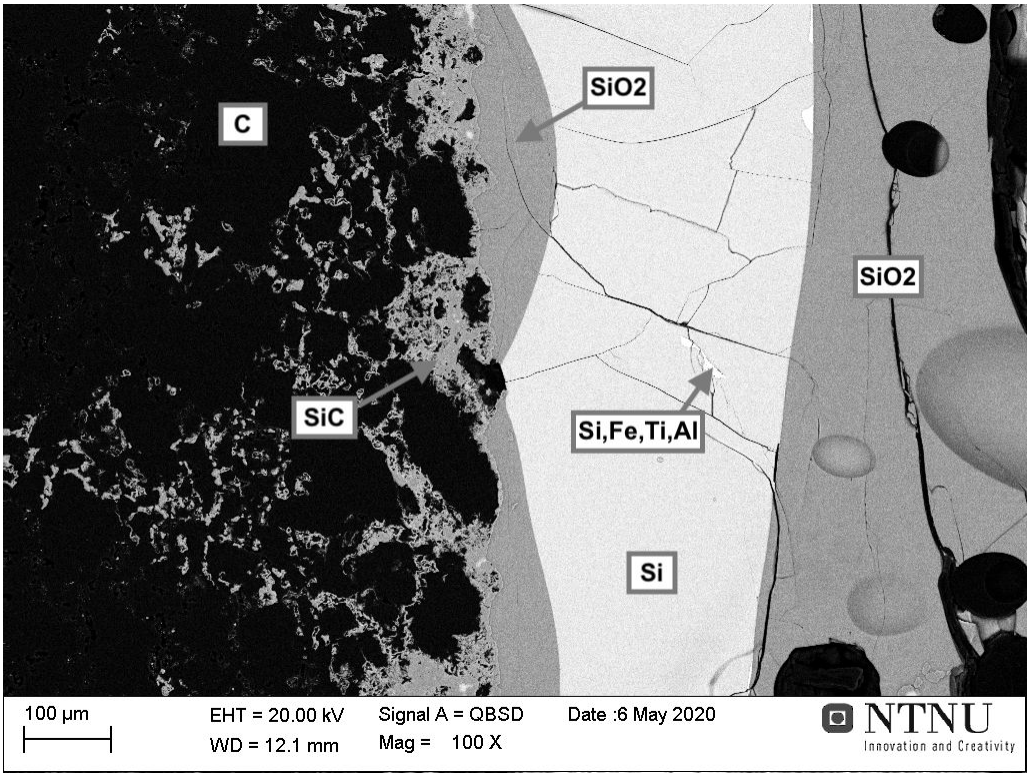

(b)

Figure 41: SEM images taken of quartz B heated to 1833°C for 60 minutes, experiment M7. Both images show the expected phases, graphite (C), silicon carbide at the crucible interface, silica and silicon with impurities at the grain boundaries.

4.4.3 Quartz C

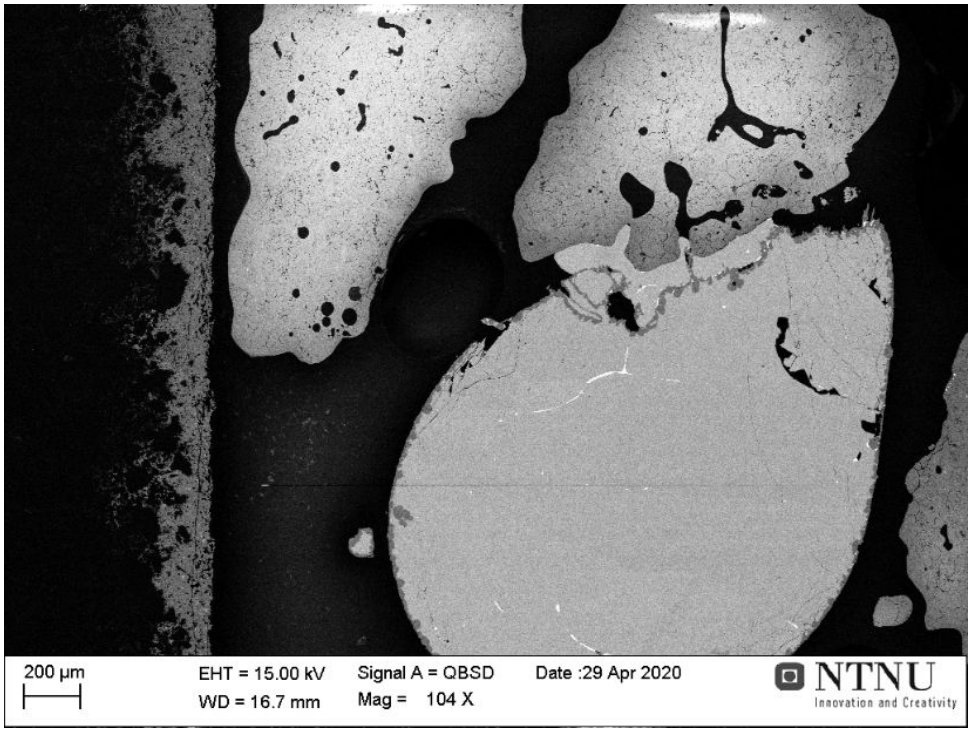

(a)

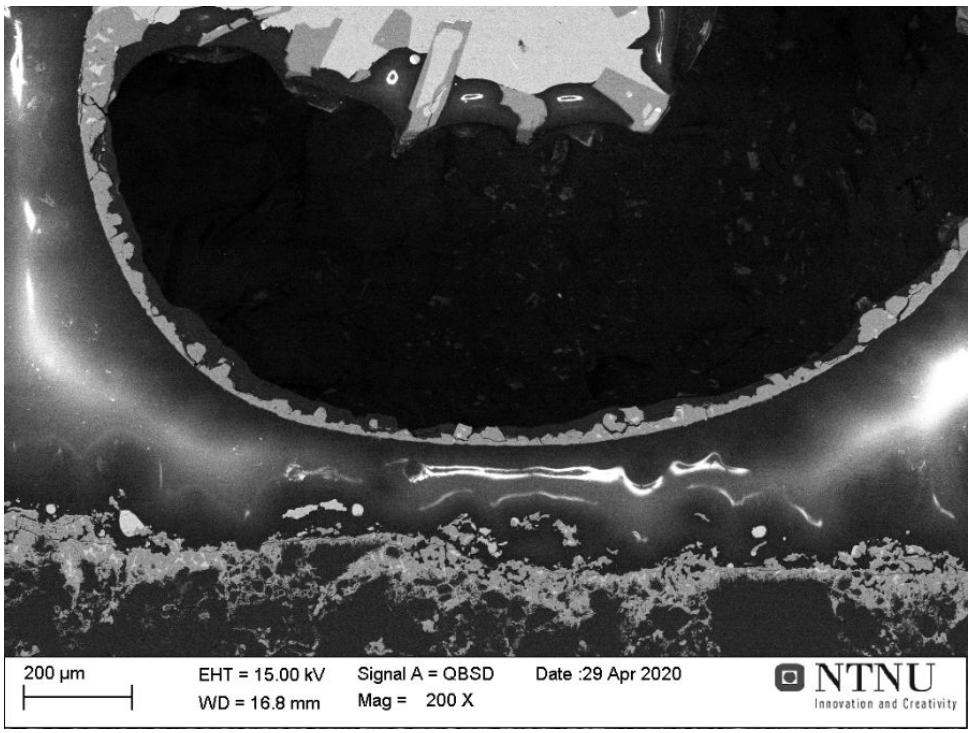

(b)

Figure 42: SEM images taken of quartz C heated to 1644°C for 120 minutes, experiment M14. Both images show a crucible and silicon droplets covered in a layer of SiC. The low quality of these images are due to charging of the surface caused by an inefficient carbon coating.

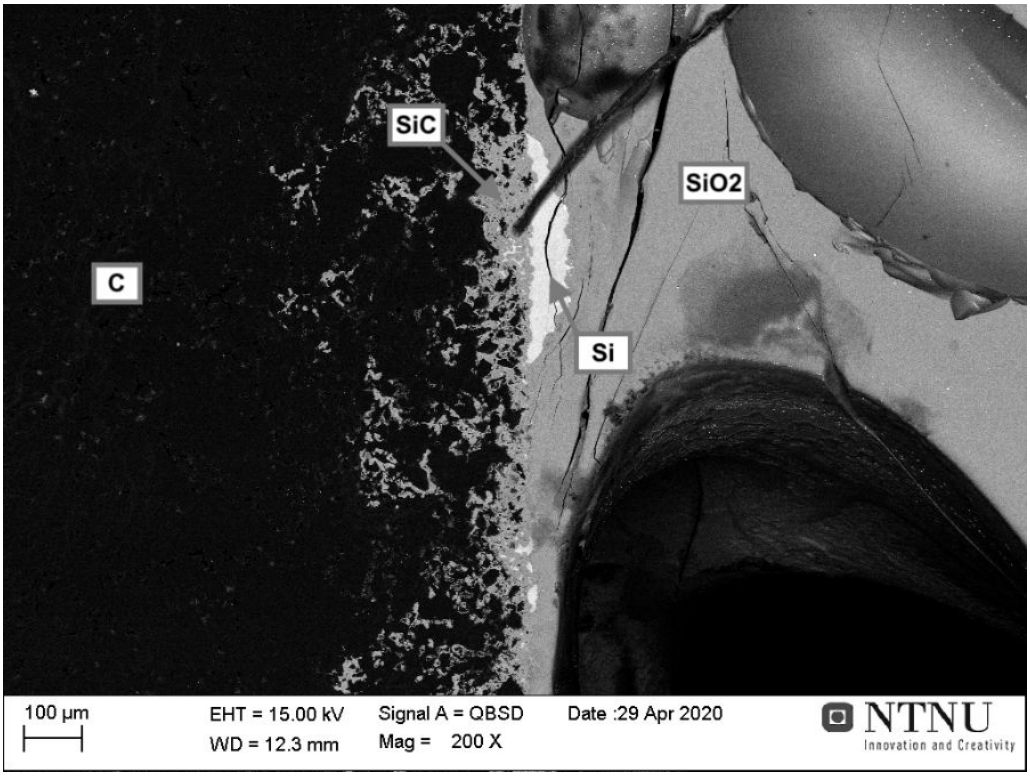

(a) Silicon and silica at the crucible interface which is covered by a layer of silicon carbide.

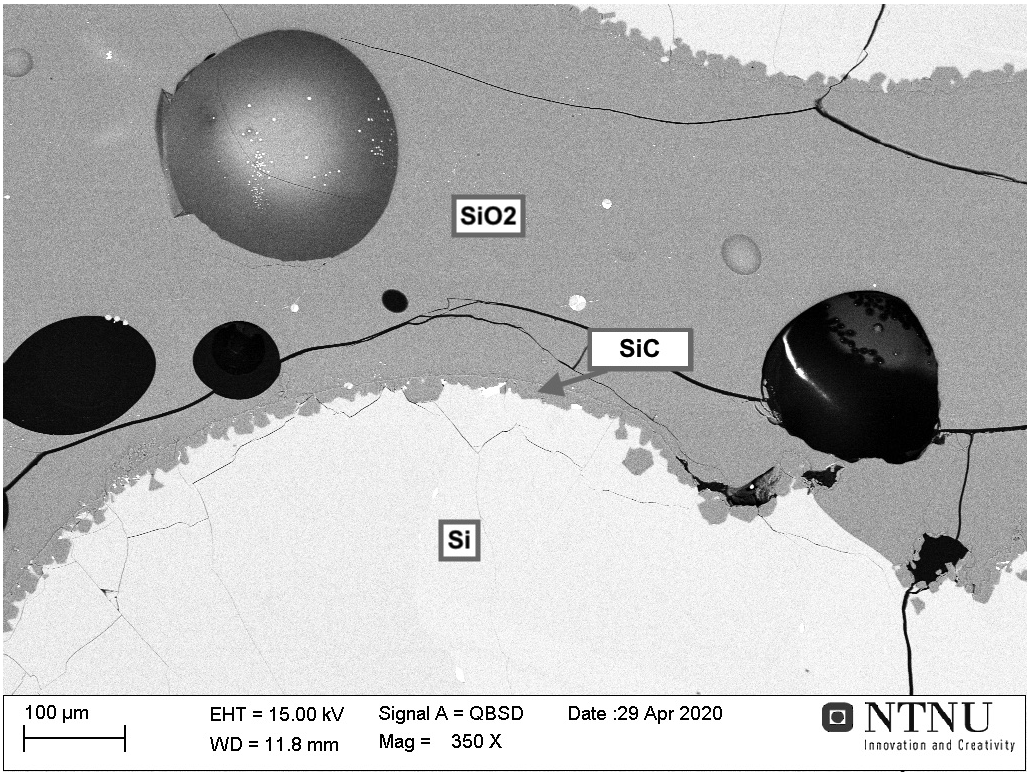

(b) A layer of silicon carbide is present between the silicon and silica phase.

Figure 43: SEM images taken of quartz C heated to 1746°C for 120 minutes, experiment M12.

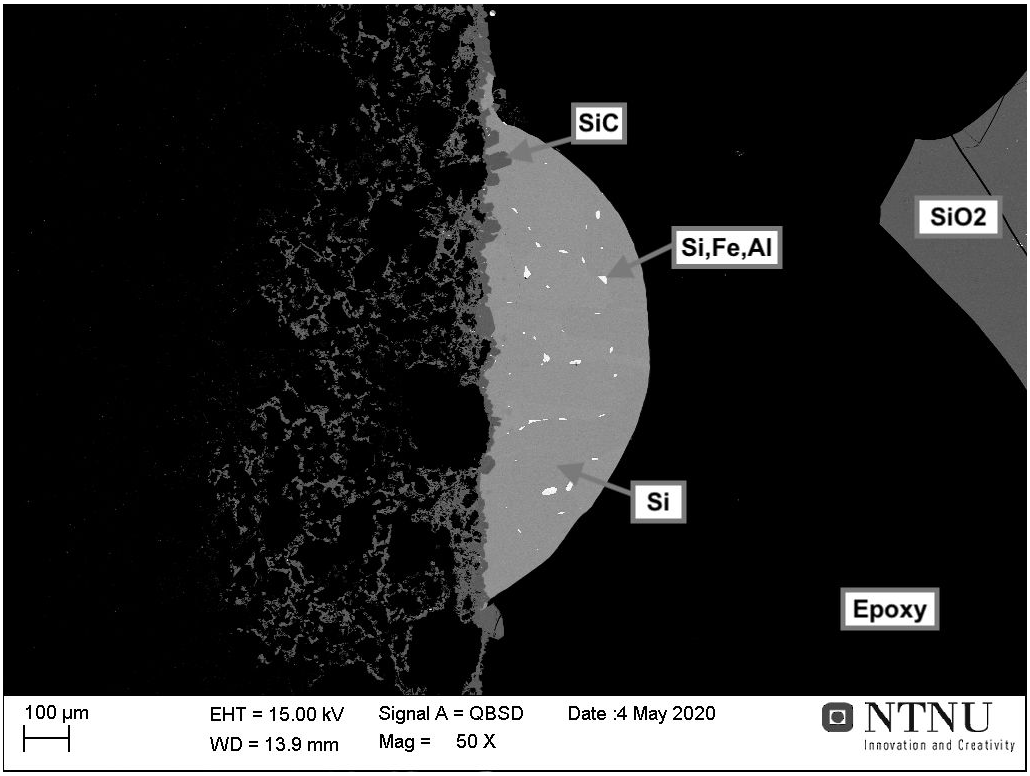

(a)

Figure 44: SEM image taken of quartz C heated to 1854°C for 60 minutes, experiment M8. The image show silicon with impurities precipitated at the grain boundaries.

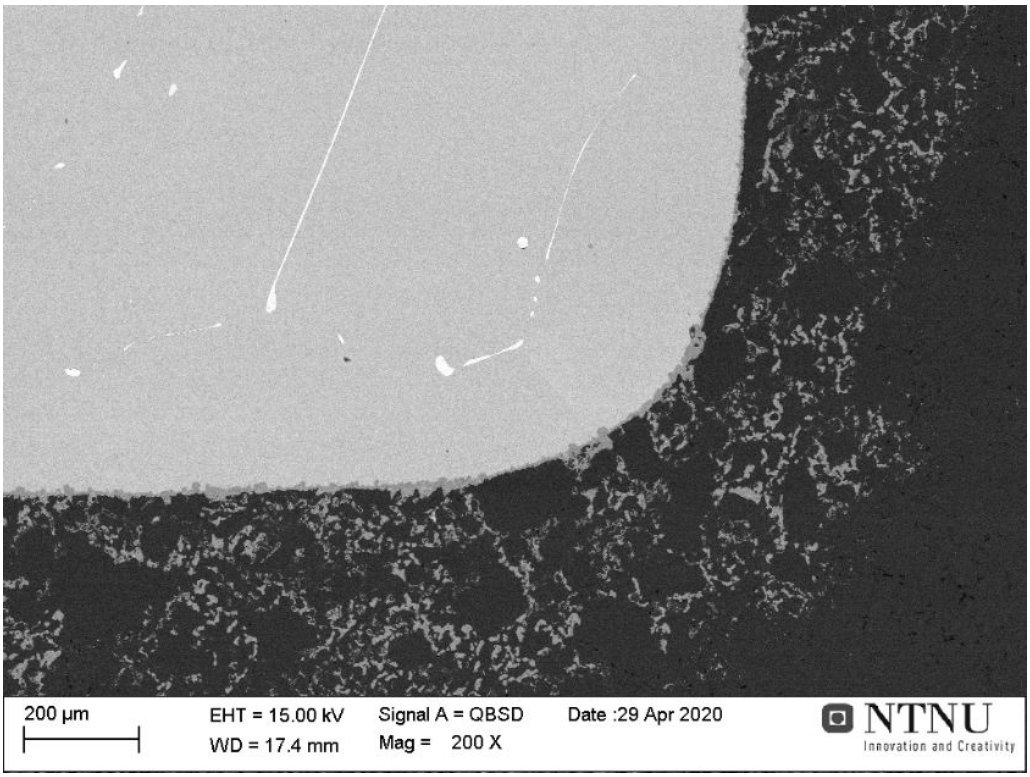

Figure 45: SEM image taken of quartz C heated to 1946°C for 30 minutes, experiment M13.

4.4.4 Quartz D

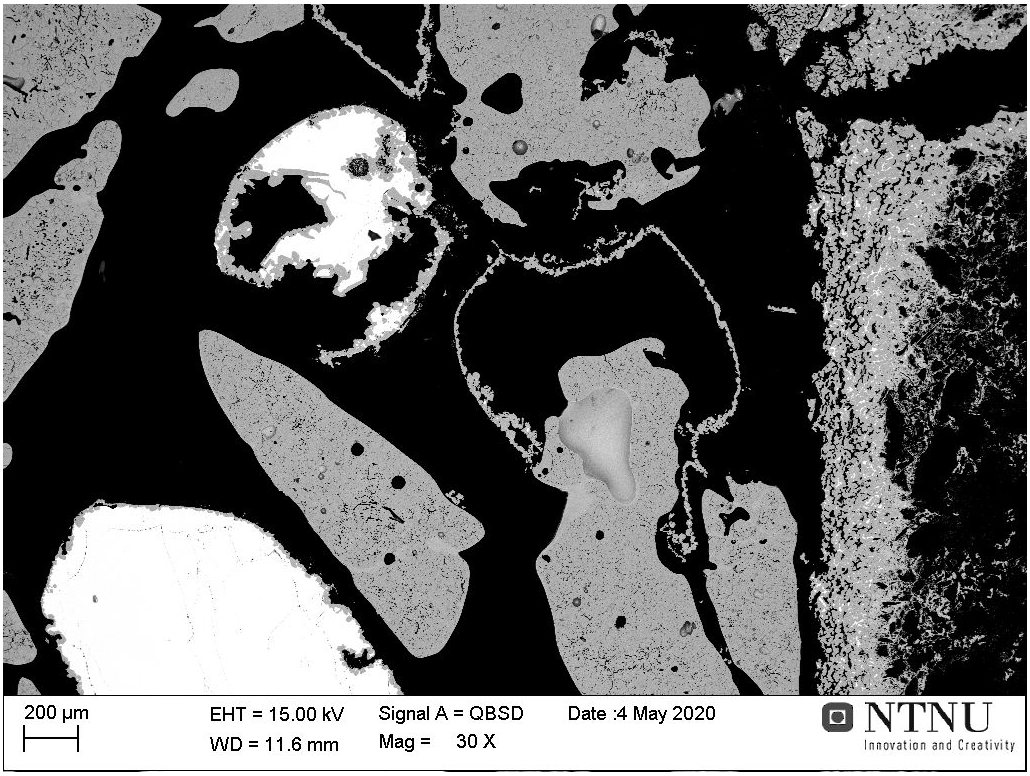

(a) The images shows a silicon particle covered in a layer of silicon carbide, a partly filled shell of silicon carbide and an empty shell. All in between silica particles.

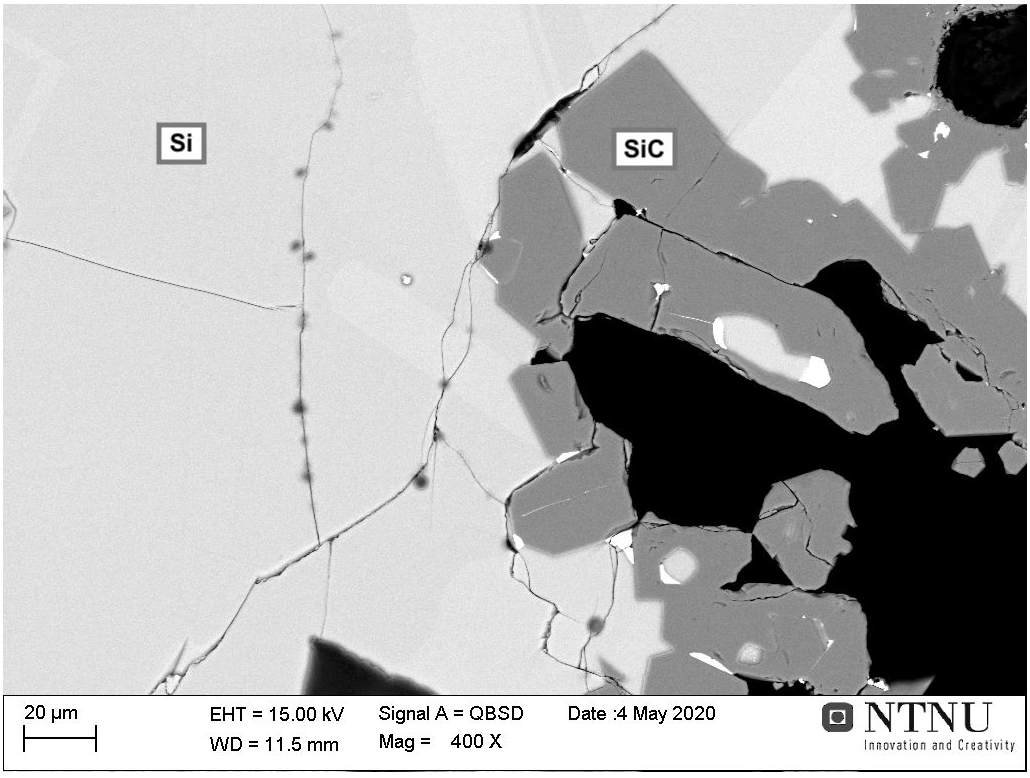

(b) Silicon carbide at the surface of a silicon particle.

Figure 46: SEM images taken of quartz D heated to 1644°C for 120 minutes, experiment M9.

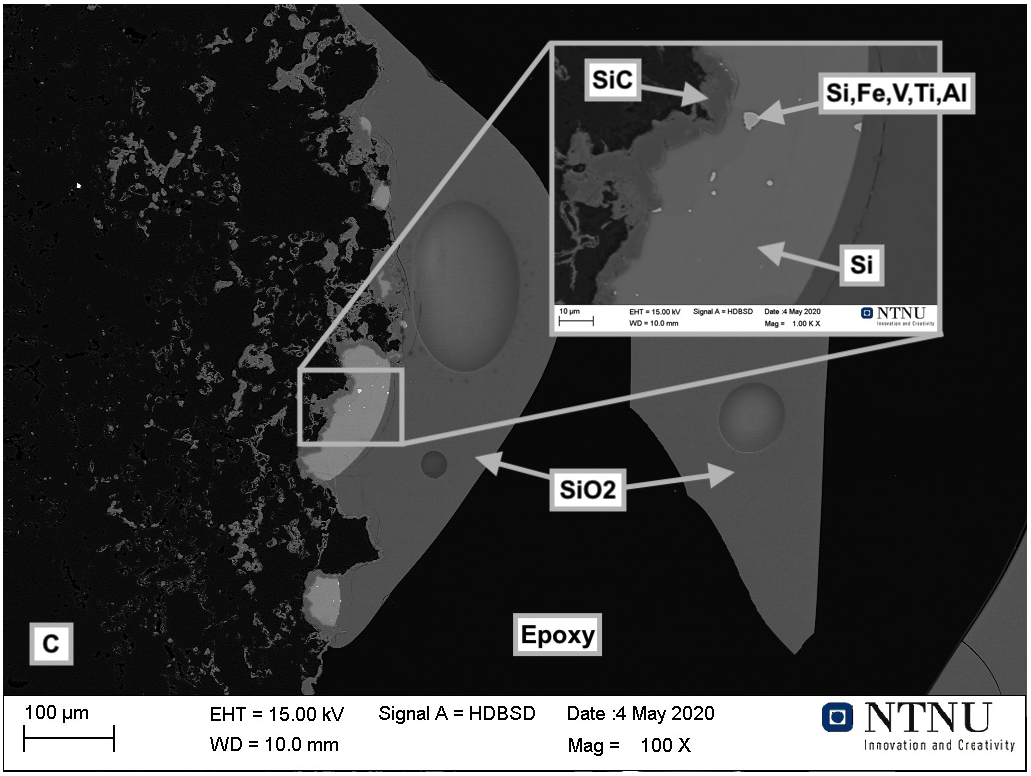

(a)

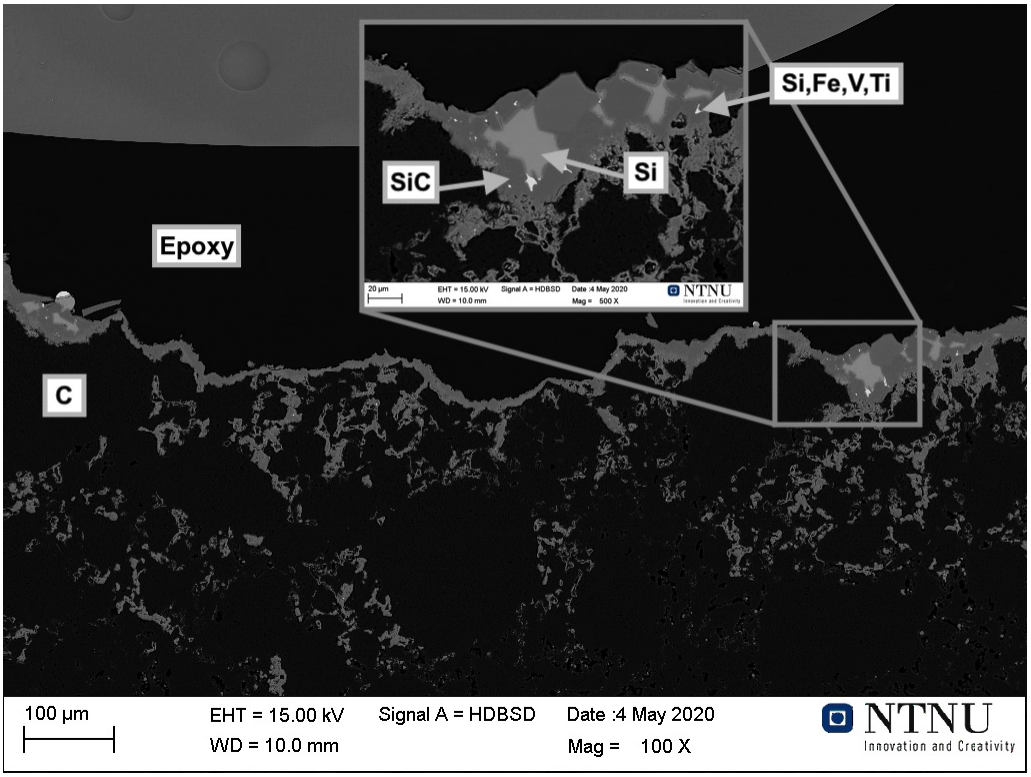

(b)

Figure 47: SEM images taken of quartz D heated to 1856°C for 60 minutes, experiment M10. The images show the expected phases, graphite (C), silicon carbide at the crucible interface, silica and silicon with impurities at the grain boundaries.

4.4.5 Quartz E, 1-2mm

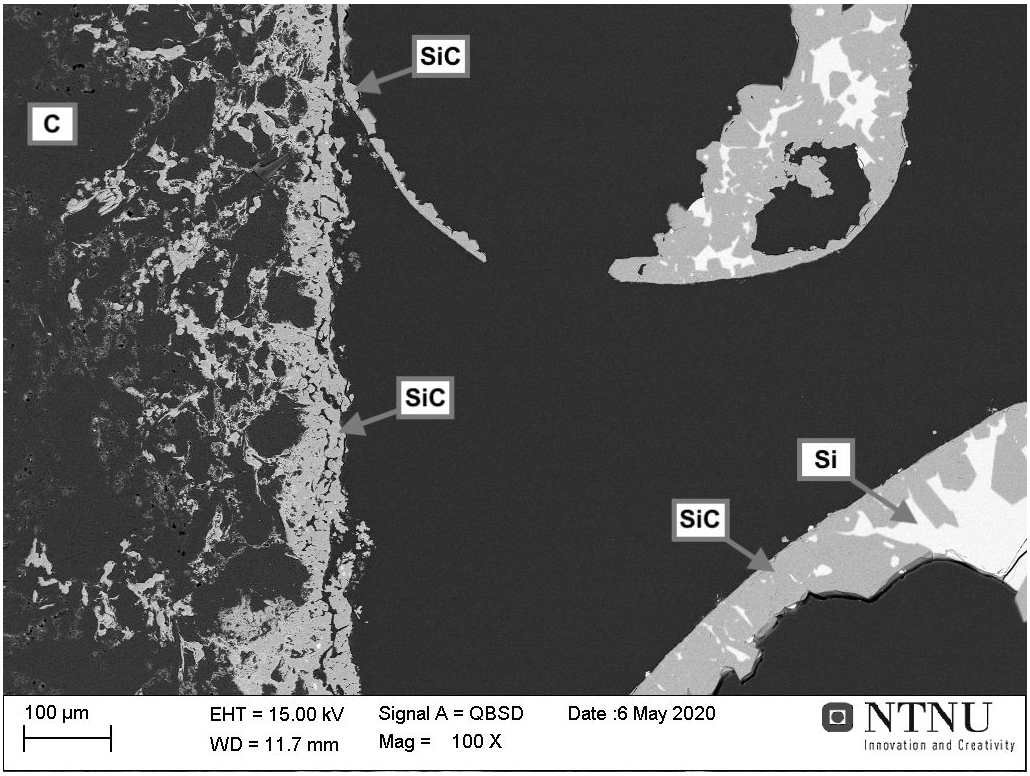

(a) Two shells of silicon carbide, partly filled with silicon.

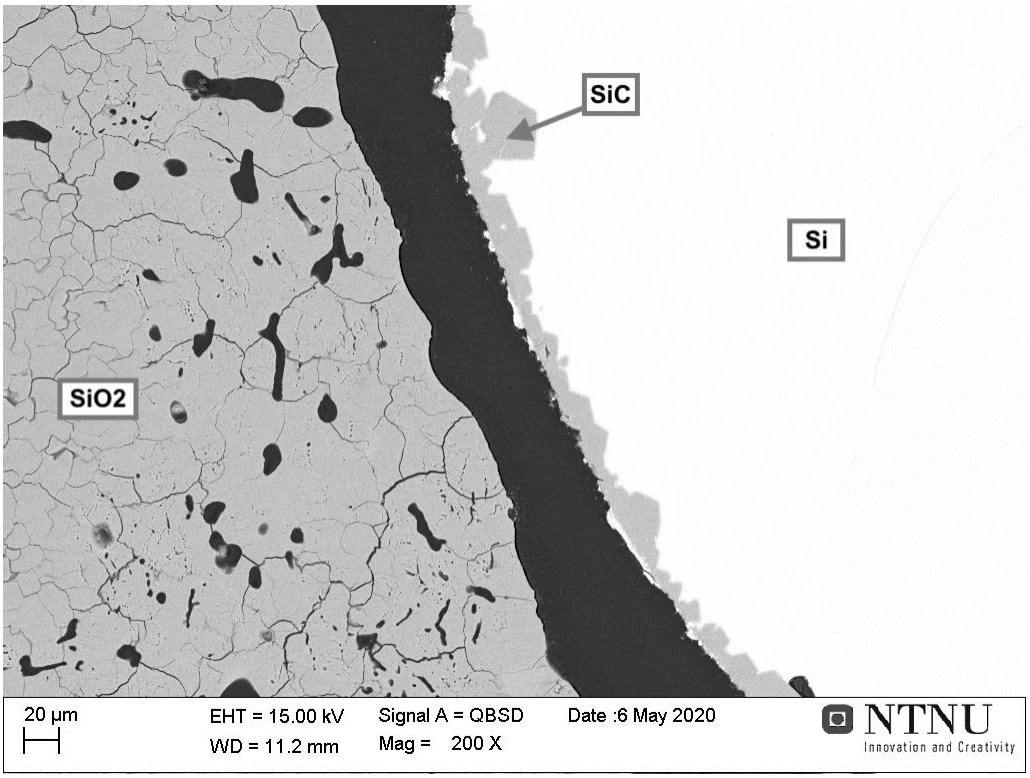

(b) Silica and a silicon particle covered in a layer of silicon carbide.

Figure 48: SEM images taken of quartz E heated to 1658°C for 120 minutes, experiment M6

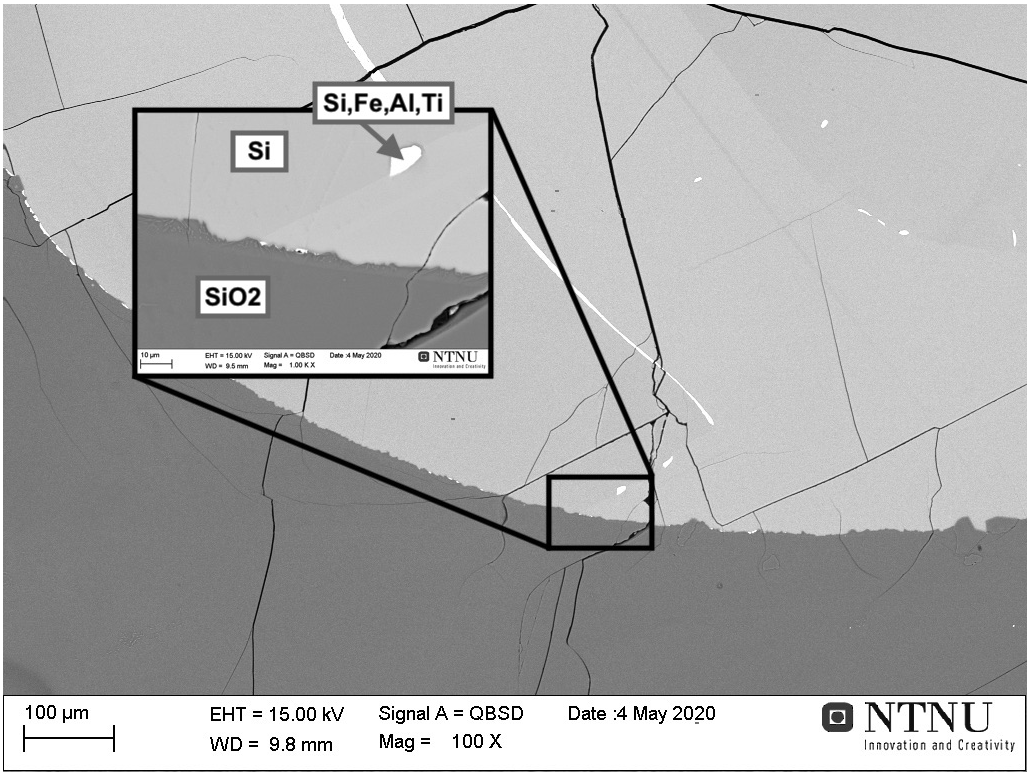

(a) Silicon and silica without any silicon carbide at the interface.

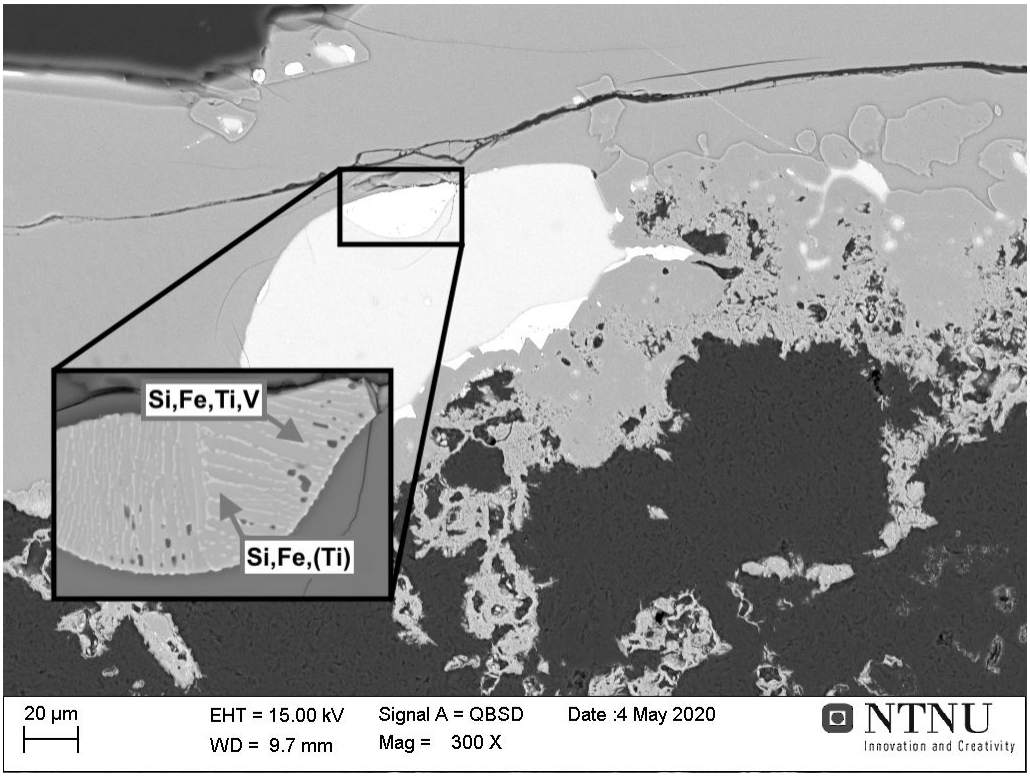

(b) A droplet of silicon with an eutectic phase at the edge towards the silica phase.

Figure 49: SEM image taken of quartz E heated to 1853°C for 60 minutes, experiment M11.

4.4.6 Quartz E, 2-5mm

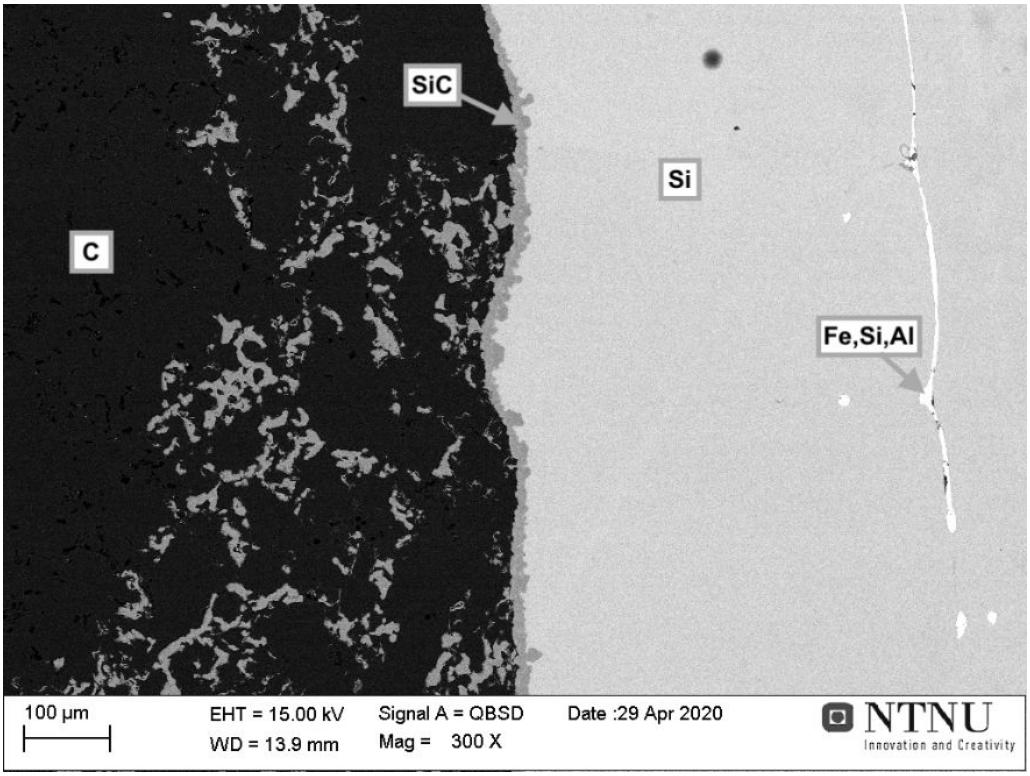

Figure 50: SEM image taken of quartz E (2-5mm) heated to 1855°C for 60 minutes, experiment M17. There is a layer of silicon carbide at the crucible interface and impurities have precipitated at the silicon grain boundaries.

4.4.7 Quartz E, 5-8mm

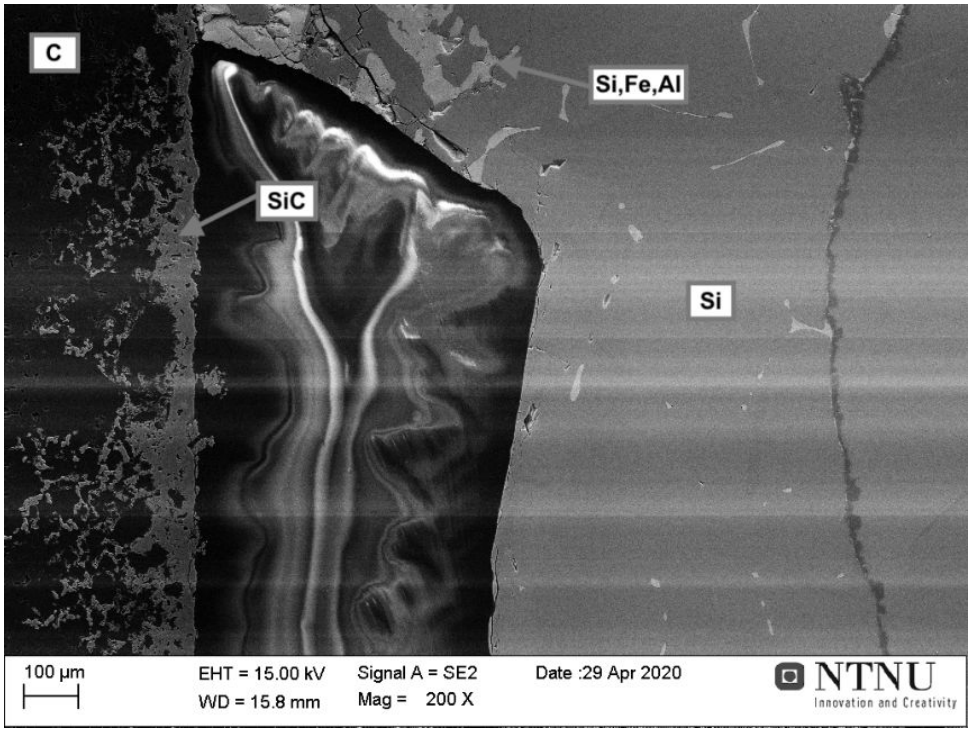

(a) Silicon with impurities at the grain boundaries and a crucible with SiC at the interface.

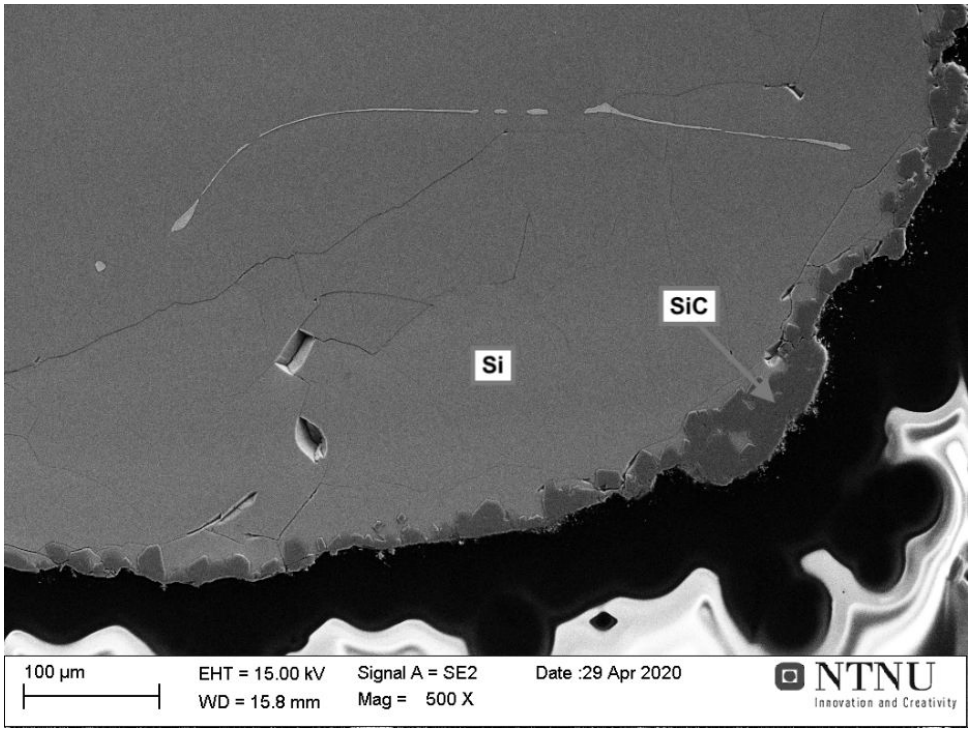

(b) Silica with a layer of SiC.

Figure 51: SEM image taken of quartz E (5-8mm) heated to 1645°C for 120 minutes, experiment M15. The low quality of these images are due to charging of the surface caused by an inefficient carbon coating.

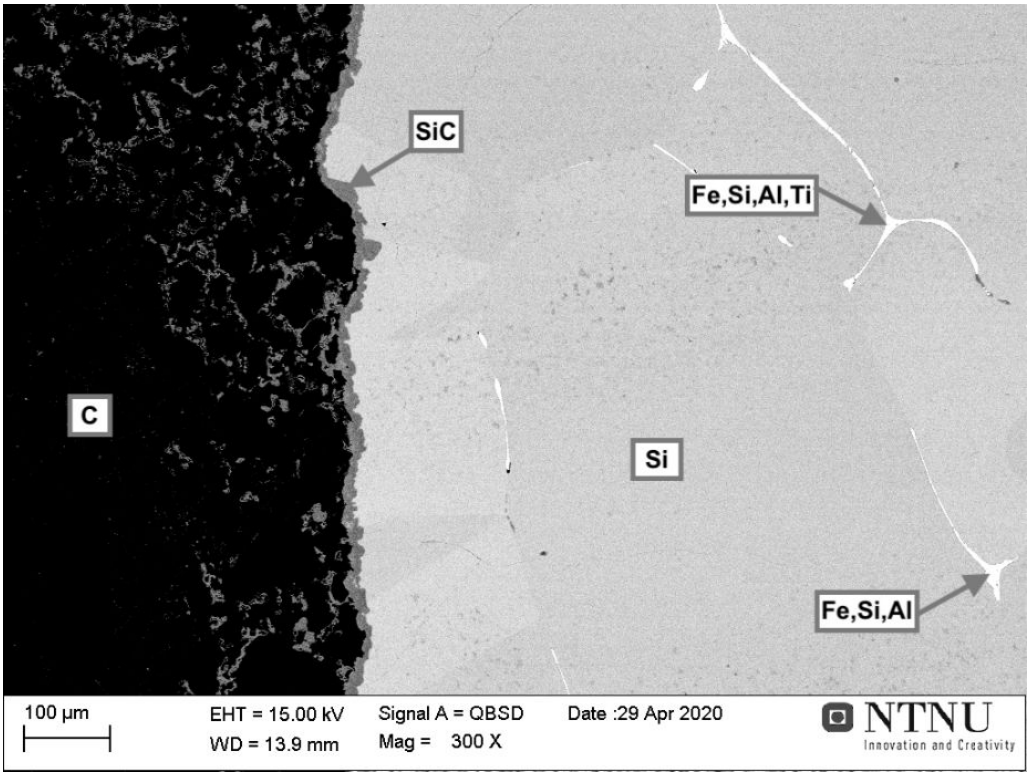

Figure 52: SEM image taken of quartz E (5-8mm) heated to 1840°C for 60 minutes, experiment M16. There is a layer of silicon carbide at the crucible interface and impurities have precipitated at the silicon grain boundaries.

4.5 X-ray diffraction (XRD) - Polymorphs of SiO_2 before and after heat treatment

XRD analysis of quartz A to E after heat treatment at 1650°C for 120 minutes (heated to 1650°C at 50°C/min) was performed by Tolchard (SINTEF). The results are presented in Figure 53 and shows the amount of different phases in each sample. There was not found quartz in any of the samples, they consist of cristobalite and amorphous phase. The results are based on an average of three parallels from each sample, except quartz A where one anomalous parallel was excluded. There is no significant difference between the samples, except quartz E who has a higher concentration of amorphous phase than the other samples. Macro images of the samples before and after heating can be found in Figure 54. There is no significant difference between the samples before and after heating, except a change in colour of each sample. The samples had multiple colours before heating but all turned grey or bright white after heating. There was no significant change in particle size, and the degree of decrepitation is therefor low for all of the samples. The amount of sample was low and all of it was needed for XRD analysis and the exact size fraction before and after was therefor not investigated by sieving.

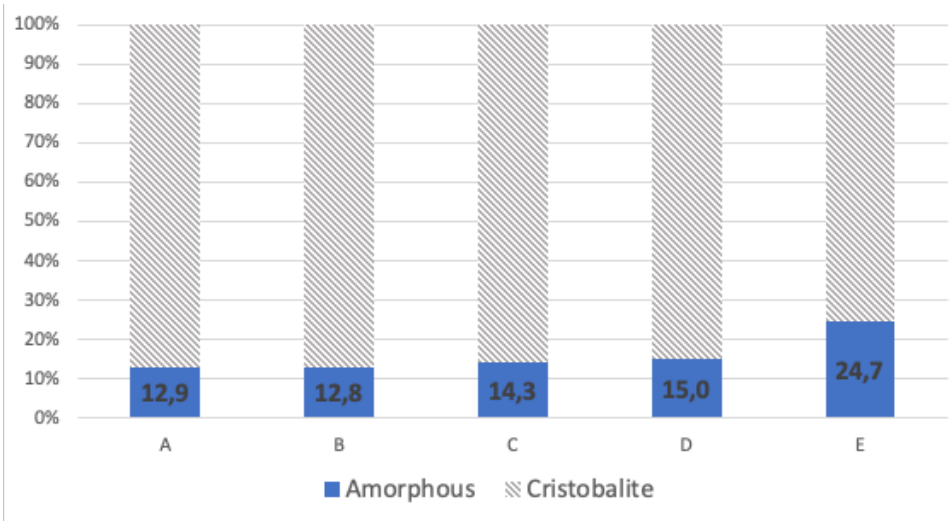

Figure 53: Amount of amorphous phase and cristobalite in the samples after heating at 1650°C for 120 minutes. There was not found quartz in any of the samples. The results are obtained by XRD analysis performed by Tolchard (SINTEF).

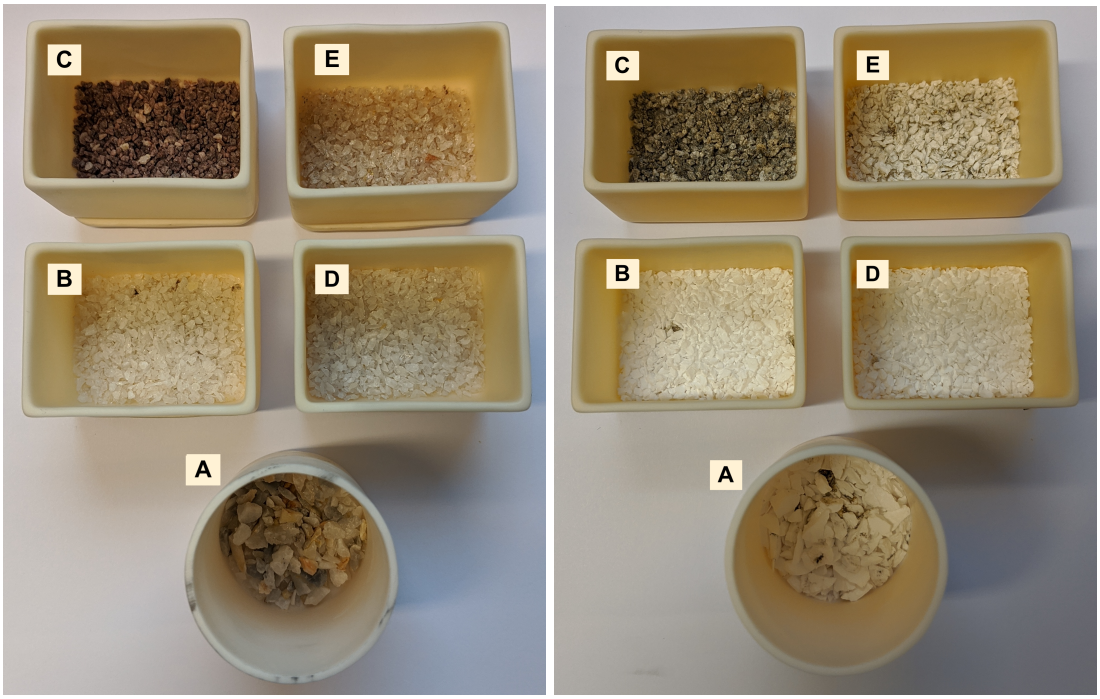

(a) Quartz samples before heating.

(b) Quartz samples after heating.

Figure 54: Images of the quartz samples before and after heating to 1650°C for 120 minutes. There is no significant difference between the samples before and after heating except a change in colour.

4.6 Wettability of silicon on quartz

The wettability of silicon on substrates made of quartz B to E has been measured by Syvertsen (SINTEF) and Sindland. Quartz A was not included in the wettability measurements due to

the lack of any large particle, which is needed to be able to make a substrate. All of the samples started to melt above the theoretical melting point of silicon and formation of a gas was observed at the silicon/silica interface, after the samples were completely melted. The wetting angle started to increase at the same time as gas started to form at the interface and the wetting angle reached a stable value after a few seconds. The droplet was moving around on the substrate during isothermal heat treatment at 1523°C but the wetting angle did not change significantly. Figure 56 shows the temperature where the initial melting was observed, the temperature where the droplet was completely melted and the temperature where an equilibrium wetting angle was observed. The value for initial wetting angle and the equilibrium angle is presented in Figure 57. All of the samples had an equilibrium angle right above 90°, except one parallel of quartz C that had an equilibrium angle of 89°. There was not observed any difference between the initial and equilibrium angle of the sample heated in furnace 2. But it should be noted that this sample was heated at a rate of 10K/min instead of 5K/min as the other samples.

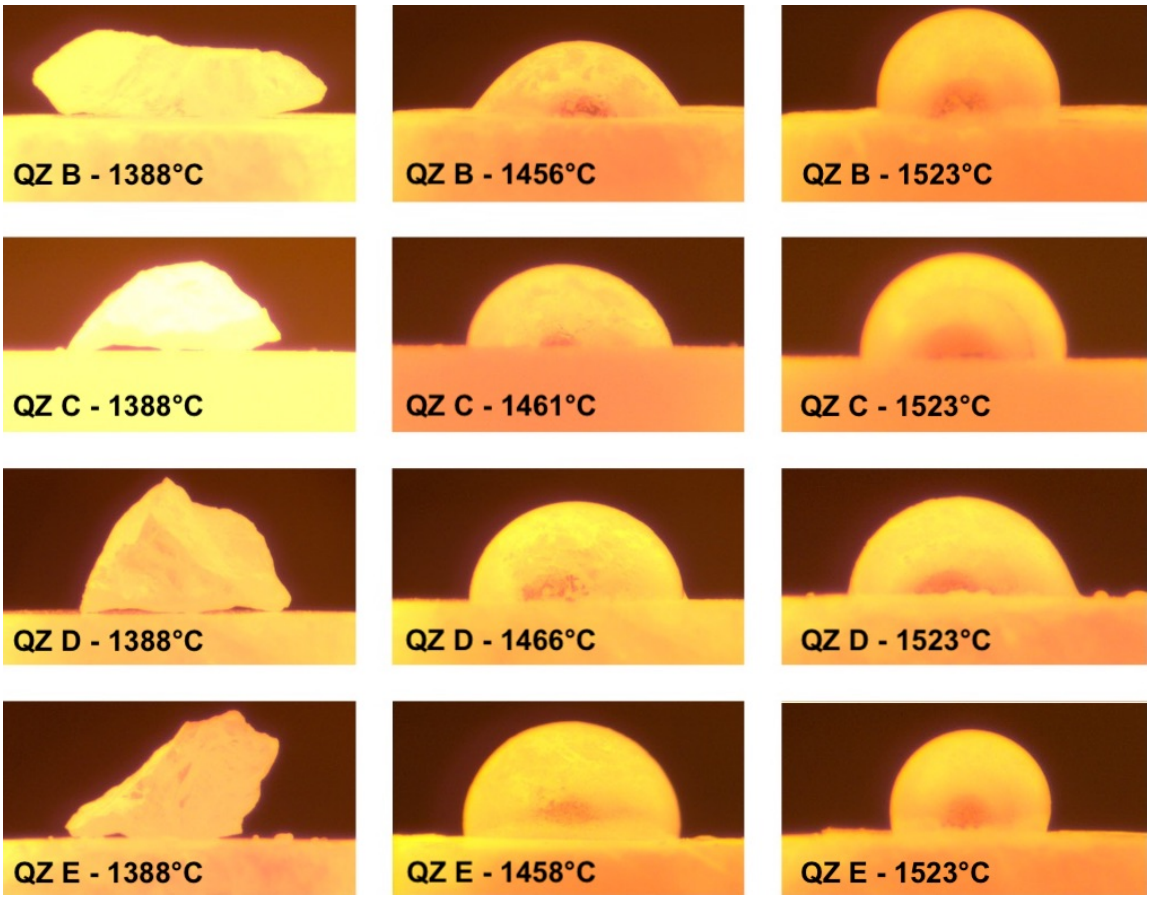

Figure 55: Images taken during heating of the silicon and silica samples in furnace 1, one image of each quartz sample before the silicon melted (images to the left), one right after complete melting (images in the middle) and one image taken during the isothermal heat treatment at 1523°C (images to the right). The type of quartz substrate and the temperature is indicated in each image.

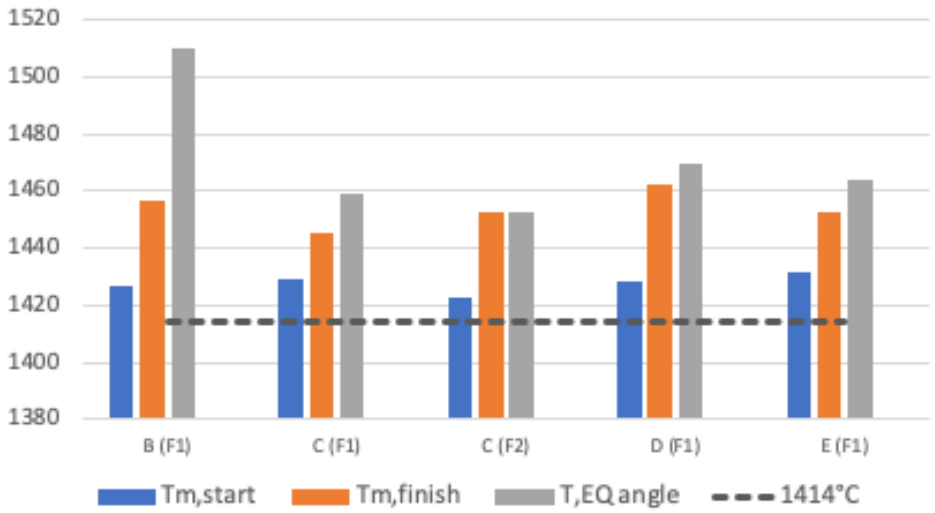

Figure 56: The figure shows the temperature where silicon started to melt on substrates of quartz B to E, temperature for complete melting and the temperature where an equilibrium angle was reached. F1 indicates that furnace 1 was used, F2 indicated that furnace 2 was used.

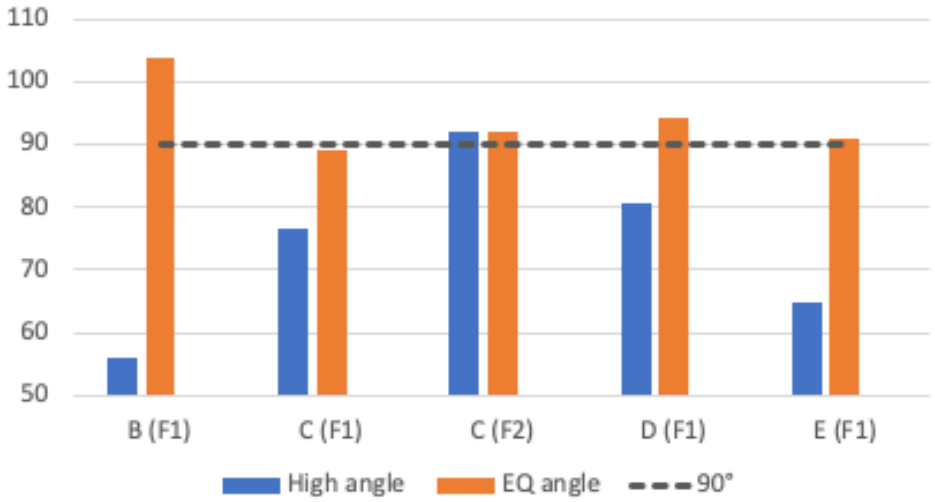

Figure 57: The figure shows the initial wetting angle (right after complete melting) and the equilibrium angle, for silicon on substrates of quartz B to E. F1 indicates that furnace 1 was used, F2 indicated that furnace 2 was used.

5 Discussion

Reactivity of silicon and silica is dependent on and increase with: available reaction area, temperature and time. This have been confirmed by 30 experiments where a a mixture of silicon and different types of industrial quartz samples have been heated at temperatures ranging from 1650 to 1950°C and times varying from 30 to 120 minutes. The degree of reaction is calculated based on weight loss of each sample and there is no significant difference between the reactivity of the different types of industrial quartz, which will be further discussed in Section 5.2.1. The phase distribution after heating of the samples have been investigated by macro and SEM images and the properties of the different quartz samples are discussed base on chemical analysis, XRD and information on each specific sample found in literature. A comparison of the two SiO producing reactions in a silicon furnace and their behaviour as a function of temperature will be discussed in the end of this chapter, based on the result of this report and literature on the silica/SiC reactivity.

5.1 Weight loss of silicon/silica mixtures

17 isothermal heat treatment experiments were performed as part of this thesis and another 13 experiments were performed in the fall of 2019 as part of Sindland's specialisation project [35][34]. Figure 58 below shows the weigh loss as function of holding time for all of the samples, 30 experiments in total. The weight loss increase with time and temperature, as indicated by a regression based on all of the data in the figure. The modelled weight loss is a function of both time, temperature and the fraction of each sample and it is therefor not included in this figure. The modelled values are however discussed and included in the next section for a selection of data and shown in Figure 60. The set up and experimental procedures is the same for experiments obtained by Sindland as part of the specialisation project in 2019 and in 2020 as part of this thesis, all of the results are therefor included and will together form a model describing silicon and silica reactivity. This will be justified in Section 5.2.4. Five different types of quartz have been used in the experiments and the difference between them will be highlighted in Section 5.2.1 and further discussed in Section 5.4.

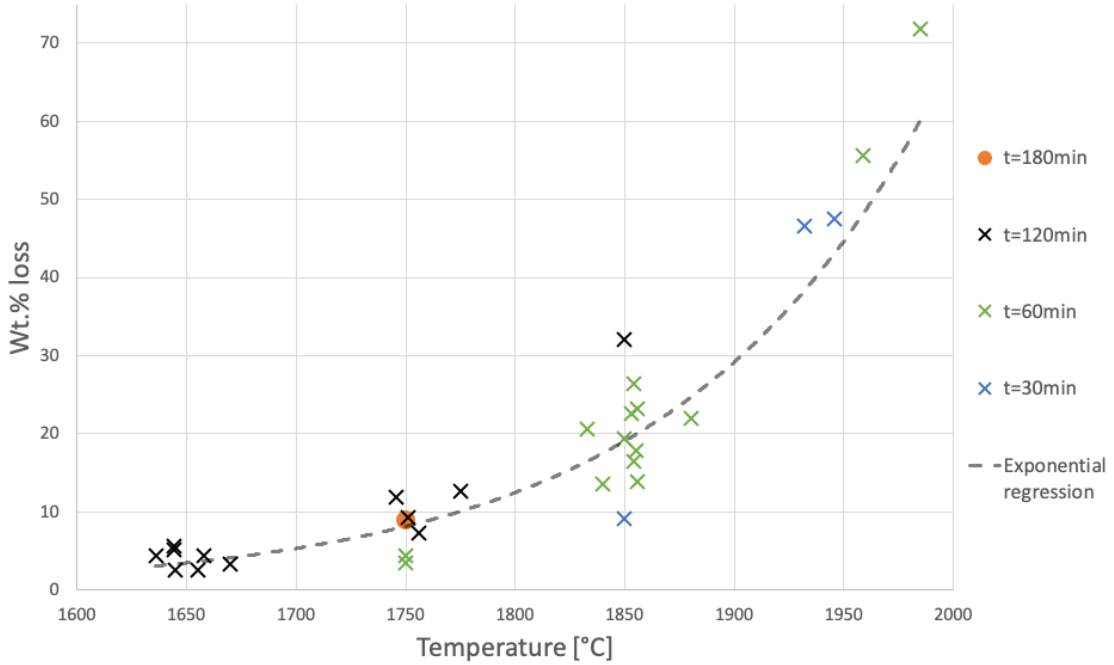

Figure 58: The weight loss after heating samples of quartz A to E mixed with silicon. The figure is including results obtained by Sindland [35][34] for quartz A in 2019 and result obtained as part of this master thesis. The colour indicate the isothermal holding temperature. The dotted line is a regression (not the reacticity model) based on all of the experimental data to indicate that weight loss increase with time and temperature.

5.2 Reaction rate of silicon and quartz mixtures - One model

One model has been developed for the reactivity of mixtures of silicon and different types of industrial quartz. There is no significant difference between the reactivity of the different quartz samples and there is not found any significant difference between the reactivity measured as part of this master thesis and the results obtained by Sindland in the fall, both discussed in sections below. It is therefor chosen to develop one model based on all of the results from 2019 and 2020. Quartz A is the quartz type used by Sindland in 2019 and in four experiments this spring, giving a total of 17 experiments with QZ A. This makes quartz A the reference sample and another 13 experiments were performed with 4 other types of quartz in the spring, to investigate the reactivity of different types of quartz.

Sindland found in her specialisation project that the reactivity of silicon and silica mixtures follow an Arrhenius equation [35]. It is assumed that the weight loss of a sample can be directly correlated to the reactivity, which means that the weight loss is assumed to be due to SiO formation only. This will be discussed and justified in Section 5.2.5. The experimental data for quartz A have a good fit to the model developed by Sindland in the fall, but an improvement regarding calculation of available reaction area was suggested for future investigations. A new model, including an agglomeration factor and an updated value for initial particle radius (based

on the size fraction of each sample) was therefor developed this spring.

The model for reactivity used in this thesis was presented in the experimental part as Equation 13, 14 and 15 and the equations are restated in this section due to their importance. Values for reaction constant (k_0) and activation energy (Q) are presented in Table 8. The values have been obtained from the linear regression in Figure 59, an Arrhenius plot of all 30 samples, including five different types of quartz heated in the fall of 2019 and spring of 2020.

$$\frac{d\alpha}{dt} = k_0 \cdot A \cdot exp(-\frac{Q}{RT}) \tag{13}$$

$$A = A_{0,Si} \cdot (1 - \alpha) \cdot F \tag{14}$$

$$T < T_{m,QZ} \Longrightarrow F = 1 \qquad T > T_{m,QZ} \longrightarrow F = 0.5 \tag{15}$$

Where α is the degree of reaction [ ], t [s] is the time, A is the available reaction area $[cm^2g^{-1}]$, $A_{0,Si}$ is the initial reaction area $[cm^2g^{-1}]$, F is the agglomeration factor and Q is the activation energy [J].

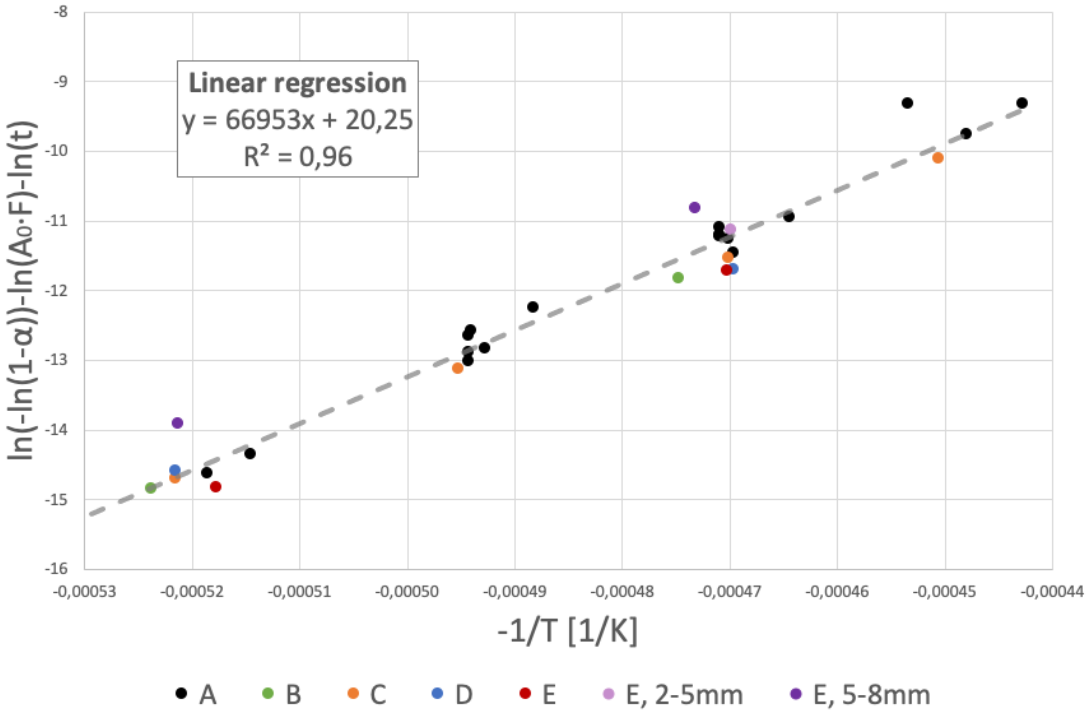

Figure 59: An Arrhenius plot of the experimental data, including results obtained by Sindland during 2019 [35][34]. The actual crucible temperature for each experiment has been used, as well as initial area (A_0) based on the particle size used in the different experiment. The different colours indicate the different types of quartz and the fraction of the raw materials in the case where different fractions were used for the same type of quartz.

Table 8: Values for reaction constant and activation energy obtained from Arrhenius plot in Figure 59, as described in Section 3.6.

k_0 $[s^{-1} \cdot cm^{-2} \cdot g]$	Q [kJ/mol]
$6.25 \cdot 10^8$	557

The modelled weight loss is a function of time, temperature and size fraction. The data points from heating at 1650 and 1750°C for 120 minutes and at 1850 and 1950°C for 60 minutes have been selected and plotted along with a model for these times and temperatures, as shown in Figure 19. The model show a good fit to the size fraction of 2-4,7mm, but it predict too high weight loss for samples of a smaller fraction and too low weight loss for samples of a higher fraction. Despite this, the model has a higher accuracy than a simple regression based on all of the data, as seen in Figure 58. The error of the model, the difference between experimental en modelled values indicate that the effect of initial area are less than what is assumed. An increase in initial reaction area (size fraction) will cause an increased reaction rate and final weight loss, but the increase is less than the model predict. This will be further discussed in Section 5.2.2. The over all fit of the model is still considered to be good and it could be used for comparison of the different SiO producing reactions in a silicon furnace.

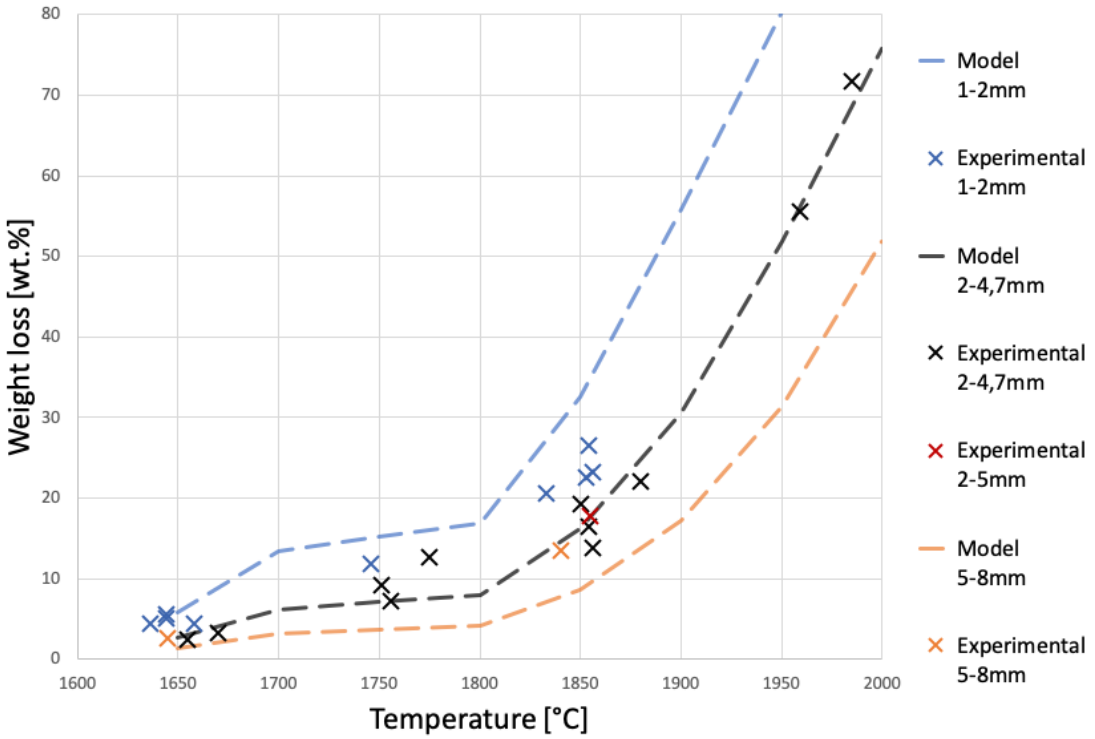

Figure 60: The weight loss after heating samples of quartz A to E mixed with silicon, including results on quartz A obtained by Sindland in 2019 [35][34]. The figure include the samples heated to 1650 and 1750°C for 120 minutes as well as 1850 and 1950°C for 60 minutes. The size fraction of the samples and the modelled value for each fraction at the given time/temperature is also included.

5.2.1 The reactivity of different industrial quartz samples

Five different types of quartz have been included in this master thesis and in the measurements of silicon/silica reactivity. The amount of impurities and their transformation rate varies significantly, but this does not seem to give any significant difference in reaction rate. Figure 61 shows an Arrhenius plot of all of the reactivity data obtained by Sindland, including a 95% confidence and a 95% prediction interval. The intervals are only based on data from heating of quartz A, which means that more than 5% of the data obtained from heating of quarts B to E would be outside this interval if there was any significant difference between the different types of quartz. It is justified to say that there is no significant difference between the reactivity of the different quartz samples, based on the fact that there is only five data point that lays at or outside the prediction interval, tree on the border of the interval and two outside. Two of these points are from the sample with a higher fraction (quartz E, 5-8mm) and one of them is from heating of quartz A. This means that only two data points from heating of 1-2mm particles of quartz B to E lay at the border of the prediction interval. The model is therefor valid for different types of industrial quartz but it might not be optimal for any size fraction.

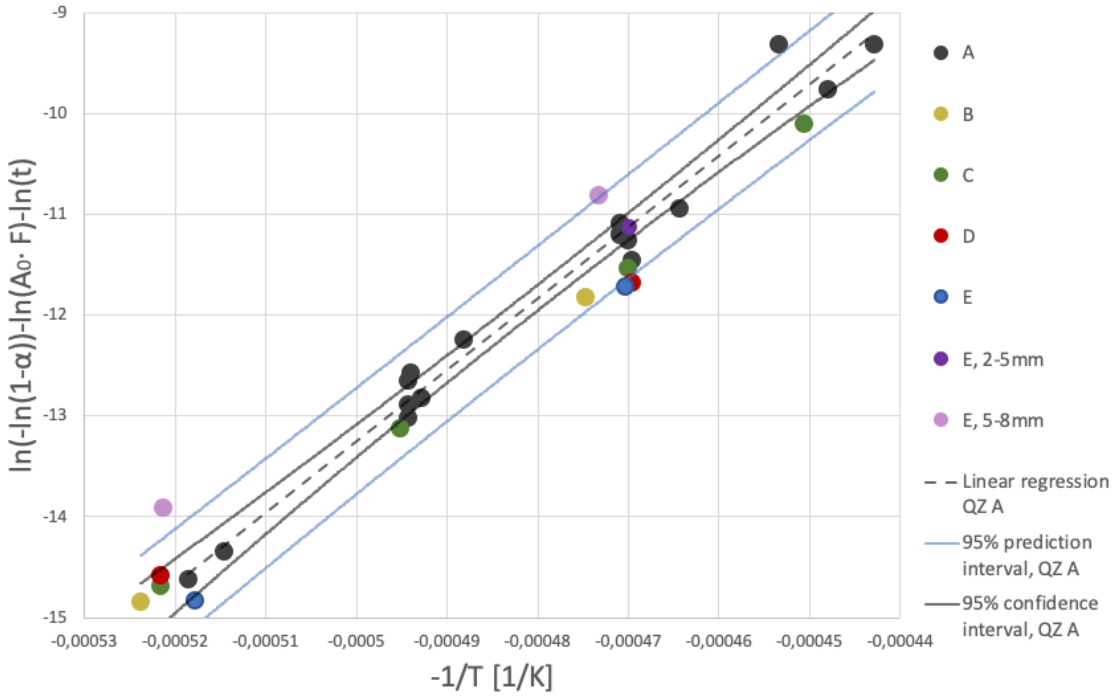

Figure 61: An Arrhenius plot of all datapoints with linear regression and intervals based on quartz A only. All types of quartz seems to follow the same model.

5.2.2 Modelling error as function of particle size and temperature

The samples have been heated at temperatures ranging from 1650°C to 1950°C. The relative error, the difference between degree of reaction (α) calculated by the model and obtained by experiments, relative to the value obtained by experiments is plotted in Figure 62 as function of temperature. There does not seem to be any trend in error as a function of temperature. The increase of reactivity with temperature is determined by the activation energy and the change in agglomeration factor in the model. No change in error with respect to temperature indicates therefor that the value for Q and F are good.

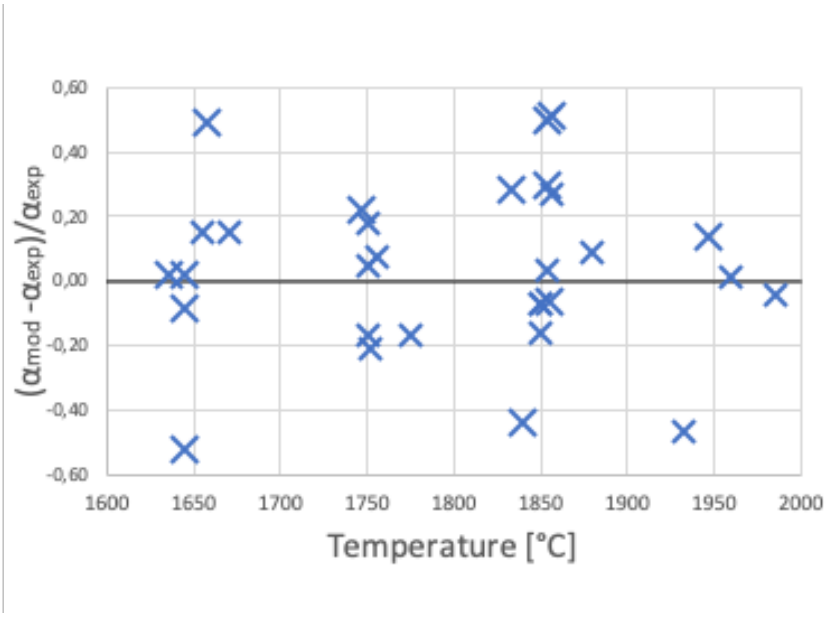

Figure 62: The difference in modelled and experimental values for degree of reaction, relative to the experimental values, plotted as function of temperature.

Samples of different particle size have been used in the isothermal heat treatment experiments. Experiments done with quartz A (17 experiments) were done with 2-4.7mm particles while experiments done with quartz B to E were done with 1-2mm particles (10 experiments), except three experiments where a higher fraction of quartz E were heated. The relative error, the difference between degree of reaction (α) calculated by the model and obtained by experiments, relative to the value obtained by experiments is plotted in Figure 63 as function of particle size. The figure shows a trend from high to lower values when the particle size increase, indicating that the reaction rate increase less with increasing initial reaction area than predicted by the model.

The experimental data for samples heated for 120minutes at temperatures below 1800°C and 60 minutes for temperatures above that is plotted in Figure 64, along with a regression for each size fraction. The regressions for each size fraction of sample shown in Figure 64 indicate that there is an increase of reactivity with increasing initial available reaction area (initial particle size). The model predict that the reactivity increase with initial area but on the other hand there is a trend in error plotted as function of particle size, indicating that the calculation of initial reaction area or the implementation in the model need optimisation. The model predict a reaction rate that is too high for samples of a small fraction and too low for samples of a higher fraction. The reactivity increase with increasing initial area (decreasing r_0) but it does not increase linear as assumed by the model. Smaller particles will have a high driving force for agglomeration (the reduction of surface energy) compared to bigger particles, this could lead to a different rate of agglomeration for the different size fractions, resulting in a smaller difference in reactivity compared to the case where there is no agglomeration. A agglomeration factor,

as function of temperature and initial particle size could correct this and reduce the error as function of particle size. But the data set in this master does not provide enough information to justify any further adjustment in the calculation of available reaction area. It is therefor suggested that further work on the reactivity of silicon and quartz focus on the reactivity of different size fractions, so that an improvement can be made.

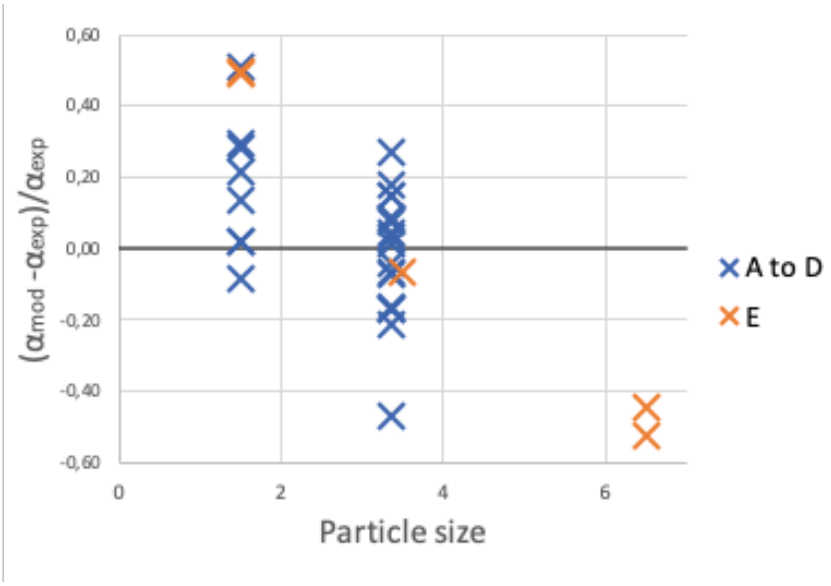

Figure 63: The difference in modelled and experimental values for degree of reaction, relative to the experimental values, plotted as function of particle size. The data points from quartz E (the sample with different size fraction) are indicated by a different colour.

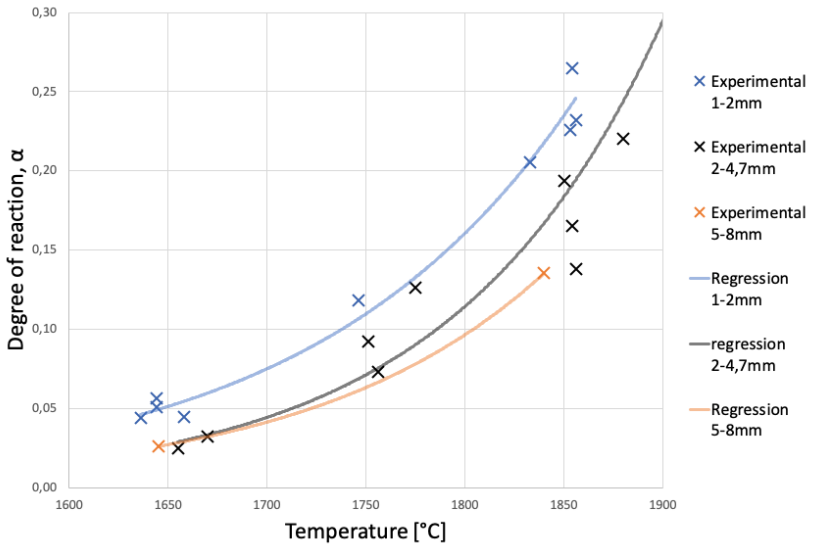

Figure 64: The degree of reaction after heating samples of quartz A to E mixed with silicon, including results on quartz A obtained by Sindland in 2019 [35][34]. The figure include the samples heated to 1650°C for 120 minutes, 1750°C for 120 minutes, 1850°C for 60 minutes and 1950°C for 60 minutes. The size fraction of the samples and a regression based on data from each fraction at the given time/temperature is also included.

5.2.3 Comparison of the reaction model with earlier work

Bao et al. [5] claimed that the reactivity of silicon and silica increase with temperature until it decreases above 1820°C. Andersen [2] claims that the reactivity increases up to 1723 °C (the theoretical melting point of silica), decreases and increase again above 1860°C. An increased reaction rate is observed in the entire temperature range from 1650 to 1950°C in this master which is not consistent with the work done by Bao showing a decrease in rate above 1820°C. However, there might be a local decrease of reaction rate between 1700°C and 1800°C, even though the results of this master show a continuous increase of reaction rate with increasing temperature, due to large temperature intervals between the experiments in this report. A decreasing reaction rate due to a silica with a high viscosity preventing removal of SiO gas right after melting might therefor be possible. On the other hand, any decrease in reaction rate observed right after silica starts to melt might be dependent on the particles size, Andersen used pellets while particles bigger than 1mm has been used in this thesis. The silica would be more evenly spread out in the case where pellets are used, resulting in a more evenly distributed viscous silica, entrapping the SiO gas. This could make the decrease of reaction rate right after melting more significant for experiments with pellets than experiments with particles. It is therefor concluded based on the work in this thesis and obtained literature that the reaction rate of silicon and silica increase with time and temperature with the possibility of a local reduction of rate around the melting point of silica. The reaction rate does not decrease at temperatures above 1820°C.

An agglomeration factor (F) has been included in the reactivity model of this master thesis due to a significant decrease in available reaction area when both silicon and silica is liquid. This was one of the suggestions that Sindland made regarding improvement of the model developed in the fall of 2019. The decrease in reaction area is due to agglomeration and separation of the silicon and silica phase, as seen in Figure 31 and 32 where one type of quartz mixed with silicon is heated to different temperatures. One constant value was chosen as agglomeration factor above the melting point of quartz to keep the model simple and 0.5 seems to give the best fit to the experimental data. Figure 65 shows an Arrhenius plot of the experimental data based on the model with an agglomeration factor (blue line) in addition to a plot of experimental values based on the model used by Sindland in 2019 (orange line). There is only a small change in the linear regression as a result of introducing the agglomeration factor but the over all fit increases from $R^2 = 0.96$ to 0.98 when an agglomeration factor is added to the model. The model with an agglomeration factor gives a better fit to the experimental and it is based on agglomeration observed after heating of samples.

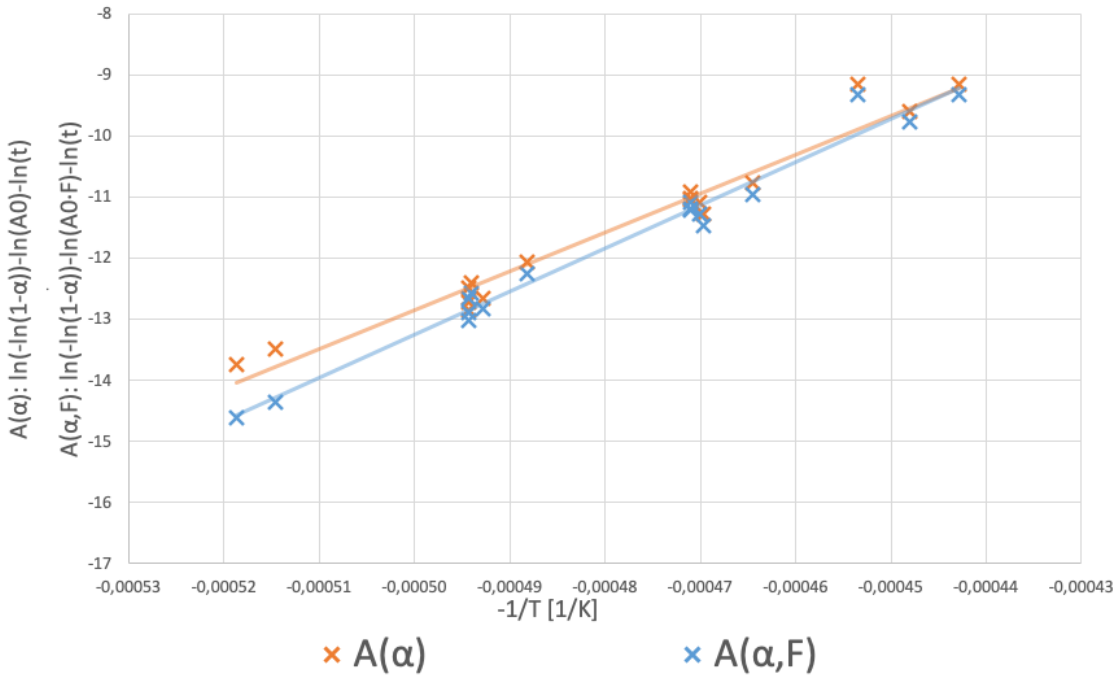

Figure 65: An Arrhenius plot of the weight loss after heating of quartz A. Comparison of two expressions for available area, the "old" one is the expression used by Sindland [35][34] in 2019 and the "new" expression is modified by the author to include an agglomeration factor.

The initial reaction area given in the reactivity model should be an area relative to the weight of silicon (or silica if that is the restricting phase), given with the unit $cm^2 \cdot g^{-1}$. This will give a reaction constant with the units $s^{-1} \cdot cm^{-2} \cdot g^1$ and the model can be used on a variety of setups and cases. A relative area was not used when Sindland developed the model in 2019, the total reaction area for a 20g sample was used instead of the available area per gram, giving

a reaction constant that was specific for the setup. The main conclusion of Sindland's report is still valid, reactivity increases with time and temperature [35] and it can be described by an Arrhenius equation. But the calculated reaction constant developed in the fall was specific for the set-up and could not be used in comparison with other reactions.

5.2.4 Reproducibility - Including earlier result in the model

Four experiments have been run this spring with the same quartz, silicon and set-up as used by Sindland in the summer and fall of 2019 [34] [35]. This was done to confirm that there were no significant changes to the furnace, set-up, procedure and samples. All of the results where a mixture of silicon and quartz A have been heated are plotted in Figure 66, in an Arrhenius plot. Two regressions have been made, one including all of the results and another regression based on the results from 2019 only. There is no significant difference between the two regressions and the reaction constant and activation energy obtained from them. All of the reactivity measurements done by Sindland previously on quartz A is therefor included when a model for silicon/silica is developed in this master thesis.

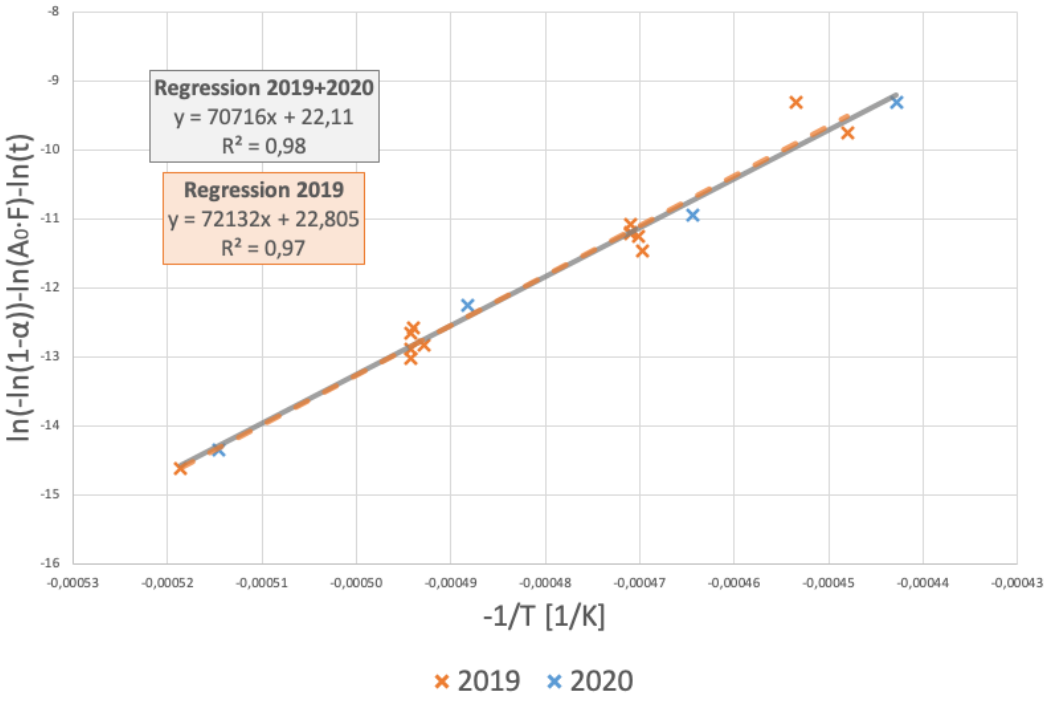

Figure 66: An Arrhenius plot of the weight loss after heating of quartz A. Comparison of results obtained by Sindland [35][34] in 2019 and result obtained by Sindland this spring.

5.2.5 Other reactions effecting the correlation between weight loss and reactivity

The reactivity model is developed based on the assumption that weight loss of a silicon/silica mixture is due to formation of SiO gas. Interaction with the graphite crucible and formation of a SiC layer at the crucible interface will cause formation of CO gas, effecting the correlation

between weight loss and SiO formation. This effect has been neglected and it is assumed that the weight loss of each sample is due to formation of SiO gas and nothing else.

The thickness of the SiC layer on each crucible was investigated by Sindland [35] in previous work on silicon/silica reactivity and calculations based on that lead to the conclusion that the weigh loss due to interaction with the graphite crucible is independent on time and temperature. A stable layer of SiC was formed after short time. Formation of CO gas due to SiC formation is calculated by Sindland to cause a weight loss of about 1.7wt.% for all samples (based on a total weight of 20g sample). A stable SiC layer is formed after heating for short time at a low temperature and the weight loss due to reaction with crucible is insignificant for samples heated at higher temperatures, where the total weight loss is high. The weight loss due to SiC formation is however significant for samples heated at lower temperatures and times due to a lower degree of reaction. The effect of correcting the results for SiC formation is shown in Figure 67 where degree of reaction is plotted as function of temperature, with and without any correction. The black point indicate the degree of reaction based on total weight loss while the blue dots indicate values corrected for weight loss due to SiC formation. Interaction with the crucible is still neglected in the entire temperature range of this model even though it is significant at 1650°C, to make the model as simple as possible. This means that the model might predict a reaction rate slightly too high at low temperature and time.

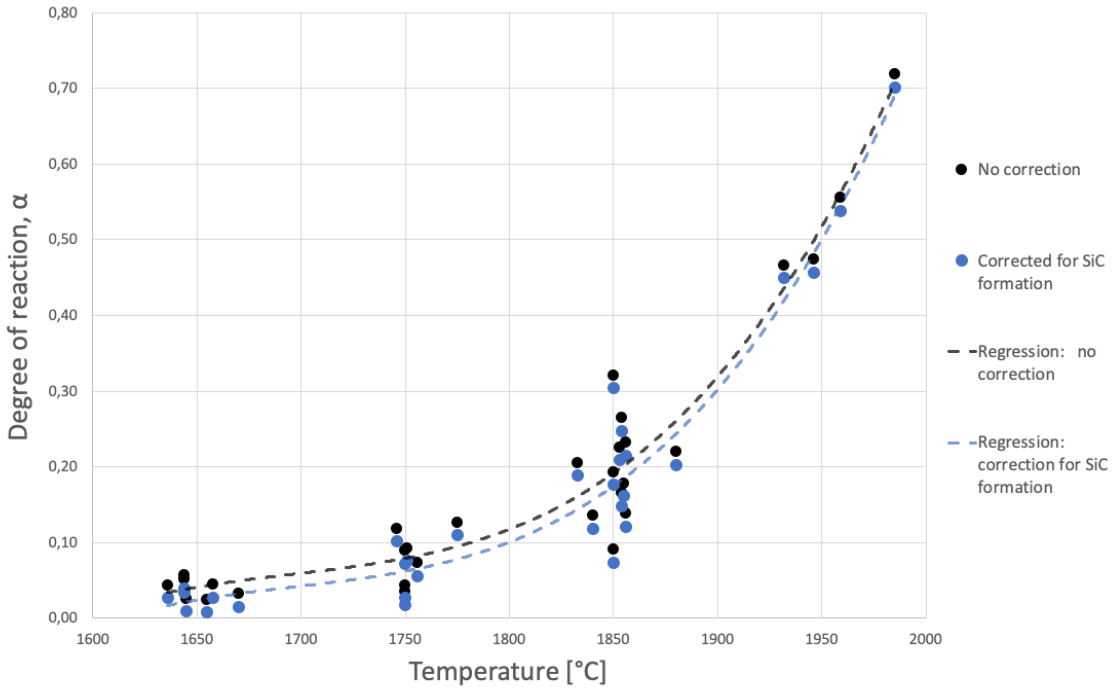

Figure 67: The degree of reaction for each sample without any correction is plotted and marked in black while the degree of reaction with correction for weight loss due to SiC formation is marked in blue. The corrected value is based on total weight loss minus the weight loss due to interaction with crucible, causing formation of CO gas. The weight loss due to interaction with crucible is assumed to be 1.7wt.% of a 20g sample, independent on time and temperature [35].

Fe_2O_3, K_2O and Na_2O are oxides that is reduced at lower temperatures than silica. Reduction of these oxides will cause formation of CO gas if they react with the carbon crucible and the amount of silicon will be reduced if the oxides are reduced by metallic silicon. The correlation between weight loss of the sample and silicon/silica reactivity will be affected in both cases. Quartz A, B and D have less than 0.03wt.% of those oxides and quartz C and E have less than 0.4wt.%. The amount of impurities are small and the amount of CO that could be produced and silicon than could be oxidised are small compared to the over all weight loss of the samples after heat treatment. The reduction of impurities in the quartz and any weight loss related to this is therefor neglected.

5.3 Phase distribution

A 1:1 molar ratio of silicon and silica particles was mixed before isothermal heating in graphite crucibles. Silicon has a melting temperature in the range of 1400-1420°C [32, p. 21] [6] and pure silica has a melting point around 1728°C [22, p. 530], depending on the references. This means that silicon will be present as a liquid for experiments at 1650°C and silica as a solid, as seen in the macro image of a sample hated to 1650°C for 120 minutes in Figure 68. Macro images of all of the samples heated to 1650°C is presented in Figure 33 and one difference between the samples can be observed, there is signs of softening or sintering for the samples with quartz C and E. Nordnes has performed experiments where industrial quartz was heated at a rate of 5°per second and softening occured at 1675-1700°C for two of the four samples she tested [25], softening could therefor be possible after heating at 1650°C for 120 minutes. There was not observed any other significant difference between the samples at 1650°C, the silicon particles/droplets seems to have agglomerated in all of the samples.

Figure 31 and 32 shows the phase distribution of samples with quartz A and C as the temperature and degree of reaction increase and Figure 68 show the phase distribution in four samples with an increasing degree of reaction. The silicon starts to agglomerate at 1650°C and both silicon and silica agglomerate at 1750 and 1850°C. The two liquid phases tends to separate and the available reaction area is decreased significant above the melting point of quartz. This is the reason why an agglomeration factor was introduced in the equation for reaction rate. The separation of the two phases is according to the findings done by Vangskaasen [40], he observed that silicon was separated from silica during heating of brown condensate, they did not wet each other. The non-wetting behaviour has also been confirmed in this thesis by heating of silicon on quartz substrates, a wetting angle less than 90°C was observed for all samples, which will be further discussed in Section 5.4.

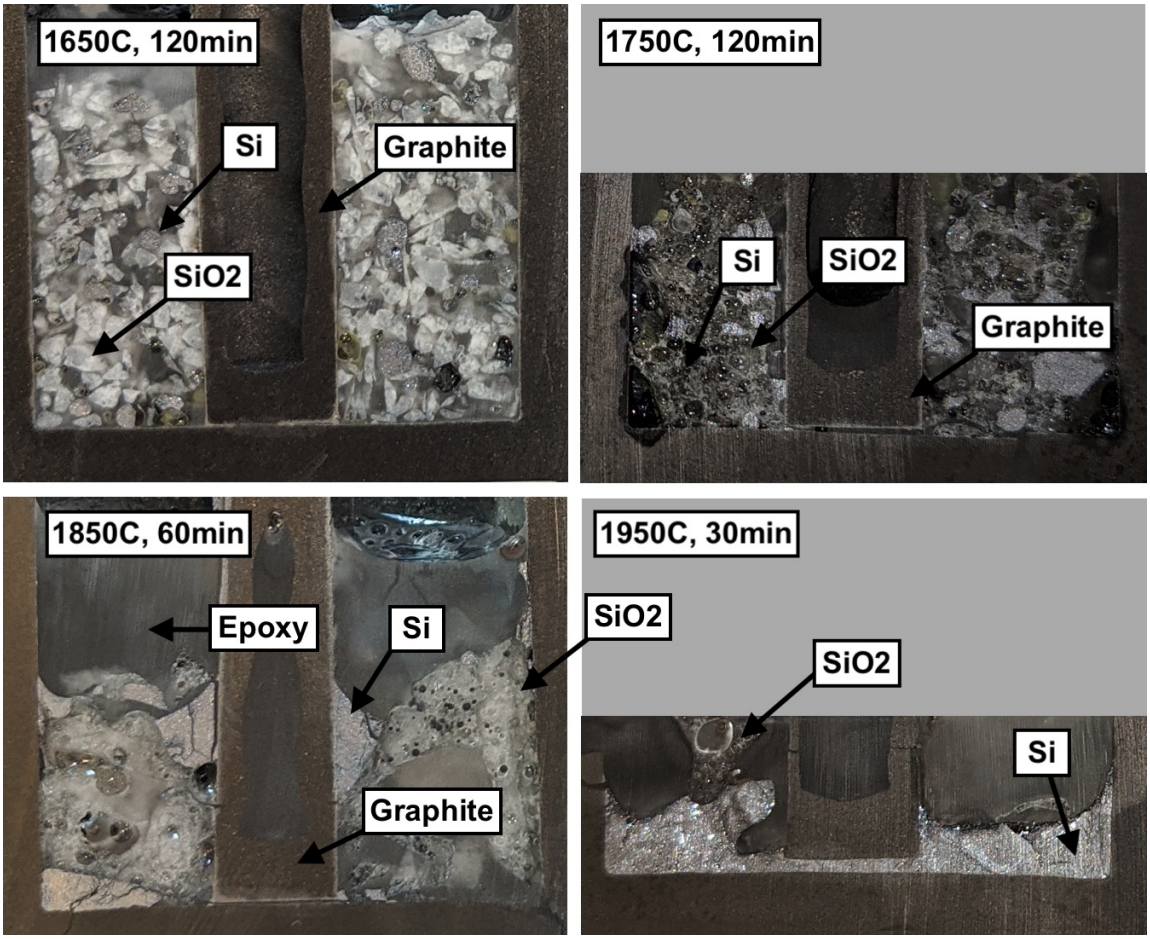

Figure 68: Phase distribution for four samples with increasing degree of reaction.

It is expected that silicon would drain to the bottom of the crucible as soon as it is melted, due to density differences between silicon and silica, leaving silica on top of the silicon. This is however not observed until a temperature of 1950°C is reached. Silicon are wetting graphite with an angle of 3-40°[11][10] and this could be one of the reasons why silicon is stopped from draining. However, Sindland performed one experiment where silicon and silica were heated in a h-BN crucible and the silicon stayed on top of the silica phase [35]. Wettability of the crucible is therefor not stopping the silicon from draining. Another possible reason is the non-wetting behaviour of silicon and silica in addition to the high viscosity of silica at low temperatures [29]. The viscous silica could stop the silicon from draining to the bottom of the crucible until a higher temperature is reached, giving a less viscous silica.

The samples were investigated in SEM and the expected phases were found: silicon, silica, graphite and silicon carbide at the crucible interface were found, as seen in Figure 41b, among others. Impurities at the grain boundaries of silicon was found in addition to this, which is expected due to a low solubility of impurities in solid silicon. There was only one unexpected finding: silicon carbide was found on the surface of the silicon heated to 1650 and 1750°C, as seen in Figure 69, this was not found in samples heated to 1850 and 1950°C. The reason for this is

not fully understood but it is assumed that silicon carbide is formed at the surface of the silicon particles/droplets at low temperature and that the silicon carbide react with silica at higher tempreature. This indicated that the silica/SiC reactivity is low at temperatures up to 1750°C. The silicon carbide is reducing the contact and reaction area between silicon and silica but there is still some contact due to the fact that the layer has a low density and "empty" shells of silicon carbide is observed, indicating that all of the silicon inside these droplets has reacted with silica. It is not known in which degree the silicon carbide layer affect the silicon/silica reactivity and it is therefor not included in the model. The model is therefor specific for silicon/silica reactivity in presence of carbon.

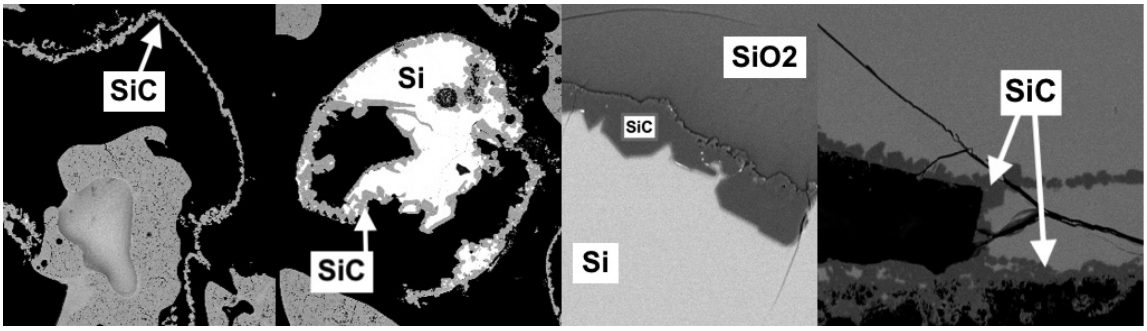

Figure 69: Silicon carbide on the surface of silicon particles/droplets in samples heated to 1650 and 1750°C.

5.4 Properties of the different quartz samples and their effect on reactivity

The total amount of impurities in each quartz sample is shown in Table 9. Quartz C and E have a relatively high amount of impurities while quartz A and B have a relatively low amount of impurities. There is a significant difference in the impurity content of each quartz sample.

Table 9: The total amount of impurities in weight percent as metal.

Sample	Total amount of impurities [wt.%]
A	0.062
B	0.013
C	0.499
D	0.121
E	0.826

It was observed that some of the samples had a higher porosity than other samples after heating. The porosity of the samples after heat treatment at 1850°C was therefor measured roughly by investigation of the macro images and the height of the crucible that was filled with sample after cooling. The height of the sample is assumed to be proportional to the volume and hence the porosity of the samples after heating. The measurements have a high uncertainty and the

porosity of the samples are therefor only listed relatively to each other, as seen i Table **??**. The samples with quartz A and B had the lowest porosity, the porosity of quartz E was a bit higher and quartz C and D had similar and even higher porosity. The difference in porosity could be due to a difference in SiO formation and a difference in viscosity (low viscosity can cause entrapment of gas). Impurities in the quartz that reduces more easily than silicon (eg. FeO) could be reduced in contact with the graphite crucible and result in formation of CO gas. They could also be reduced in contact with metallic silicon, resulting in formation of SiO gas or SiO_2. This could cause a difference in gas formation (weight loss) and porosity of the samples, but the total amount of impurities in the samples are low. Reduction of impurities are therefor neglected when it comes to porosity as well as weight loss, as mentioned in the previous section.

The experiments done in a sessile drop furnace show that silicon has a wetting angle below 90°on quartz substrates made of quartz B, C, D and E right after complete melting of the silicon, except for the one experiment run in furnace 2 (the rest of the experiments were run in furnace 1). Formation of bubbles at the silicon/silica interface start right after melting of the silicon, and this is assumed to be formation of SiO gas. The wetting angle starts to increase at the same time and a wetting angle right above 90°is reached for all samples except for quartz C. The wetting angle increase for a few minutes and reaches an equilibrium before the isothermal temperature of 1523°C is reached. It took between 0 to 3 minutes (corresponding to heating 0 to 14°C above melting temperature) for the samples to reach equilibrium angle after complete melting, except quartz B that reached equilibrium after 11min (53°C). The wetting angle has been measured by image analysis in ImageJ (three parallels for each sample at equilibrium) and the numbers have an uncertainty equal to the difference between the samples, except sample B that has a significant higher wetting angle. The equilibrium angle is reached a short time after melting and the equilibrium angle is therefor believed to be the angle of importance, both in the experiments performed in this report and for behaviour in an industrial furnace. It is therefor concluded that silicon is not wetting either of the industrial quartz samples and they all have a wetting angle in the range of 90 to 95°, except quartz B who has a wetting angle in the range of 100 to 110°. It should be noted that quartz B is the sample with the lowest impurity content. Literature reports a wetting angle between silicon and pure silica of 90 to 95°[1][20][14], which is in agreement with the measured wetting angle for the industrial quartz in this thesis.

Increasing wettability of silicon on silica would most likely give an increased available reaction area for silicon and silica mixtures. A difference in wettability could therefor explain a difference in reaction rate of the different quartz samples. There is however no significant difference in either of the properties, the reactivity of each quartz are within the same range and the same could be said about the wettability, except quart B who has a higher wetting angle. It is not possible to say whether the reactivity of silicon and quartz is dependent on the wettability of silicon on that specific sample or not. The reaction rate could be independent on the wettability since no difference in reaction rate was observed for quartz B compared to the other samples but one sample is not enough to say anything specific about the relation between wettability

and reaction rate.

There was not observed any significant difference between the initial and equilibrium angle of the sample heated in furnace 2, in opposite to the samples hated in furnace 1 where the initial angle was significant lower than the equilibrium angle. This sample in Furnace 2 was heated at a rate of 10K/min, a doubled rate compared to all of the other samples that was heated at a rate of 5K/min in Furnace 1. This could affect the reaction rate (formation of SiO gas) and the melting rate. The fact that no significant difference was observed by the angles in furnace 2 where the sample was heated at a higher rate can be explained in the case where the reaction rate increase more rapidly with temperature than the melting rate. This would cause formation of a significant amount of SiO gas during melting of the sample, which could cause the sample to melt directly into a droplet with an equilibrium angle. The samples heated at a lower rate would in this case melt before the amount of SiO gas formed at the surface is high enough to cause an increase in wetting angle.

A difference in the substrates roughness could also cause a difference in initial wetting angle. A rough surface would give a lower wetting angle due to the fact that SiO gas can leak through grooves and dimples while a smooth surface would lead to a higher amount of entrapped gas and a higher wetting angle [20]. All of the samples were grind to the same roughness before each experiment but some deviation could occur. But it is likely that all of the quartz surfaces would approach the same roughness after reaction with silicon. This could explain why there is a significant higher difference in initial wetting angle of each sample compared to the difference in equilibrium wetting angle. The initial angle varies from 56 to 92°while the equilibrium angle varies from 89 to 104°for all samples.

Furnace 2 can reach a higher vacuum than furnace 1, giving a lower oxygen pressure during heating of samples. Formation of an oxide layer has been observed on the surface of samples heated in furnace 1 previously and this was a concern when furnace 1 had to be used due to the fact that furnace 2 was out of order. However, there was not observed any oxide layer on the surface of silicon heated in furnace 1 and the difference in vacuum of the two furnaces does not seem to have affected the results.

All of the quartz samples were heated to 1650°C in alumina crucibles and held for 120 minutes before they were cooled and investigated by XRD, to investigate tge phase distribution in each sample. There were no significant difference between the phase composition of the samples, except quartz E which had a higher amount of amorphous phase, as seen in Figure 53. All types of quartz will transform to cristobalite at 1650°C after long enough time. It seems like the chosen holding time of 120 minutes (corresponding to the holding time used for silicon/silica samples heated to 1650°C) are long enough for all of the samples to approach equilibrium phase composition. However, work done by Jusnes show that there is a significant difference in transformation rate of quarts B, C and D [17] (her work does not include quartz A and E). The relevant information from her work is extracted and presented in Figure 70, where the phase

composition after heating for three different times at 1650°C are presented for quartz B, C and D. Quartz A has a higher rate of transformation than quartz C which again has a higher rate than quartz D, as presented in Table **??**. It can hence be concluded that the transformation rate is not affecting the SiO formation of the silicon/silica mixtures in this report. This could be due to the fact that most of the samples in this work were heated at higher temperatures, where all of the samples will be transformed in to cristobalite and start melting before the isothermal temperature is reaches.

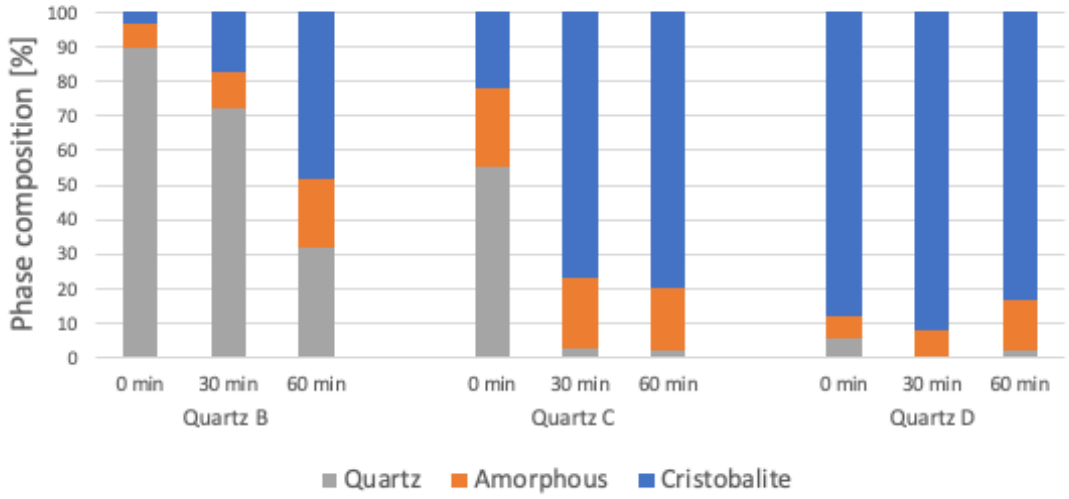

Figure 70: Phase transformation in quartz B, C and D after heating at 1600°C for 0, 30 and 60 minutes obtained from work done by Jusnes [17].

Jusnes has obtained values for decrepitation after shock heating of quartz B, C and D while Nordnes has obtained values for melting rate of quartz B and C [19][25]. The relevant values have been extracted from their work and it is presented in Figure 71. It seems to be a significant difference in decrepitation, a low amount of particles below 10mm (<5%) were found after shock heating of quartz C while the amount of particles below 10mm was about 30% for quartz B and about 75% for quartz D. There was however not observed any significant difference in particle size before and after heating of the quartz samples at a rate of 50°C/min prior to XRD analys, as seen in Figure 54. The amount of sample was low in these experiments and the change in size fraction and degree of decrepitation was only observed by the naked eye and not determined by sieving. The silicon/silica mixtures are hated at a rate of 50°C/min in the experiments performed as part of this master thesis and the difference in decrepitation might not be as big as when the samples are shock heated. It is reasonable to assume that the heating rate of the silicon and silica mixtures up to isothermal holding temperature is low enough to prevent significant decrepitation. There is a significant difference in the quartz samples decrepitation after shock heating but there might not be any significant difference between the samples decrepitation in the main experiments. The surface of silicon is lower than the surface of silica in the experiments

where weight loss is measured, due to a density difference giving a difference before heating and the possibility of agglomeration of the silicon when its melted, before the silica starts to melt. Any decrepitation of the quartz would further reduce the surface area of silicon relative to the silica. This verifies that the surface area of silicon is the limiting factor when it comes to available reaction area, and the surface area of silicon is a good assumption of available reaction area. As used in this reaction model, $A_{0,model} = A_{0,Si}$.

There is a significant difference in the melting rate of quartz B and C but no information has been obtained for the other samples. The melting rate of each quartz sample is assumed to be quite different in the present experiments, due to a large difference observed between quartz B, C and other industrial samples [25]. As this has not effected the reaction rate bewteen silicon and silica this verifies that the over all reaction rate is independent on the melting rate. It should however be noted that the experiments have been performed at 1650, 1750, 1850 and 1950°C, at relatively large temperature intervals and there might be a local variation in reaction rate due to a difference in melting rate.

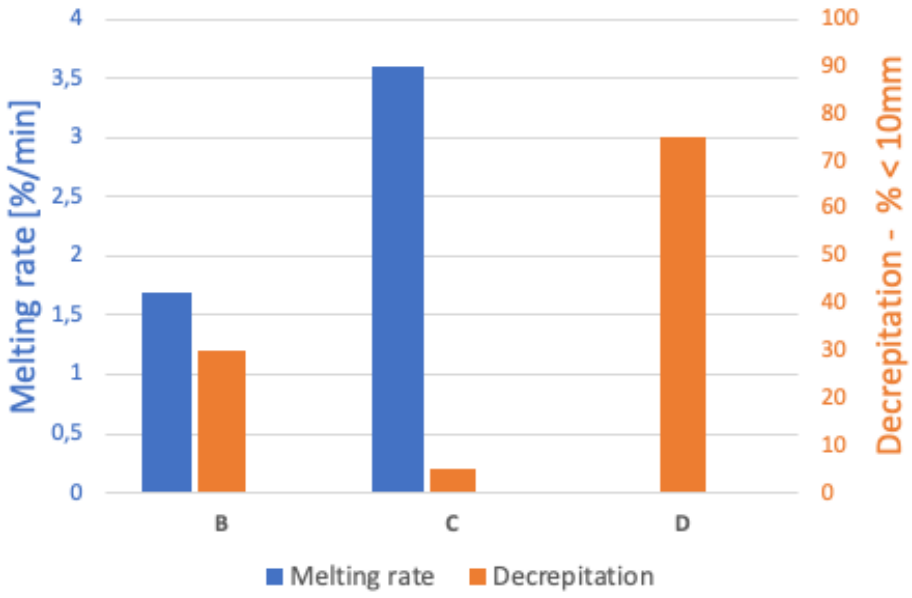

Figure 71: Melting rate of quartz A and B at 1750°C obtained from work done by Nordnes [25]. Decrepitation of quartz B, C and D after shock heating to 1500°C obtained from work done by Jusnes [19], given as percentage of particles that are below 10mm.

There is a significant difference in content of impurities, decrepitation after shock heating and rate of phase transformation between the different types of quartz. There is no significant difference in reaction rate and therefor it is assumed that impurities, decrepitation after shock heating and phase transformation rate has a low and insignificant impact on the reactivity of silicon and silica mixtures when the samples are heated at a rate of 50°C. However, the difference in decrepitation of the quartz samples could lead to a difference in reactivity if the samples are shock heated, due to the fact that a higher amount of fines would give a higher available reaction

area. There is a significant difference in melting rate of each sample and it is assumed to not affect the over all reaction rate but there could be a local difference between the different quartz samples in the temperature range where the samples soften and melt. The reason for varying porosity after heating is not known and the wettability does not show a significant difference, it is therefor not possible to say if there is a correlation between wettability, porosity and reactivity.

Table 10: A summary of properties of the quartz samples. The different quartz samples are listed from least/lowest to most/fastest where a significant difference between the different quartz samples was found.

Property	Significant difference?	From least to most of the property
Reaction rate	no	-
Impurities [wt.%]	yes	B < A < D < C < E
Porosity	yes*	A ∼ B < E < C ∼ D
Wettability	no	-
Phase transformation rate	yes	D < C < B
Melting rate [%/min]	yes*	B < C
Decrepitation** [% <10 mm]	yes	C < B < D

*data of low quality or not enough data. **after shock heating to 1600°C.

5.5 A comparison of the two SiO producing reactions in a silicon furnace

There are two SiO forming reactions in a silicon furnace, the reaction between silicon and silica as described by Equation 3 and the reaction between silicon carbide and silica as described by Equation 6. It is interesting to compare them, to be able to say something about the formation of SiO gas in a silicon furnace and factors leading to an increased amount of SiO in the off gases. The work in this report and previous work on the SiO_2/SiC reaction show that the reaction rate of both reactions are independent on the quartz quality [39], any calculations presented on reaction rate in this section will therefor be valid for various types of quartz.

Figure 72 shows the reaction rate of both SiO producing reactions on a logarithmic scale and Figure 73 shows the same on a linear scale, both in a temperature range from 1650 to 2150°C. The figures are based on initial reaction rate calculated by the model developed in this thesis, described by Equation 13 and the model for SiC/SiO_2 reactivity developed by Tangstad [39], described by Equation 10. The reaction area (A) is set to be 17,4 $cm^2 g_{Si}^{-1}$ for the silica/silicon reaction and 15,1 $cm^2 g_{SiO_2}^{-1}$ for the silica/SiC reaction. This is based on calculation of available reaction area for the two reactions, where 1-2mm particles of silicon is limiting the reaction rate of Si/SiO_2 and 1-2mm particles of SiO_2 is limiting the reaction rate of SiO_2/SiC. The calculations are described in Section 4.2 for 1-2mm particles of silicon and the same calculations have been performed for 1-2mm particles of silica, with 2,65g/cm^3 as the density of silica. The black line in Figure 72 and 73 are representing reactivity of silicon and silicon carbide based on the average

activation energy and the error bars indicate rate based on maximum and minimum values reported by Tangstad. It should also be noted that the dotted part of the lines are calculations done outside the temperature range where the models where developed. But the extrapolation is included in the figure due to the fact that a silicon furnace can reach temperatures up to 2000°C in the high temperature zone [28].

There is a difference between the reaction rate of the two reactions in this case, as seen in Figure 72. However, the difference is not significant at lower temperatures due to the fact that the maximum value for silica/SiC activation energy gives a reactivity that is higher than the one obtained for silicon/silica reactivity. There is a significant difference between the two reactions at higher temperatures which is particularly evident in Figure 73 where the reaction rates are plotted on a linear scale. It could therefor be argued that there is a significant difference between the rate of each reaction for the given available reaction area but both reactions are highly dependent on this, the available reaction area used to calculate the rate. The available reaction area is therefor considered the main factor determining which of the reactions that produces the highest amount of SiO gas. This leads to the conclusion that the production of SiO gas in a silicon furnace is highly dependent on the available reaction area for the two possible reactions.

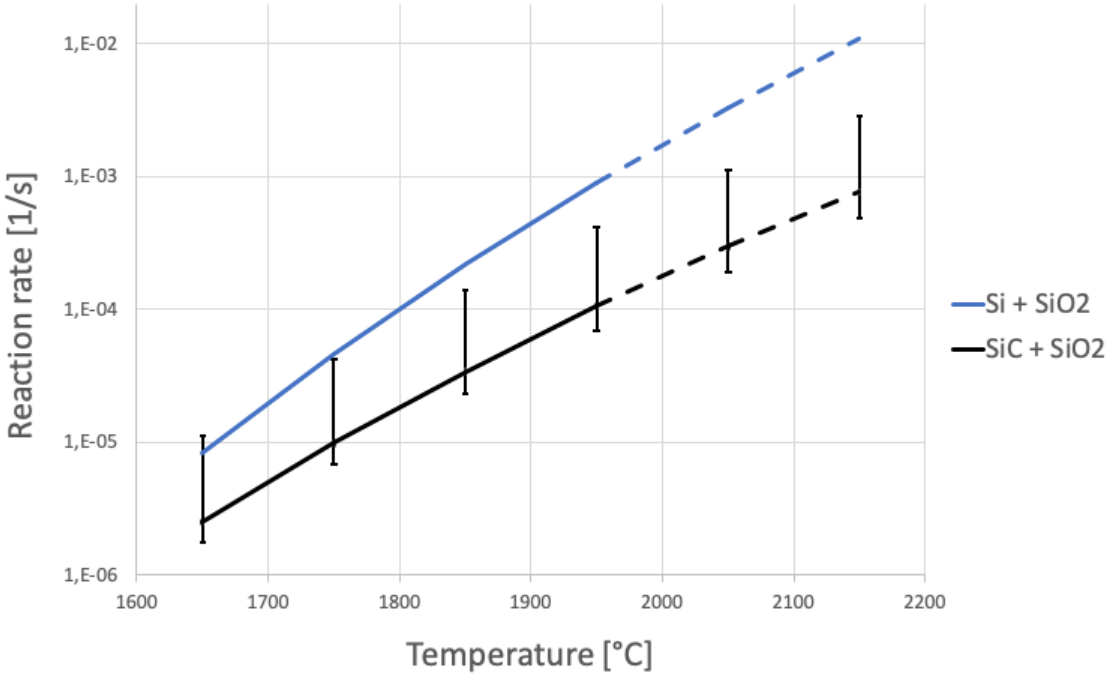

Figure 72: The reaction rate of the two SiO producing reactions in a silicon furnace for a given reaction area on a logarithmic scale. The reaction area (A) is set to be determined by 1-2mm silicon particles for the silicon/silica reaction and 1-2mm silica particles for the silica/SiC reaction. The reaction rate for SiO_2/SiC reactivity was obtained from a model developed by Tangstad [39]. The reaction rate for SiO_2/Si was obtained by the model developed in this thesis. The dotted line is outside the temperature range of the models.

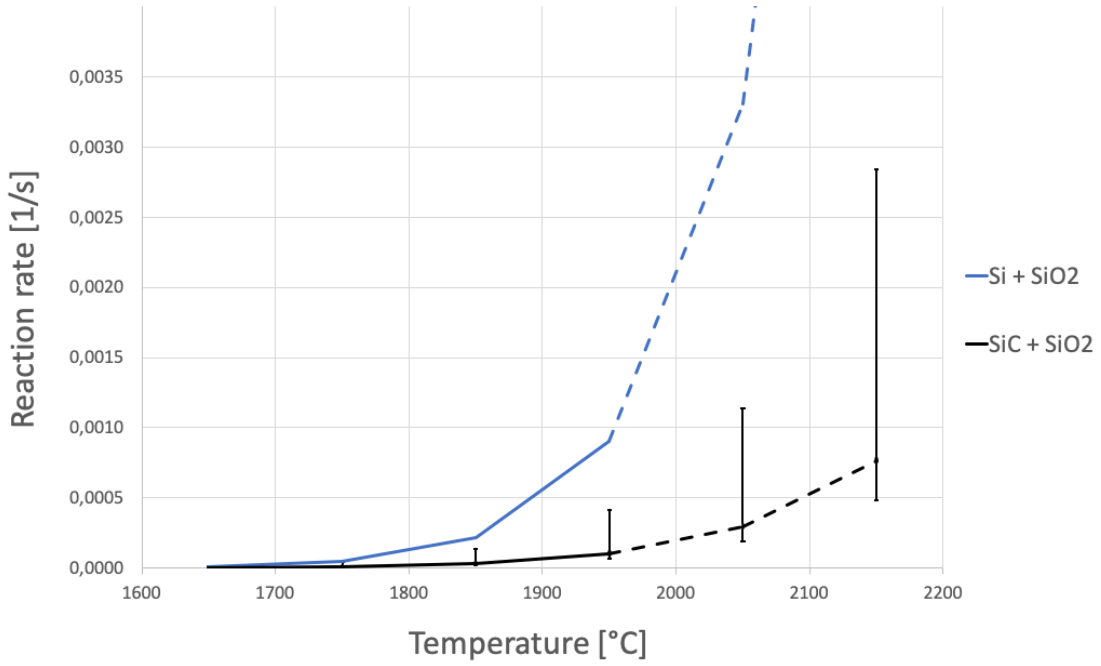

Figure 73: The reaction rate of the two SiO producing reactions in a silicon furnace for a given reaction area as shown i Figure 72, but on a linear scale in stead of a logarithmic scale.

5.6 The reaction model and an industrial furnace

Problem with tapping can cause a build up of silicon in the bottom of a furnace, the amount of silicon increase as you descend in a silicon furnace and different types of quartz have different properties, all being factors that could affect the over all $SiO_{(g)}$ formation in a silicon furnace. This section will address this topic and how the formation of SiO change with increasing temperature and depth in the furnace.

The reactivity of a silicon and silica mixture is proportional to the available reaction area, a doubling of the available reaction area will give a doubled reaction rate. Jusnes has done experiments with shock heating of quartz samples and found that the surface area of a 200g sample increased by a factor of 9 after shock heating [19]. This does not necessarily mean that the available area for silicon/silica reaction in a silicon furnace will increase by a factor of 9. The area of silica will increase as a result of decrepitation but it will eventually decrease again due to agglomeration. But the surface area of silica could increase below the melting point of quartz (before agglomeration) and most likely increase slightly in the hot zone as well. One could therefor assume that a high degree of decapitation will lead to a higher rate of $SiO_{(g)}$ formation, especially at temperatures below the melting point of quartz. However, the reaction rate of the two SiO producing reactions is determined by the surface area of the limiting phase. There is a very low amount of silicon in the low temperature zone, making silicon the limiting phase. The increase of silica surface area due to decrepitation is therefor significant higher than any increase in reaction rate due to decrepitation. Decrepitation might even be insignificant

to the silicon/silica reaction rate in the low temperature zone due to a low available area of silicon being the rate determining and in the high temperature zone due to agglomeration and separation of silicon and silica.

Production of silicon starts at 1811°C in theory and formation of SiO gas at lower temperatures is unwanted, to keep the SiO losses as low as possible [32, p. 29]. The reactivity of silicon and silica is relatively low at at 1650°C compared to 1850°C, with a factor of 26 times lower. The low reaction rate and low amount of silicon in the low temperature zone makes it possible for the two phases to descend in the furnace without reacting reacting completely before 1811°C. On other words, the amount of SiO produced from the $Si + SiO_2$ reaction is low in the low temperature zone compared to the hot temperature zone.

The amount of silicon is increased when you go deeper in a silicon furnace, which will increase the available reaction area for the silicon/silica reaction significantly. This will increase the formation of SiO gas in the hot zone compared to the cold zone. The SiO forming reactions are dependent on available reaction area between silicon/silica and silica/SiC, which is determined by the surface of the metal bath, the amount of slag droplets falling into the metal bath, the amount of SiC at the furnace wall, etc. The four main cases where SiO could be formed in a silicon furnace is summarised by the four points below [37]:

1. $Si_{met.bath} + SiO_{2,\,slag}$, low A_{Si} and low a_{SiO_2}.
2. $Si_{met.bath} + SiO_{2,\,droplets}$
3. $SiC_{furnace\,wall} + SiO_{2,\,droplets}$
4. $SiO_{2,\,slag} + SiC_{slag}$, low a_{SiO_2} but high A_{SiC} due to $r_{SiC} \approx 20\mu m$

The first case, the reaction area between a slag containing silica and the silicon bath is low and this combined with the fact that the activity of silica is low in the slag makes this a small contributor to the over all SiO production. The contact area between quartz dripping down from a crust into the metal bath could be high, depending on the amount of droplets. The same goes for contact area between silicon carbide along the furnace walls and droplets of silica. The last and fourth case are small particles of SiC finely distributed in a slag containing SiO_2. SiC particles of about 20 µm have been observed in slag excavated from a silicon furnace, giving a high reaction area and rate of reaction, even though the activity of silica can be low in the slag.

The four different cases listed above does not explain why industry report increased SiO loss when they have trouble with tapping. Trouble with tapping will increase the amount of silicon in the bottom of a furnace, but the available reaction area will not increase significantly, as long as the silicon is present as a metal bath in the bottom of the furnace and reacts according to case 1 and 2 above. An increased amount of silicon in the bath will increase the height of the bath but it will not increase the surface where silica is dripping down.

The reaction rate of the two SiO forming reactions in a silicon furnace does not vary with

different types of quartz, according to experiments done so far in this thesis and literature on silicon/SiC reactivity [39]. There is no significant difference between the rate of the two reactions when the particle size of the limiting phase is within the same range, giving them an available reaction area within the same range. The formation of SiO gas is therefor mainly dependent on the available reaction area for both reactions. Whether the reaction $Si + SiO_2$ or $SiO_2 + SiC$ produce the most SiO in a silicon furnace is determined by the phase distribution on the hot temperature zone.

6 Conclusion

The reactivity of a silicon and silica mixture increase with time and temperature and can be described by Equation 1 for various types of industrial quartz. This is based on 30 experiments where five different types of industrial quartz have been mixed with silicon and heated at temperatures ranging from 1650 to 1950°C in graphite crucibles. The reaction $Si + SiO_2$ has a reaction constant (k_0) equal to $6.25 \cdot 10^8 s^{-1} m^{-2} g$ and an activation energy (Q) equal to 557 kJ/mol.

$$\frac{d\alpha}{dt} = 9.81 \cdot 10^7 \cdot A \cdot exp(-\frac{557 \cdot 10^3}{RT}) \tag{1}$$

Where α is the degree of reaction (varying from 0 to 1) and A is the available reaction area given by Equation 14 when the initial area of silicon ($A_{0,Si}$) is limiting the reaction area. The agglomeration factor (F) is included to correct for agglomeration of the silicon and silica, causing a reduction in available reaction area during heating. The value of the agglomeration factor is set to be 1 below the melting point of quartz and 0,5 above.

$$A = A_{0,Si} \cdot (1 - \alpha) \cdot F \tag{14}$$

The reaction rate of the two SiO producing reactions in a silicon furnace, $Si + SiO_2$ and $SiO_2 + SiC$ is within the same range as long as their available reaction area is within the same range. The reaction rate of both reactions increase significantly with temperature and so does their available reaction area as you go deeper in a silicon furnace. This means that the phase distribution in the hot temperature zone is determining weather reaction with silicon or silicon carbide contributes the most towards formation of SiO gas.

The weakness of the model is the calculation of available reaction area. There is a trend in the difference between experimental data and modelled data as a function of particle size used in each experiment. This indicate that the expression for available reaction area could be improved. The reaction rate of silicon and silica is shown to increase with time and temperature but work done by Andersen indicate that there might be a local reduction of rate around the melting point of silica. It would therefor be interesting to run a few experiments at temperatures ranging from 1700 to 1750°C to see weather a local drop in reactivity due to a high silica reactivity can be observed. Despite that, the model is considered to predict reasonable values for reaction rate of a silicon and silica mixture in the range from 1650 to 1950°C.

References

[1] L. D. Alphei et al. "Reaction enhanced wetting of quartz by silicon droplets and its instabilities". In: *Journal of Materials Science* 48 (2013), pp. 7350–7359.

[2] V. Andersen. "Condensate formation in the silicon process". MA thesis. Norwegian University of Science and Technology, 2011.

[3] F. O. Bakken and C. O. Paulsen. *Thermal stability of quartz for silicon process*. Norwegian University of Science and Technology, 2013.

[4] D. Bandyopadhyay. "The Ti-Si-C system (titanium-silicon-carbon)". In: *Journal of phase equilibria and diffusion* 25.5 (2004), pp. 415–420.

[5] S. Bao et al. "Production og SiO gas in the silicon process". In: *The thirteenth International Ferroalloys Congress - Efficient technologies in ferroalloy industry*. 2013, pp. 273–282.

[6] Blackman and Gahan. *Si Chemical Data*. 7th ed. Wiley, 2014.

[7] L. Brewer and R. K. Edwards. "The Stability of SiO Solid and Gas". In: *The Journal of Physical Chemistry* 58.4 (1954), pp. 351–358.

[8] W. D. Callister and J. D. G. Rethwisch. *Materials science and engineering and introduction*. 8th ed. Wiley, 2009, p. 464.

[9] J. A. Champion, B. J. keene, and S. Allen. "Wetting of refractory materials by molten metallides". In: *Journal of Materials Science* 8 (1973), pp. 423–426.

[10] A. Ciftja, T. A. Engh, and M. Tangstad. "Wetting Properties of Molten Silicon with Graphite Materials". In: *Metallurgical and Materials Transactions A* 41 (2010), pp. 3183–3195.

[11] O. Dezellus et al. "Wetting and infiltration of carbon by liquid silicon". In: *Journal of Materials Science* 40 (2005), pp. 2307–2311.

[12] B. Drevet et al. "Wetting and adhesion of Si on Si3N4 and BN substrates". In: *Journal of the European Ceramic Society* 29 (2009), pp. 2263–2367.

[13] E.Fadeeva et al. *Laser Surface Modification of Biomaterials*. Woodhead Publishing, 2016.

[14] H. Fujii et al. "Effect of gas evolution at solid-liquid interface on contact angle between liquid Si and SiO2". In: *Journal of Materials Science* 34 (1999), pp. 3165–3168.

[15] J. Hjelen. *Scanning elektron-mikroskopi*. Metallurgisk institutt, NTH, 1986.

[16] R. Johnson and A. Myan. "Phase Diagrams for the Systems Si-O and Cr-O". In: *Journal of the American Ceramic Society* 51.8 (1968), pp. 430–433.

[17] K. F. Jusnes. unpublished, to be published in monograph. 2020.

[18] K. F. Jusnes, M. Tangstad, and E. Ringdalen. "Phase transformations in quartz used in silicon and ferrosilicon production". unpublished. 2020.

[19] K. F. Jusnes, M. Tangstad, and E. Ringdalen. "Shock Heating of Quartz used in Silicon and Ferrosilicon Production". In: *Infacon XV: International Ferro-Alloys Congress*. Ed. by R. Jones and P. den Hoed. 2018.

[20] H. Kanai et al. "Wetting and reaction between Si droplet and SiO2 substrate". In: *Journal of Materials Science* 42 (2007), pp. 9529–9535.

[21] M. E. Kjelstadli. "Kinetics and Mechanism of Phase Transformations from Quartz to Cristobalite". MA thesis. Norwegian University of Science and Technology, 2016.

[22] C. Klein and C. S. Hurlbut. *Manual of Mineralogy*. 21st ed. Wiley, 1993, pp. 527–530.

[23] S. Nishimurab, S. Matsumotoa, and K. Terashima. "Variation of silicon melt viscosity with boron addition". In: *Journal of Crystal Growth* 237-239 (2002), pp. 1667–1670.

[24] E. Nordnes. *Softening and Melting Properties of Quartz*. Norwegian University of Science and Technology, 2018.

[25] E. Nordnes. "Softening and Melting Properties of Quartz". MA thesis. Norwegian University of Science and Technology, 2019.

[26] S. M. Production. *Newsletter Q1/17, New projects: Controlled Tapping*. URL: https://www.ntnu.edu/documents/1263635097/1271002173/SFI+Metal+Production+Newsletter+Q1+2017.pdf/2c329143-b923-4597-a8a9-9a63aa5cd3aa. (accessed: 02.08.2019).

[27] E. Ringdalen. "Quartz properties in the silicon production". In: *Silicon for the Chemical and Solar Industry XII. Trondheim.* 2014, pp. 7–18.

[28] E. Ringdalen et al. "Melting properties of quartz and their effect on industrial Si and FeSi production." In: *XXV CONFERENCE «ALUMINIUM OF SIBERIA»*. 2019, pp. 611–620.

[29] E. Ringdalen and M. Tangstad. "Softening and Melting of SiO2, an Important Parameter for Reactions with Quartz in Si Production". In: *Advances in Molten Slags, Fluxes, and Salts: Proceedings of The 10th International Conference on Molten Slags, Fluxes and Salts (MOLTEN16)*. Ed. by R. G. Reddy et al. 2016, p. 44.

[30] T. Rosenqvist. *Principles of Extractive Metallurgy*. Tapir Academic Press, Trondheim, 2004, pp. 112–114.

[31] Y. Satoa et al. "Viscosity of molten silicon and the factors affecting measurement". In: *Journal of Crystal Growth* 249 (2003), pp. 404–415.

[32] A. Schei, J. K. Tuset, and H. Tveit. *Production of High Silicon Alloys*. Trondheim: Tapir, 1998, pp. 21–29.

[33] S. Schurre, J. Gröbner, and R. Scgmid-Fetzer. "Thermodynamics and phase stability in the Si-O System". In: *Journal of Non-Crystalline Solids* 336 (2004), pp. 1–25.

[34] C. Sindland. *Internal report, Reactivity of silicon and silica mixtures*. Norwegian University of Science and Technology, June 2019.

[35] C. Sindland. *Reactivity of silicon and silica mixtures, specialisation project*. Norwegian University of Science and Technology, December 2019.

[36] S. J. Stevens, R. J. Hand, and J. H. Sharp. "The polymorphism of silica". In: *Journal of Materials Science* 32 (1997), pp. 2929–2935.

[37] M. Tangstad. personal communication. Nov. 2019.

[38] M. Tangstad. *Metal Production in Norway*. Trondheim: Akademika Publishing, 2013.

[39] M. Tangstad et al. "Reaction Rates of 2SiO2+SiC=3SiO+CO in Pellets at Elevated Temperatures". In: *Aspects Min Miner Sci* 3.2 (2019).

[40] J. Vangskåsen. “Condensate formation in the silicon process”. MA thesis. Norwegian University of Science and Technology, 2011.

[41] R. E. Walpole et al. *Probability and Statistics for Engineers and Scientists*. 9th ed. Pearson Education Limited, 2017, pp. 409–431.

[42] Z. Yuan, W. L. Huang, and K. Mukai. “Wettability and reactivity of molten silicon with various substrates”. In: *Applied Physics A* 78 (2004), pp. 617–622.

Appendix I - Derivation of Equation 16

Copy of Equation 13, 14 and 16.

$$\frac{d\alpha}{dt} = k_0 \cdot A_{Si} \cdot exp(-\frac{Q}{RT}) \tag{13}$$

$$A_{Si} = A_{0,Si} \cdot (1-\alpha) \cdot F \tag{14}$$

$$ln(-ln(1-\alpha)) - ln(A_{0,Si} \cdot F) - ln(t) = ln(k_0) - \frac{Q}{RT} \tag{16}$$

Derivation of equation 16 from Equation 13 and 14.

Rearrangement of equation 13 with Equation 14 inserted gives:

$$\frac{1}{1-\alpha} \cdot d\alpha = k_0 \cdot A_{0,Si} \cdot F \cdot exp(-\frac{Q}{RT}) \cdot dt \tag{19}$$

Integrating both sides from $\alpha = 0$ and t=0 to α and t gives:

$$ln(1-\alpha) \cdot (-1) = k_0 \cdot A_{0,Si} \cdot F \cdot exp(-\frac{Q}{RT}) \cdot t \tag{20}$$

Taking the natural logarithm of both sides gives:

$$ln(-ln(1-\alpha)) = ln(k_0) + ln(A_{0,Si} \cdot F) - \frac{Q}{RT} + ln(t) \tag{21}$$

Further rearrangement gives Equation 16

Appendix II - Macro images

The images of cut crucibles is presented in Figure 74 to 88 below.

Quartz A

Figure 74: Crucible after the first cutting, from experiment M2 where quartz A was heated to 1650 °C for for 120min.

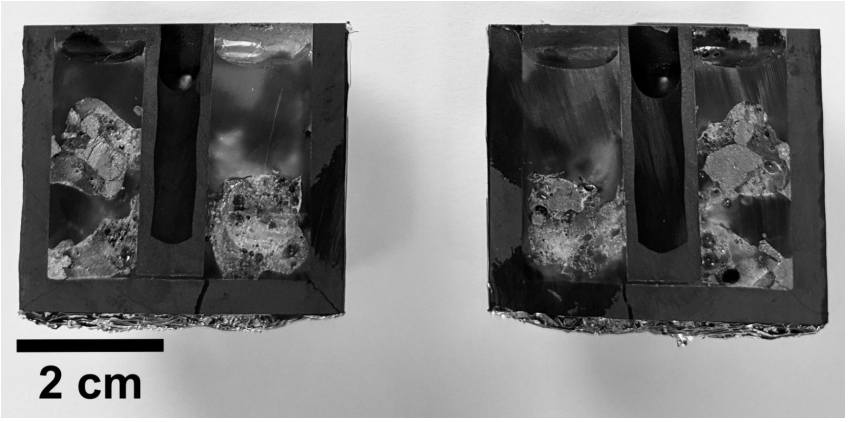

Figure 75: Crucible after the first cutting, from experiment M1 where quartz A was heated to 1750 °C for for 120min.

Figure 76: Crucible after the first cutting, from experiment M3 where quartz A was heated to 1850 °C for for 60min.

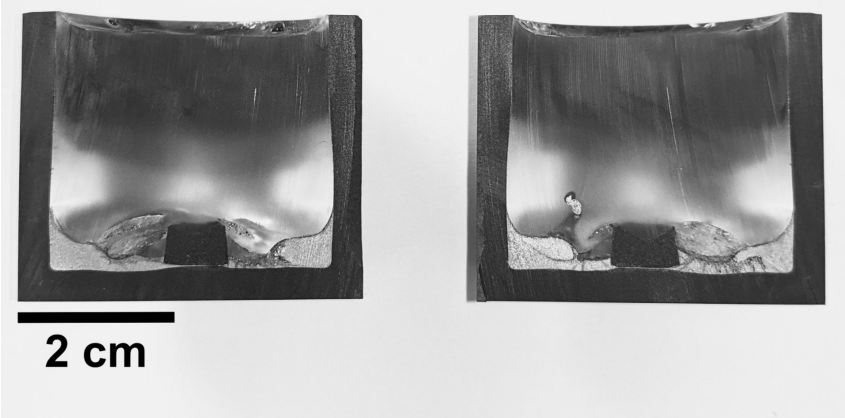

Figure 77: Crucible after the first cutting, from experiment M4 where quartz A was heated to 1950 °C for for 60min.

Quartz B

Figure 78: Crucible after the first cutting, from experiment M5 where quartz B was heated to 1650 °C for for 120min.

Figure 79: Crucible after the first cutting, from experiment M7 where quartz B was heated to 1850 °C for for 60min.

Quartz C

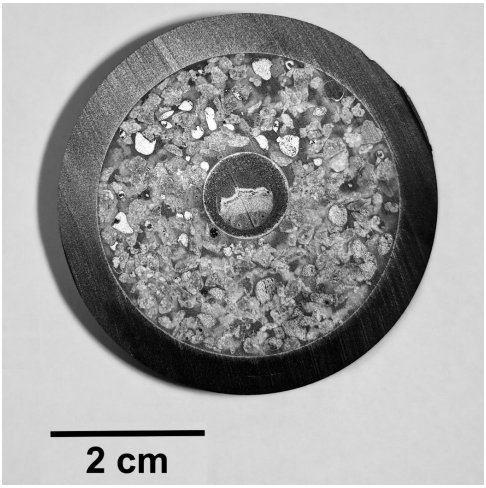

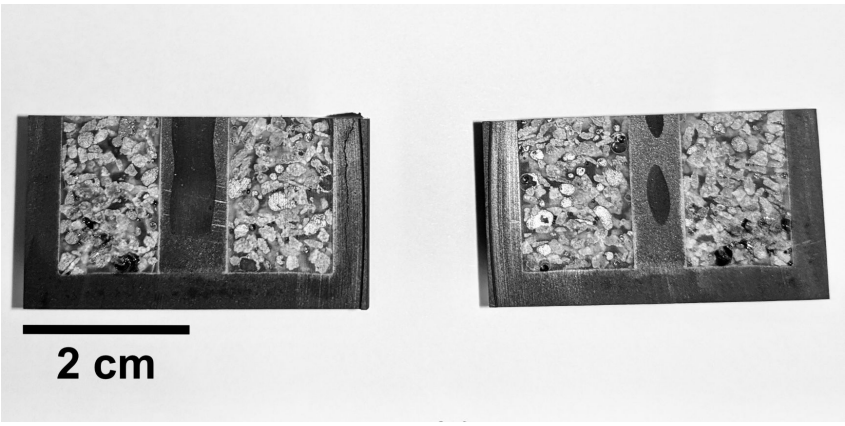

Figure 80: Crucible after the first cutting, from experiment M14 where quartz C was heated to 1650 °C for for 120 min.

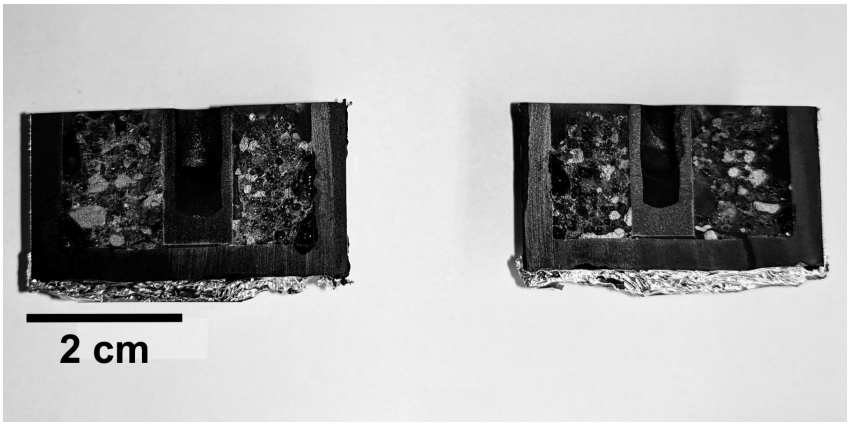

Figure 81: Crucible after the first cutting, from experiment M12 where quartz C was heated to 1750 °C for for 120 min.

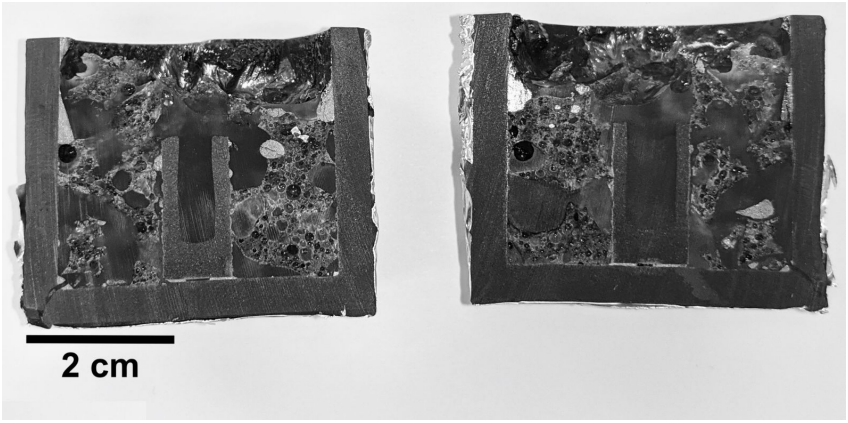

Figure 82: Crucible after the first cutting, from experiment M8 where quartz C was heated to 1850 °C for for 60min.

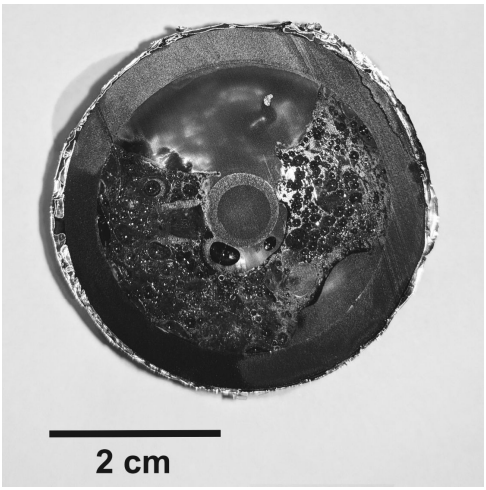

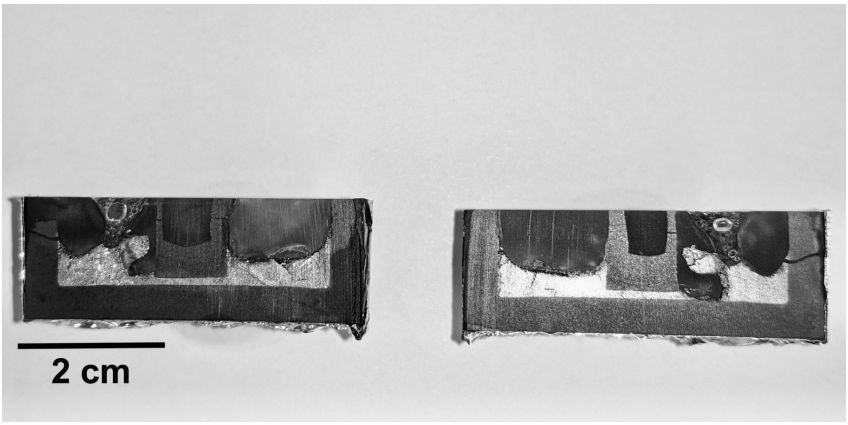

Figure 83: Crucible after the first cutting, from experiment M13 where quartz C was heated to 1950 °C for for 60 min.

Quartz D

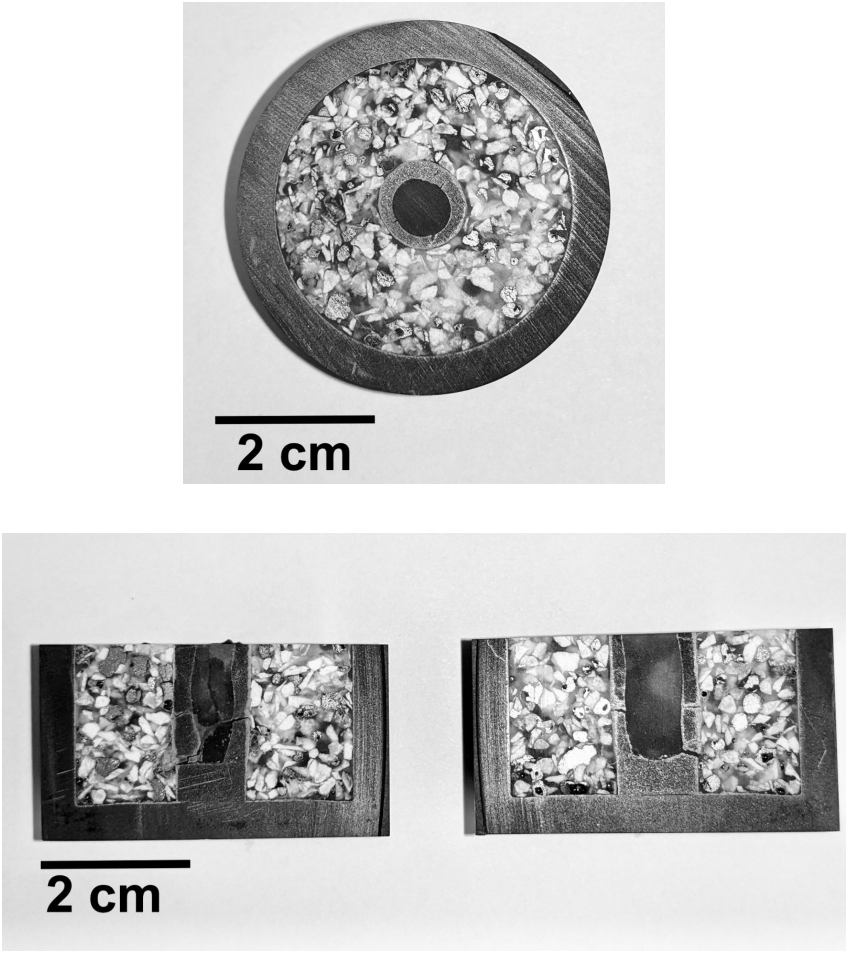

Figure 84: Crucible after the first cutting, from experiment M9 where quartz D was heated to 1650 °C for for 120 min.

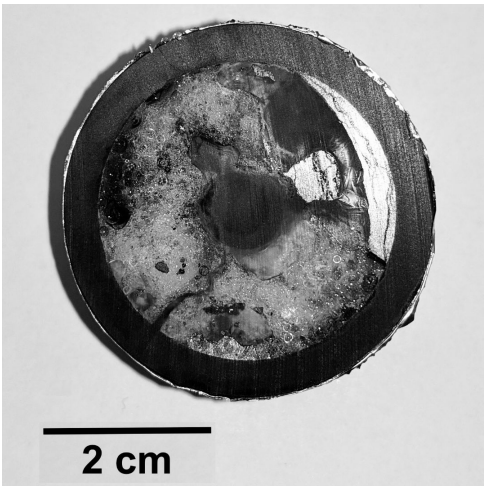

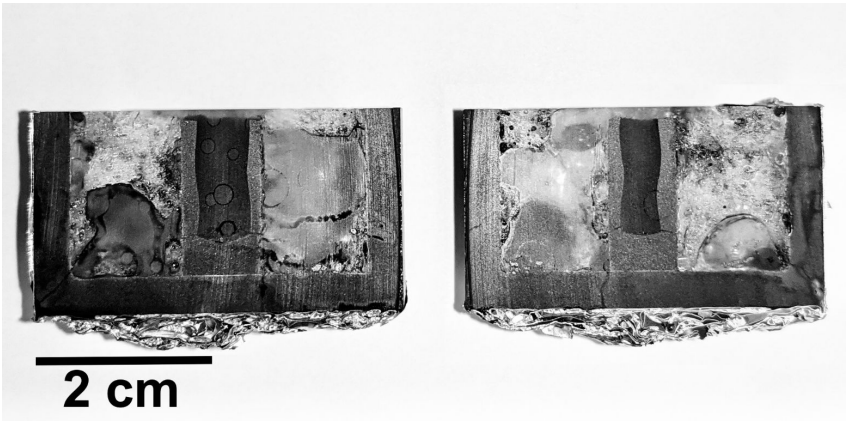

Figure 85: Crucible after the first cutting, from experiment M10 where quartz D was heated to 1850 °C for for 60 min.

Quartz E

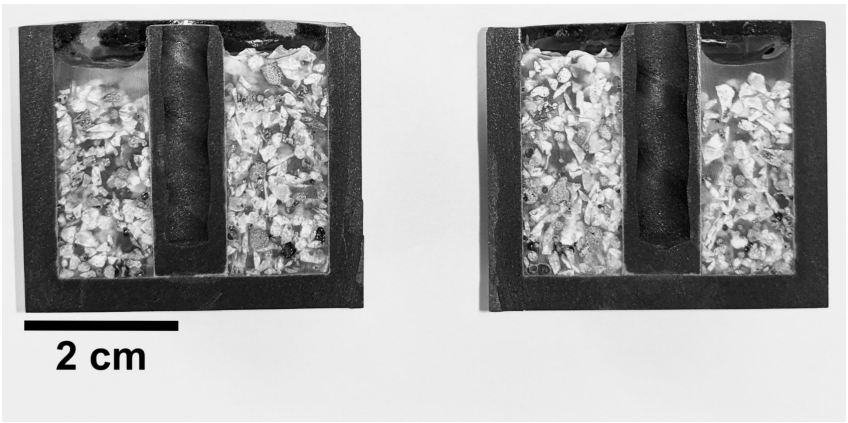

Figure 86: Crucible after the first cutting, from experiment M6 where quartz E was heated to 1650 °C for for 120min.

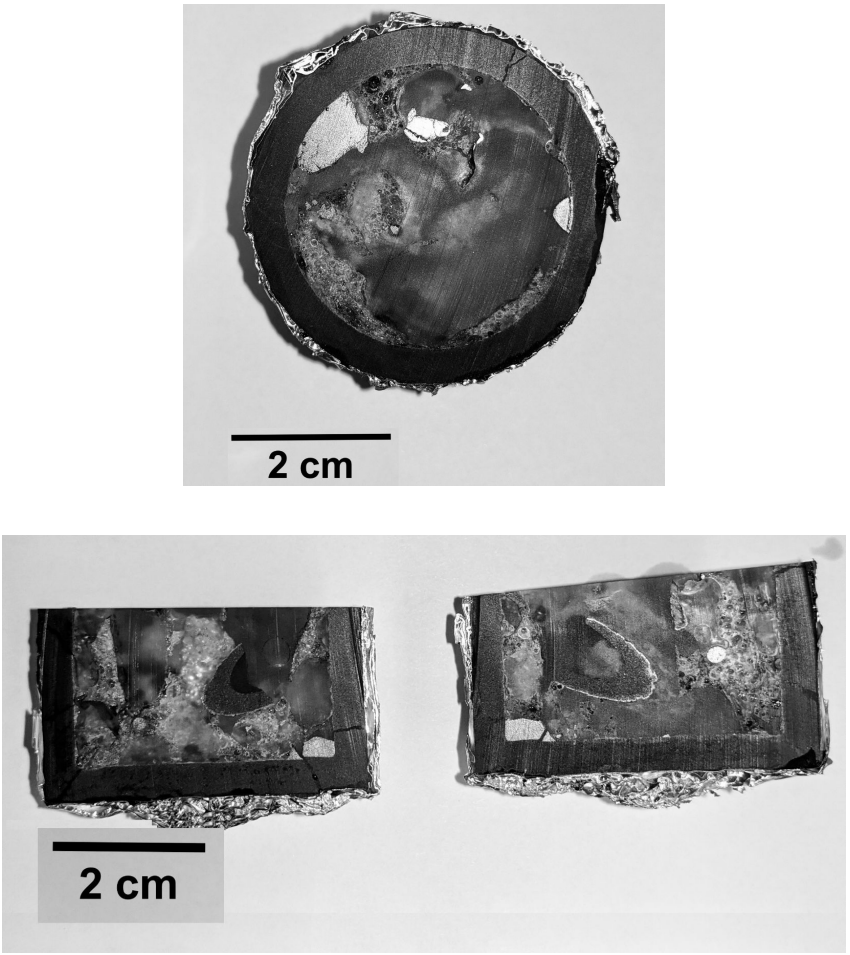

Figure 87: Crucible after the first cutting, from experiment M11 where quartz E was heated to 1850 °C for for 60 min.

Quartz E, 2-5mm

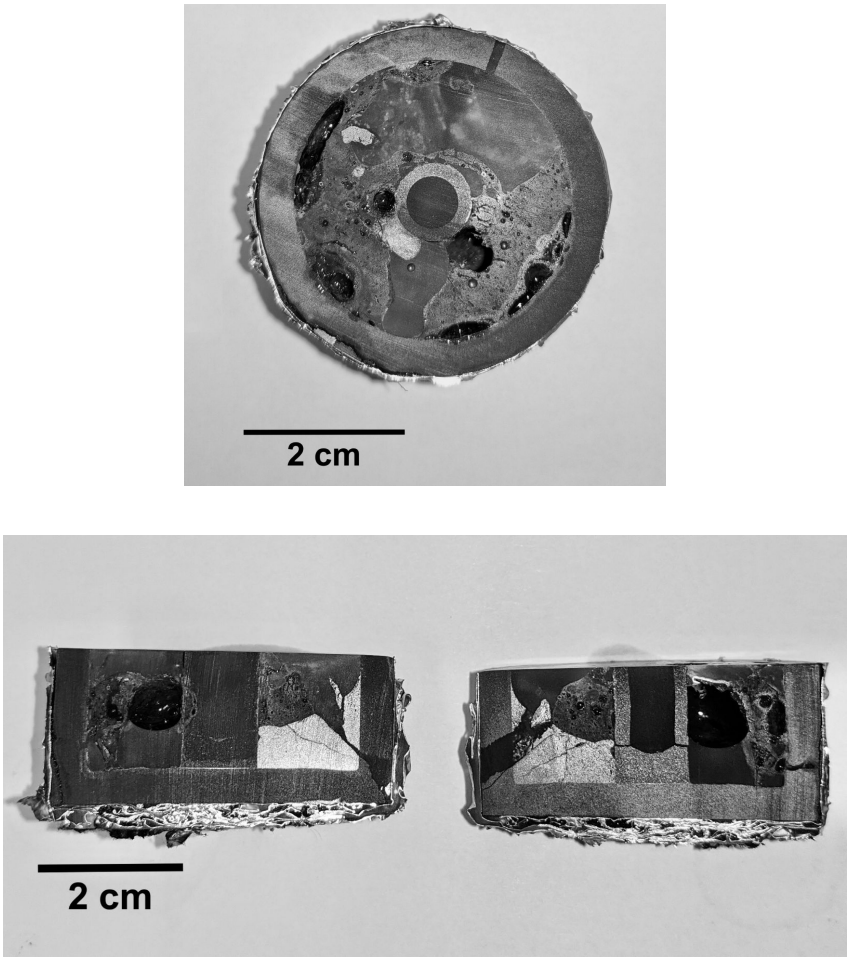

Figure 88: Crucible after the first cutting, from experiment M17 where quartz E was heated to 1850 °C for for 60 min.

Quartz E, 5-8mm

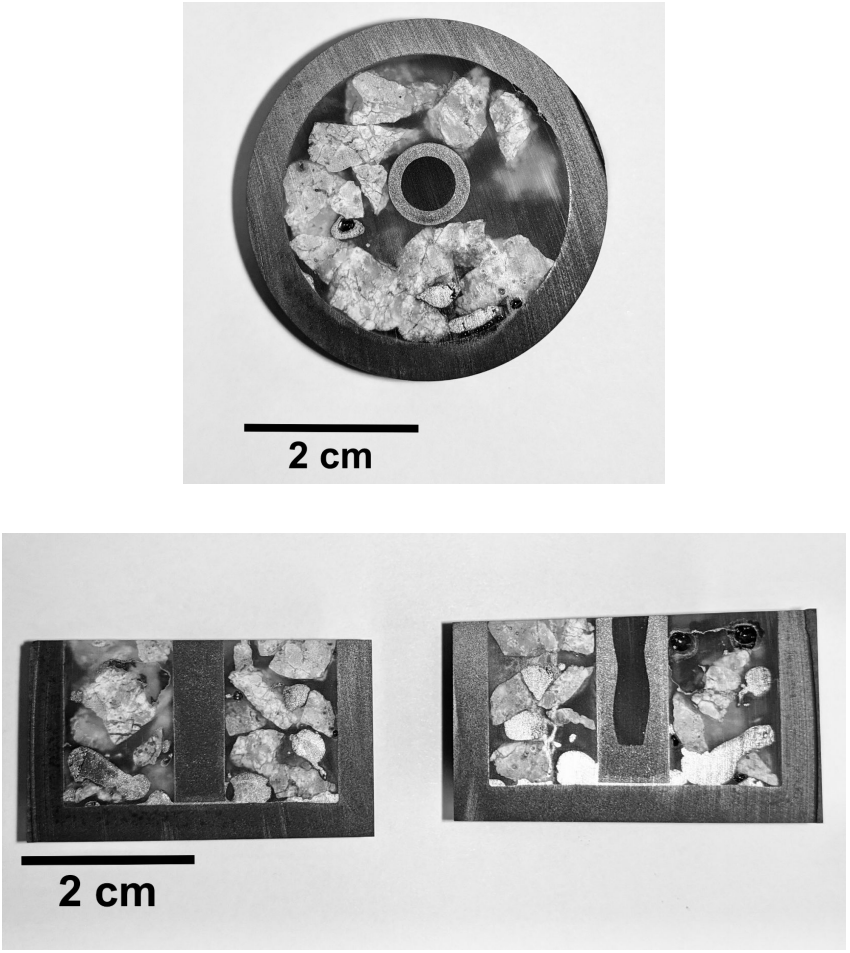

Figure 89: Crucible after the first cutting, from experiment M15 where quartz E was heated to 1650 °C for for 120 min.

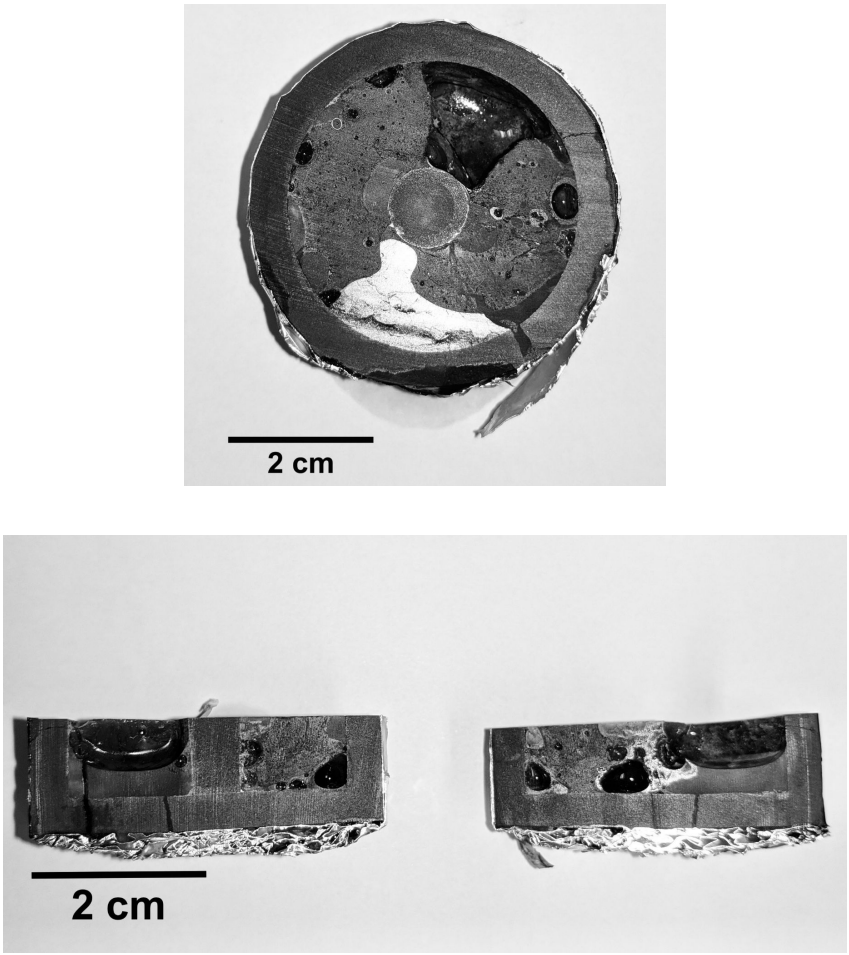

Figure 90: Crucible after the first cutting, from experiment M16 where quartz E was heated to 1850 °C for for 60 min.

Appendix III - Light Optical Microscopy images (LOM)

LOM images was taken at positions as illustrated in Figure 91. All of the samples have been investigated in LOM and the images is presented in Figure 92 to 108.

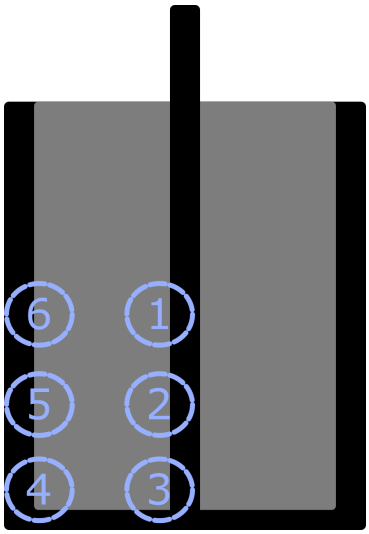

Figure 91: The LOM images was taken at specific areas indicated by numbers in this figure. Each LOM image below are marked with the position it was taken.

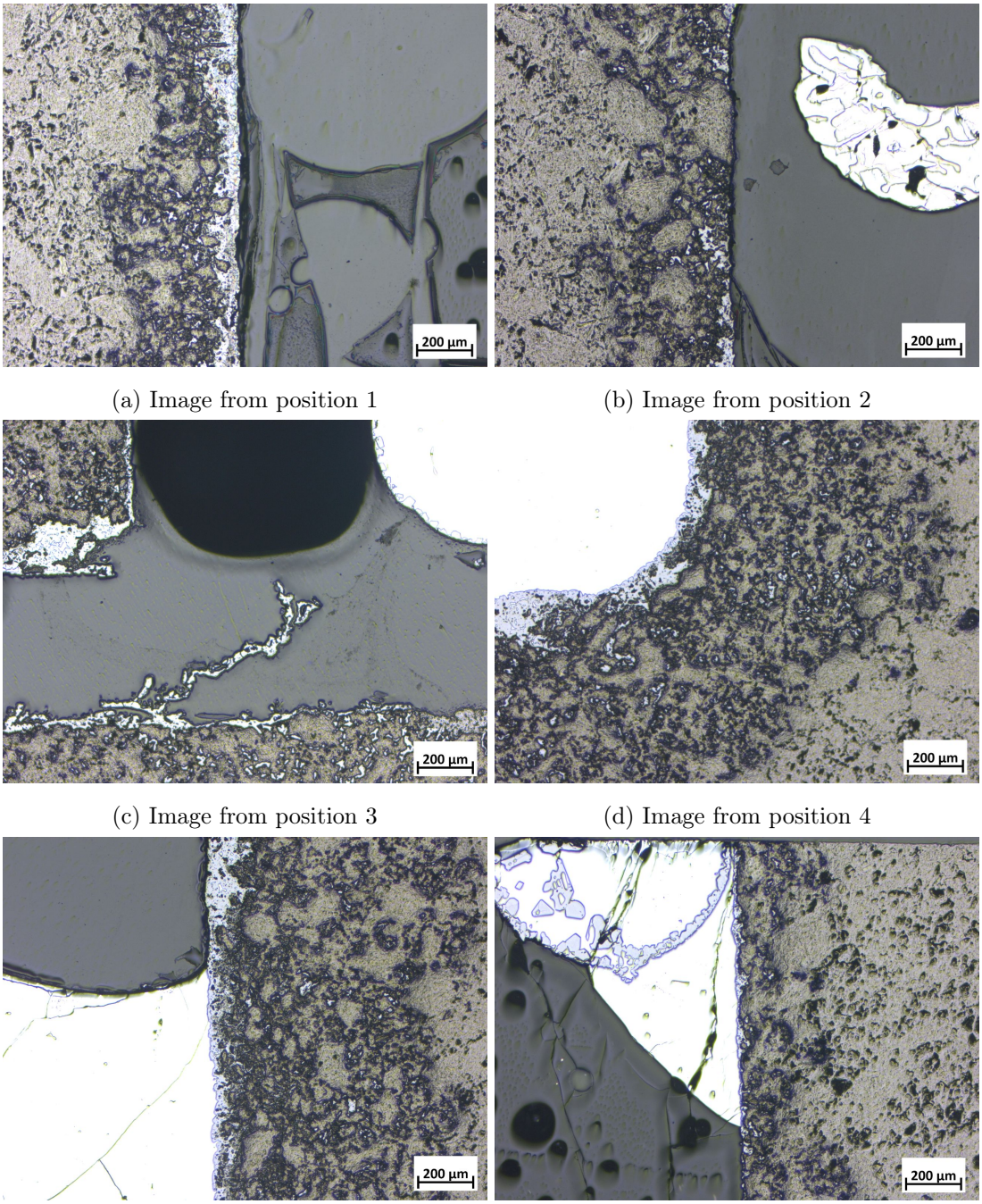

(a) Image from position 1

(b) Image from position 2

(c) Image from position 3

(d) Image from position 4

(e) Image from position 5

(f) Image from position 6MaCen

Figure 92: Image taken by LOM of sample where QZ A was heated at 1750C for 2h, M1.

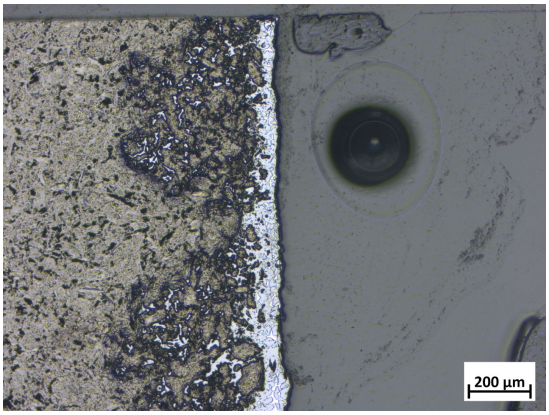

(a) Image from position 1

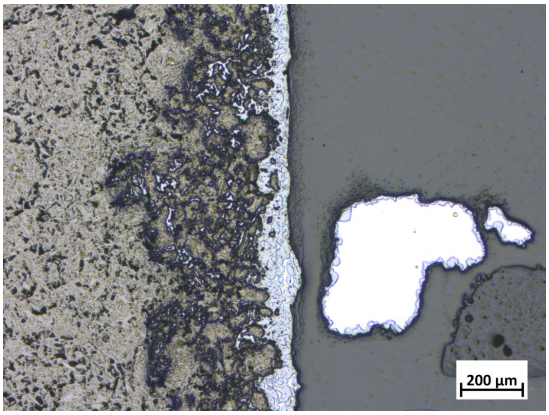

(b) Image from position 2

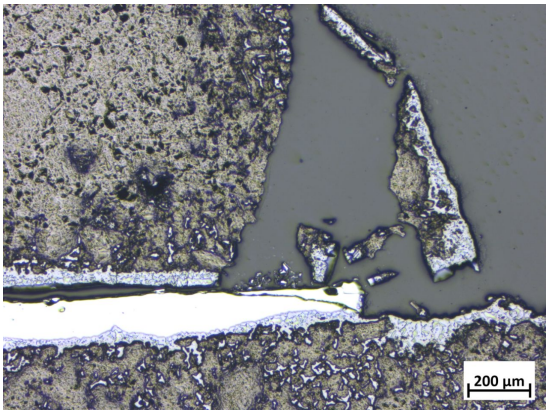

(c) Image from position 3

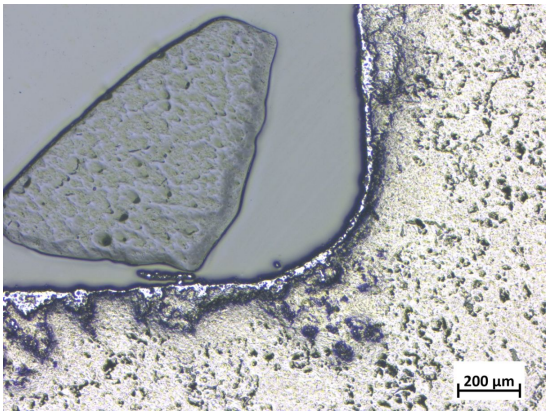

(d) Image from position 4

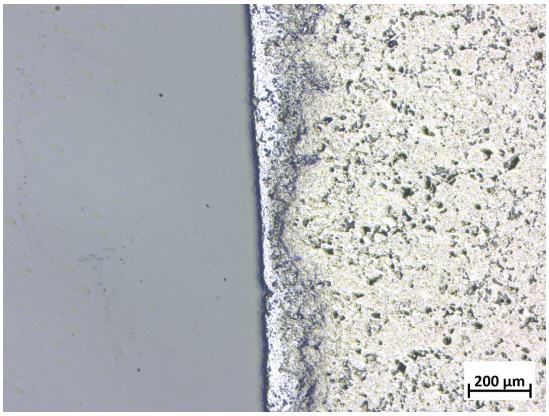

(e) Image from position 5

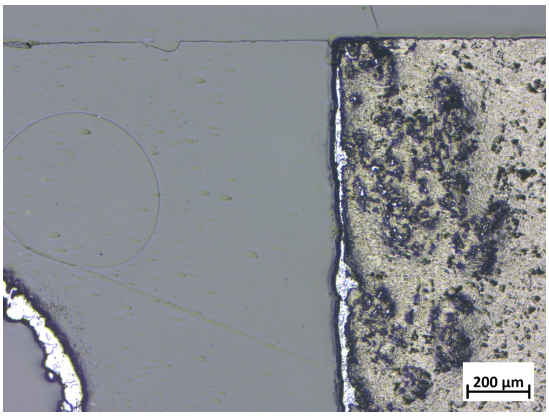

(f) Image from position 6

Figure 93: Image taken by LOM of sample where QZ A was heated at 1650C for 2h, M2.

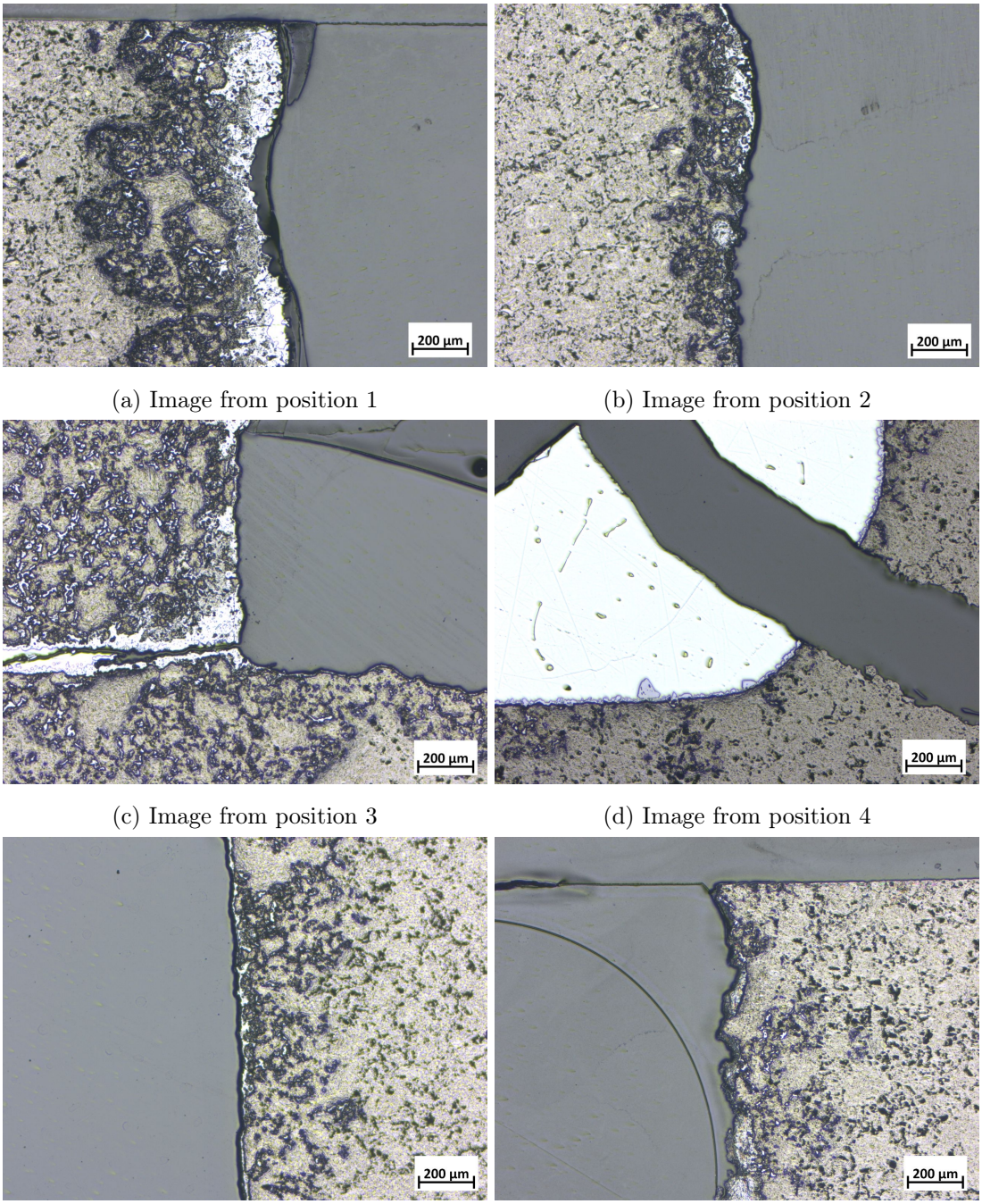

(a) Image from position 1

(b) Image from position 2

(c) Image from position 3

(d) Image from position 4

(e) Image from position 5

(f) Image from position 6

Figure 94: Image taken by LOM of sample where QZ A was heated at 1850C for 1h, M3.

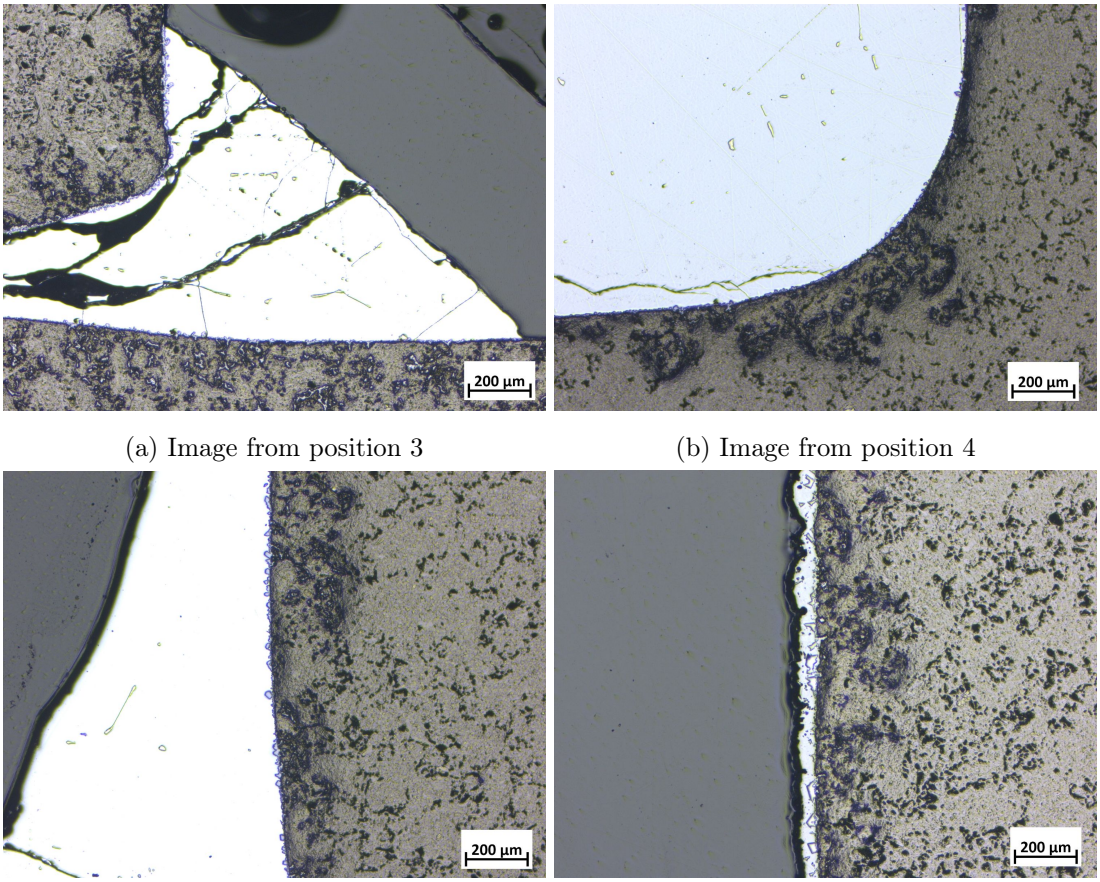

(a) Image from position 3

(b) Image from position 4

(c) Image from position 5

(d) Image from position 6

Figure 95: Image taken by LOM of sample where QZ A was heated at 1950C for 1h, M4.

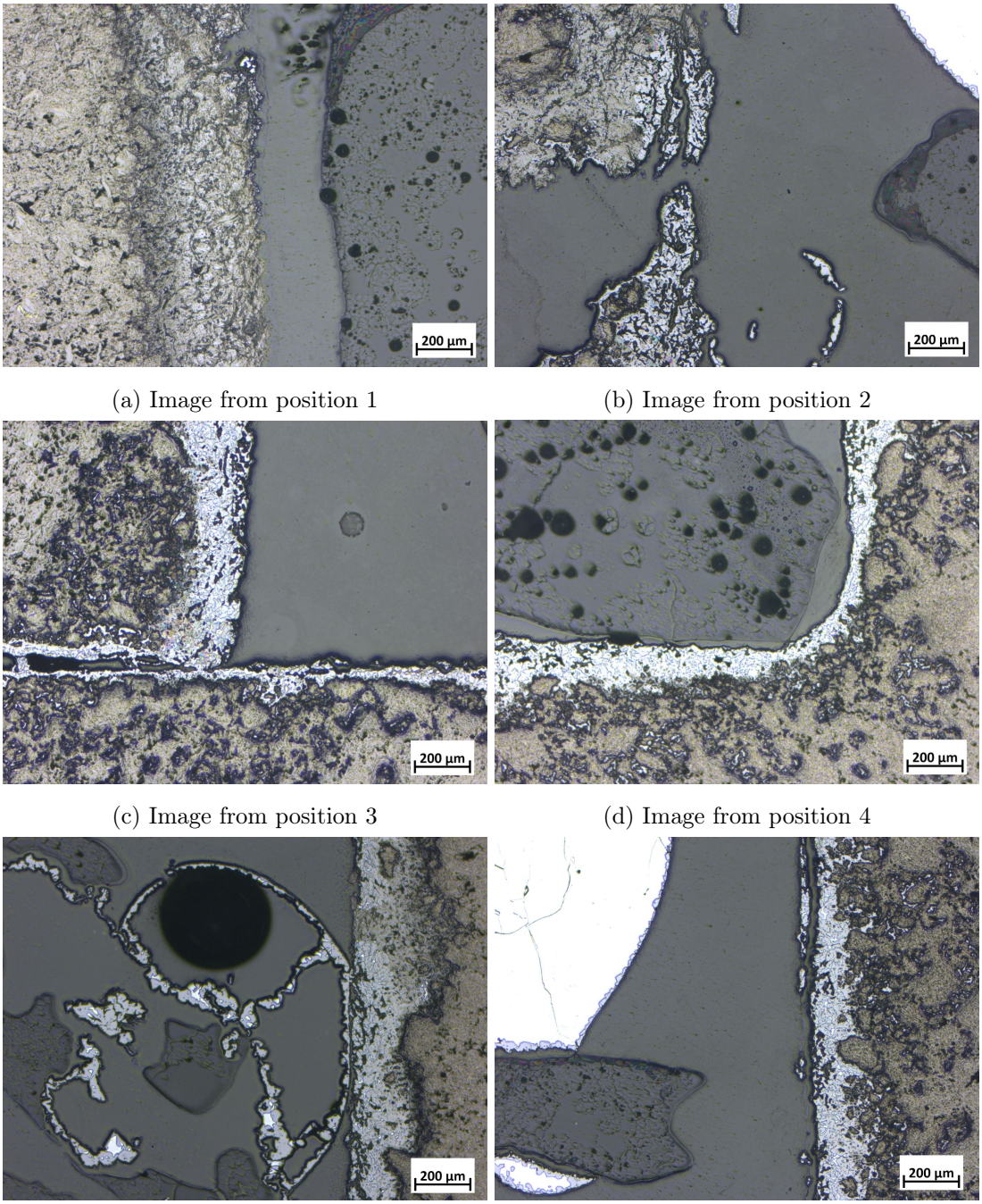

(a) Image from position 1

(b) Image from position 2

(c) Image from position 3

(d) Image from position 4

(e) Image from position 5

(f) Image from position 6

Figure 96: Image taken by LOM of sample where QZ B was heated at 1650C for 2h, M5.

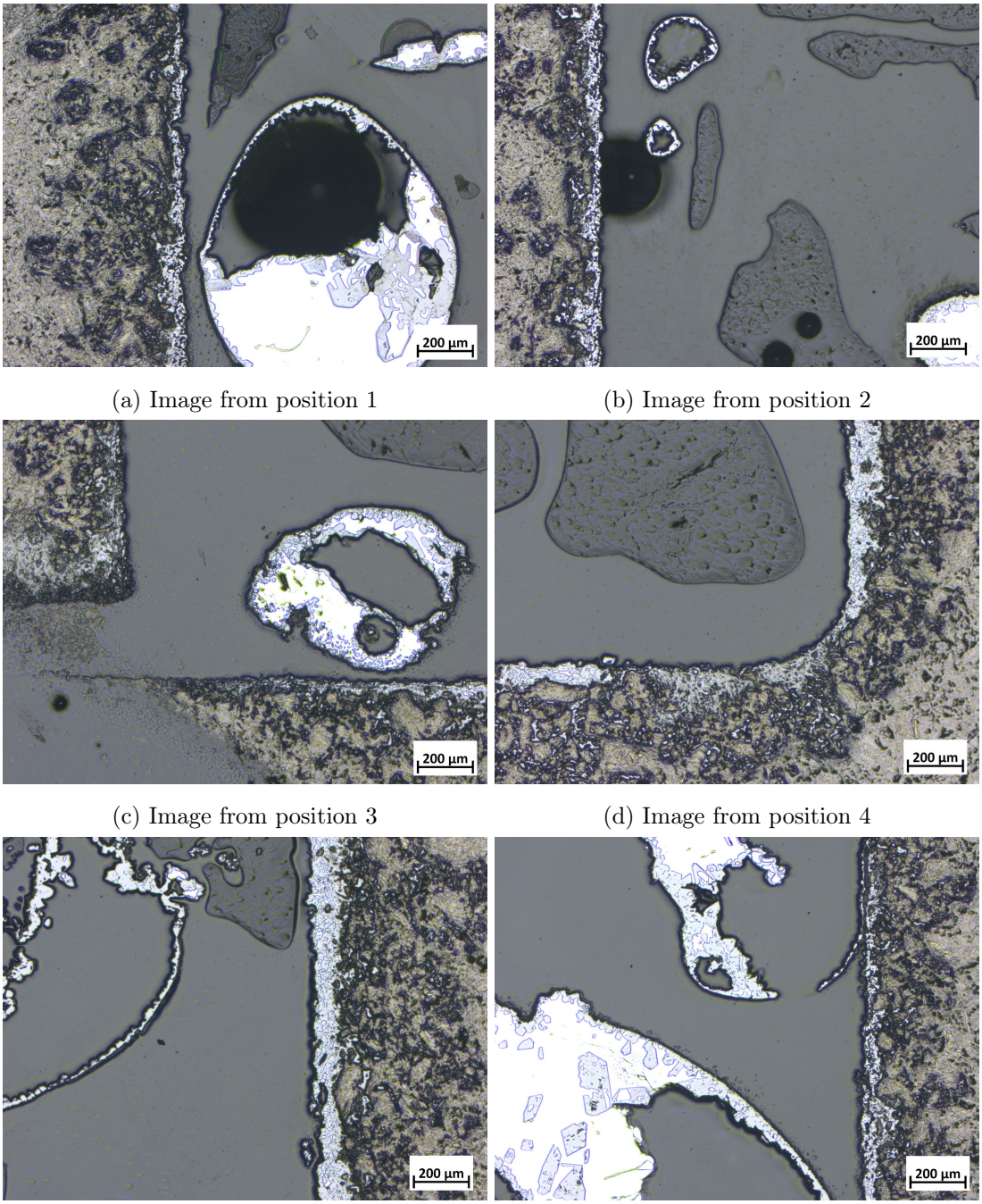

(a) Image from position 1

(b) Image from position 2

(c) Image from position 3

(d) Image from position 4

(e) Image from position 5

(f) Image from position 6

Figure 97: Image taken by LOM of sample where QZ E was heated at 1650C for 2h, M6.

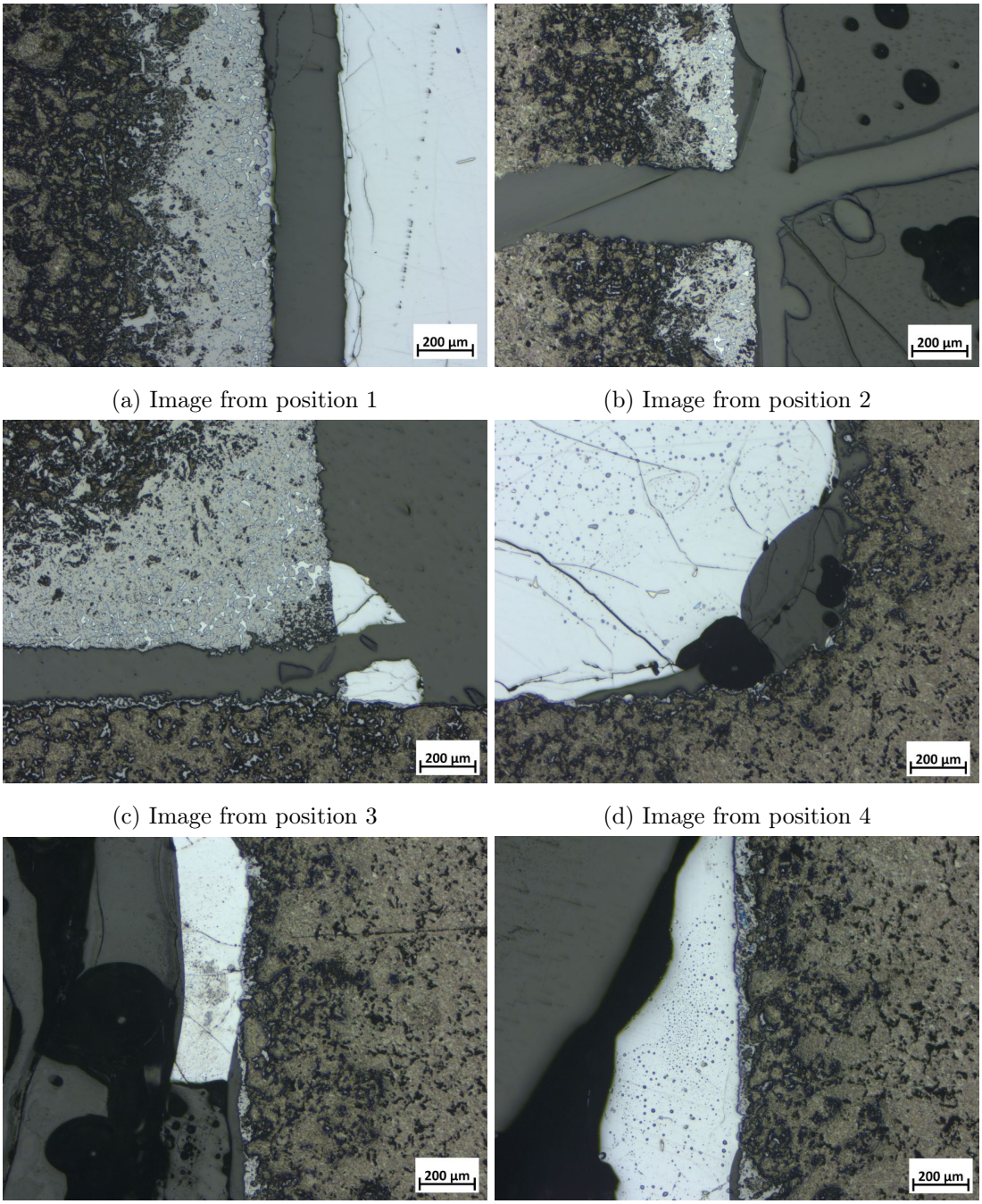

(a) Image from position 1

(b) Image from position 2

(c) Image from position 3

(d) Image from position 4

(e) Image from position 5

(f) Image from position 6

Figure 98: Image taken by LOM of sample where QZ B was heated at 1850C for 1h, M7.

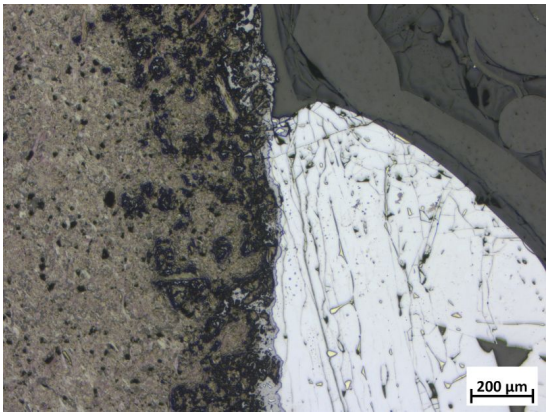

(a) Image from position 1

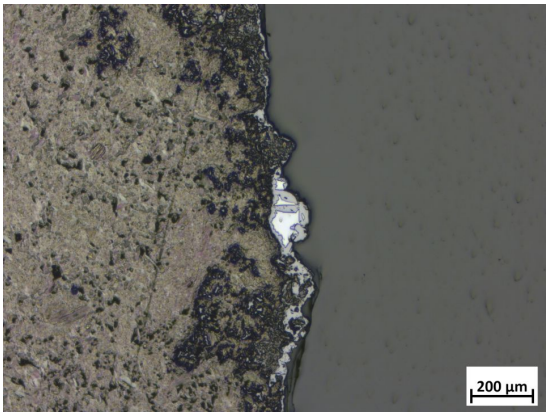

(b) Image from position 2

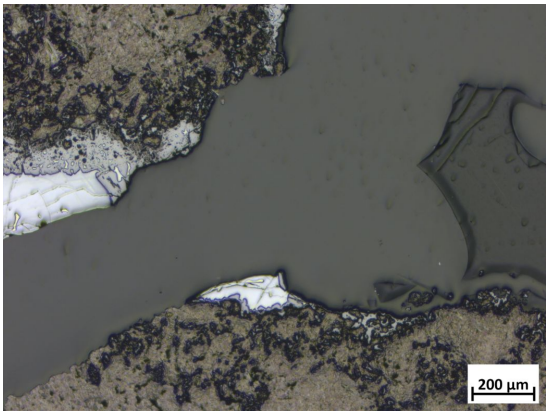

(c) Image from position 3

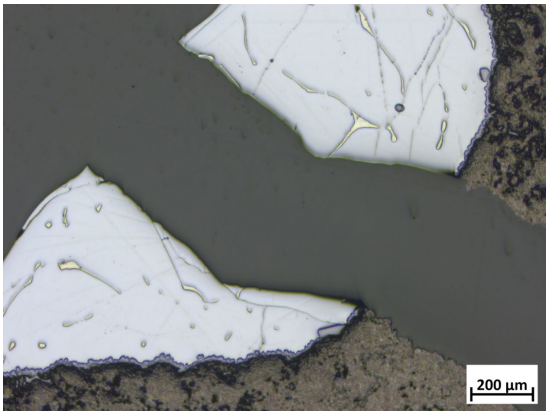

(d) Image from position 4

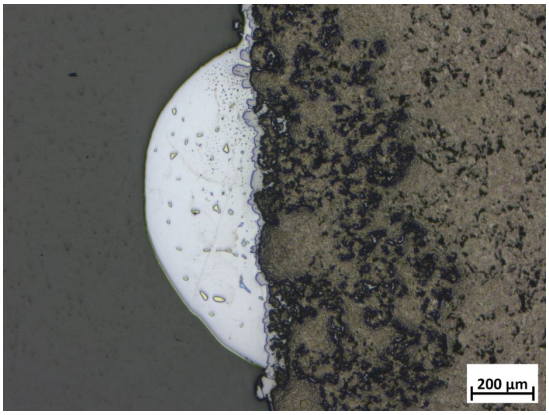

(e) Image from position 5

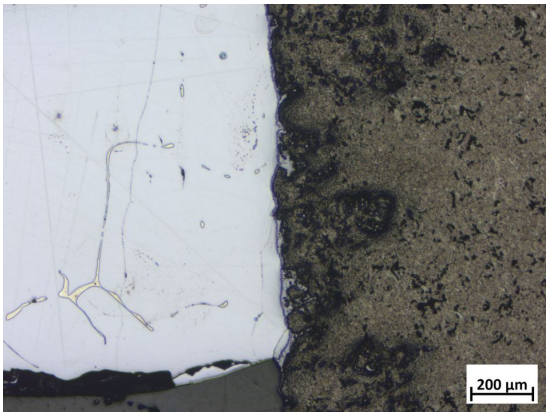

(f) Image from position 6

Figure 99: Image taken by LOM of sample where QZ C was heated at 1850C for 1h, M8.

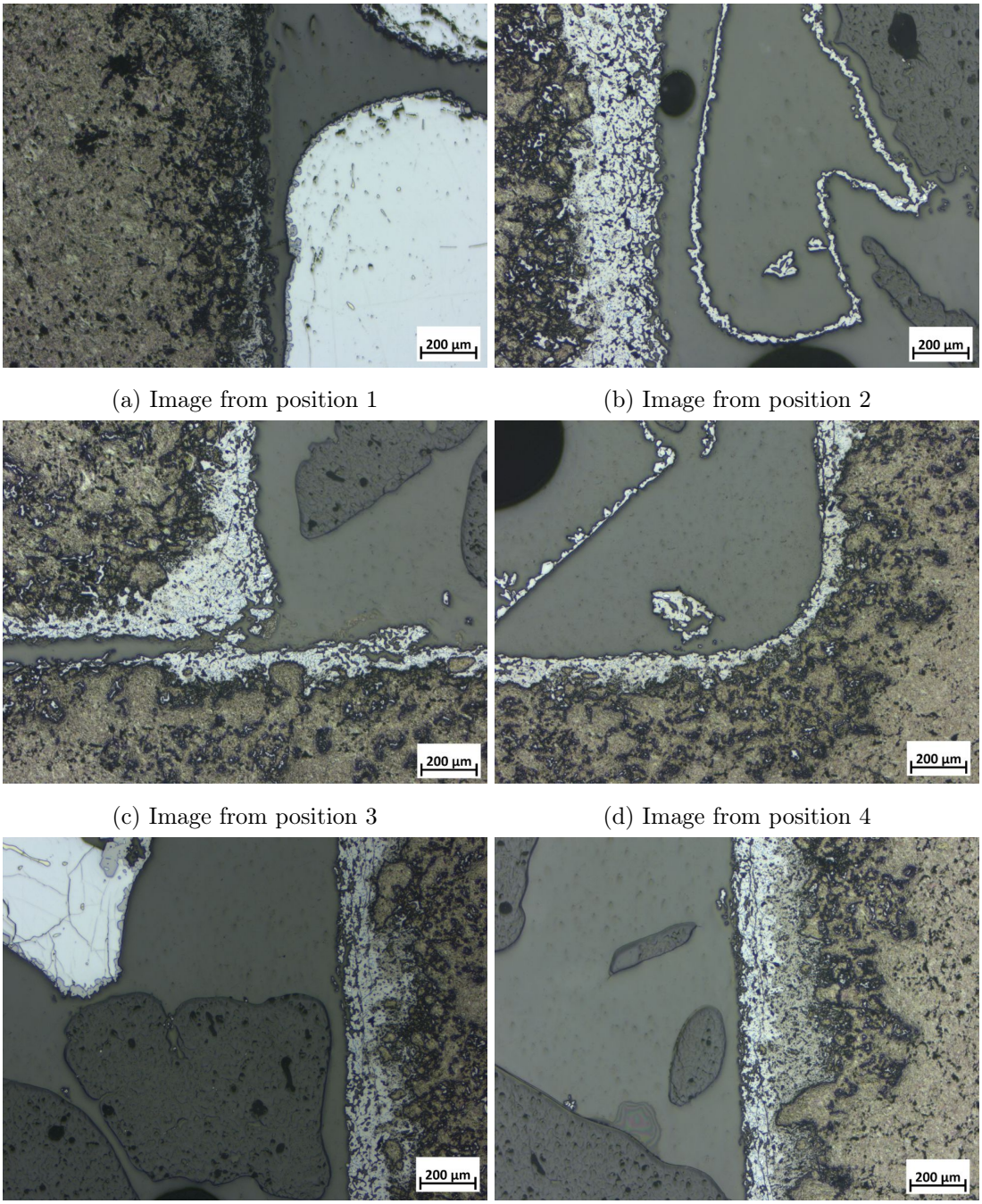

(a) Image from position 1

(b) Image from position 2

(c) Image from position 3

(d) Image from position 4

(e) Image from position 5

(f) Image from position 6

Figure 100: Image taken by LOM of sample where QZ D was heated at 1650C for 2h, M9.

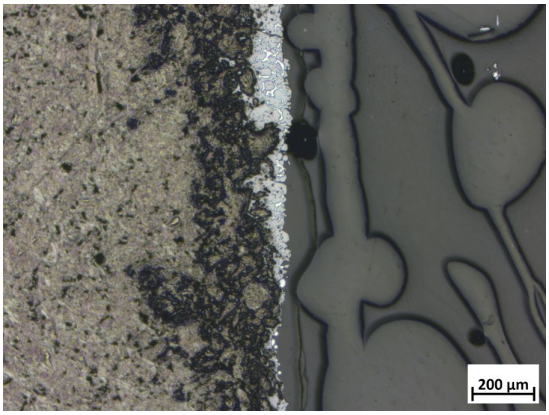

(a) Image from position 1

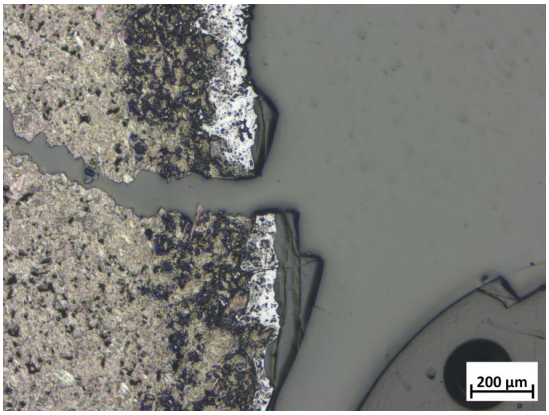

(b) Image from position 2

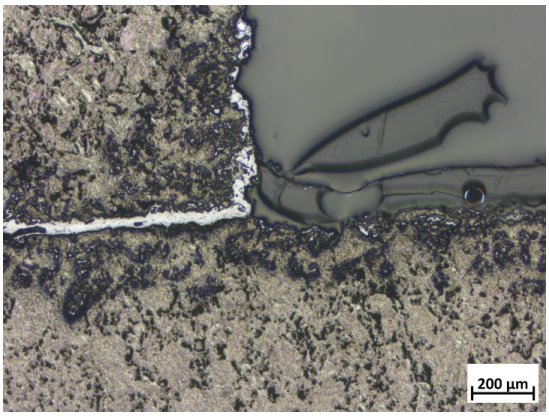

(c) Image from position 3

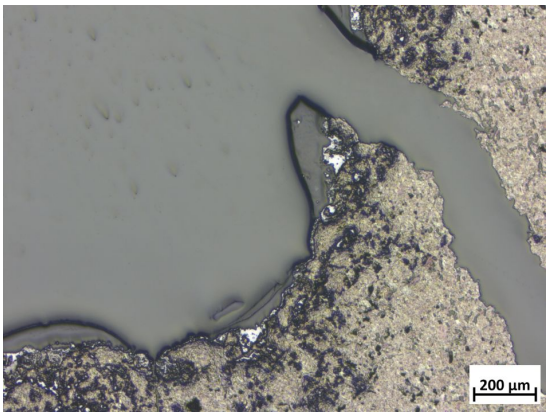

(d) Image from position 4

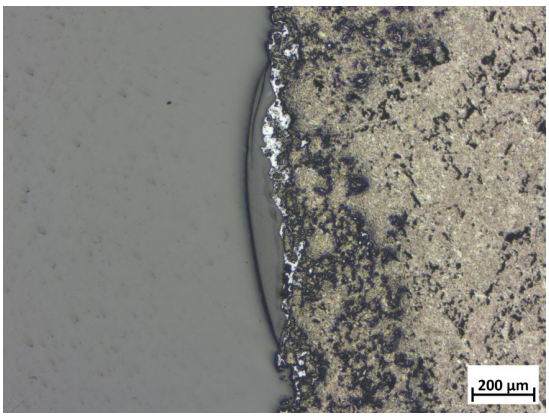

(e) Image from position 5

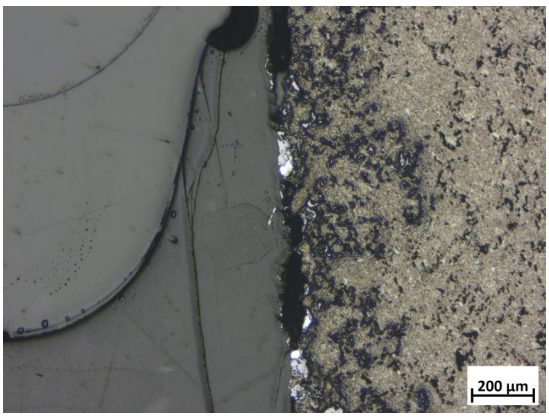

(f) Image from position 6

Figure 101: Image taken by LOM of sample where QZ D was heated at 1850C for 1h, M10.

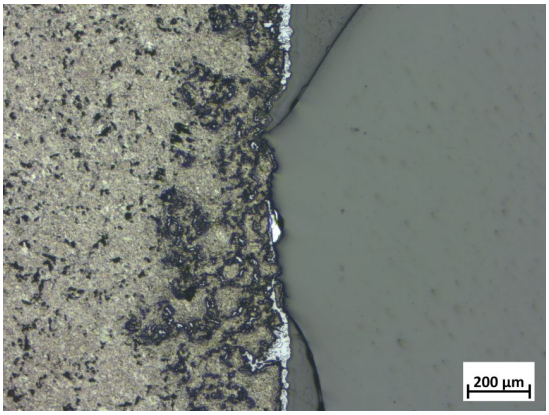

(a) Image from position 1

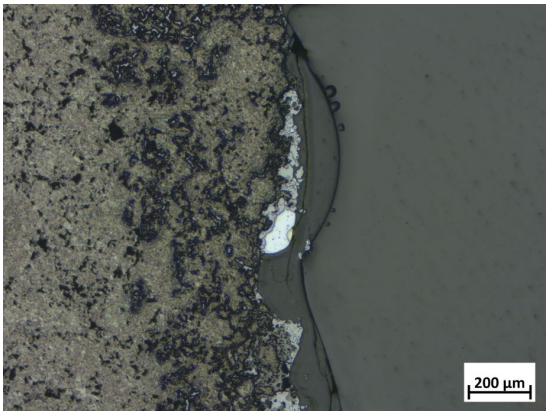

(b) Image from position 2

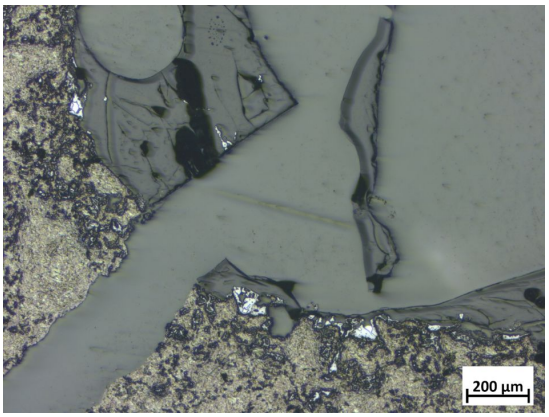

(c) Image from position 3

Figure 102: Image taken by LOM of sample where QZ E was heated at 1850C for 1h, M11.

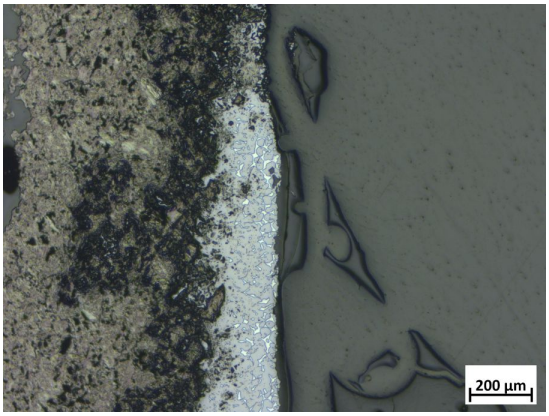

(a) Image from position 1

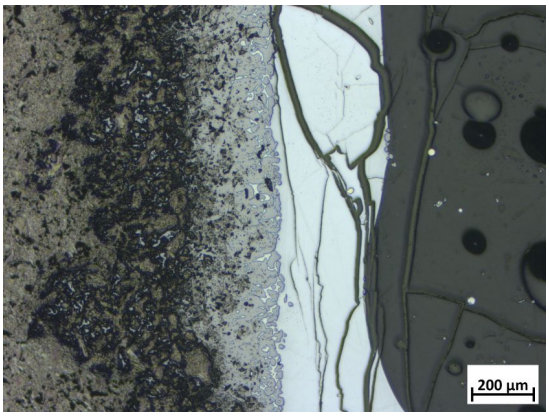

(b) Image from position 2

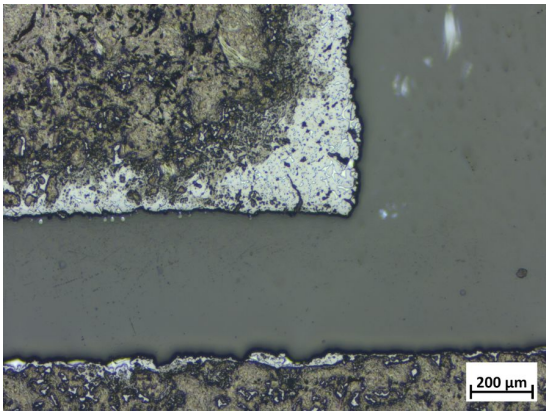

(c) Image from position 3

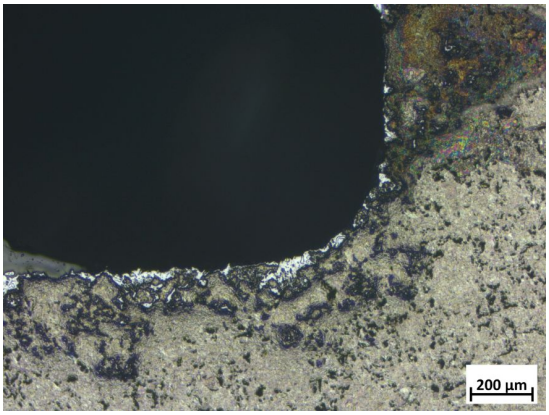

(d) Image from position 4

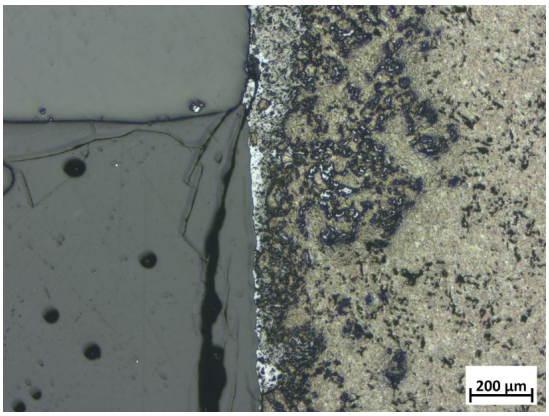

(e) Image from position 5

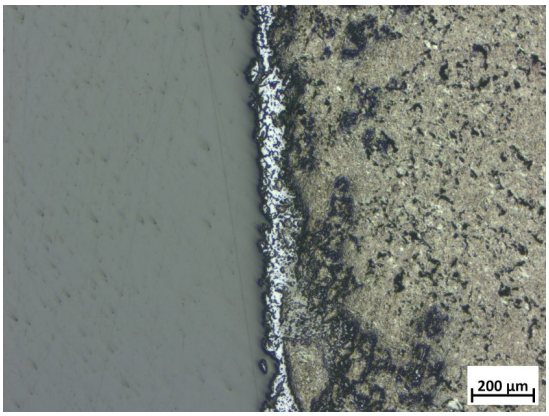

(f) Image from position 6

Figure 103: Image taken by LOM of sample where QZ C was heated at 1750C for 2h, M12.

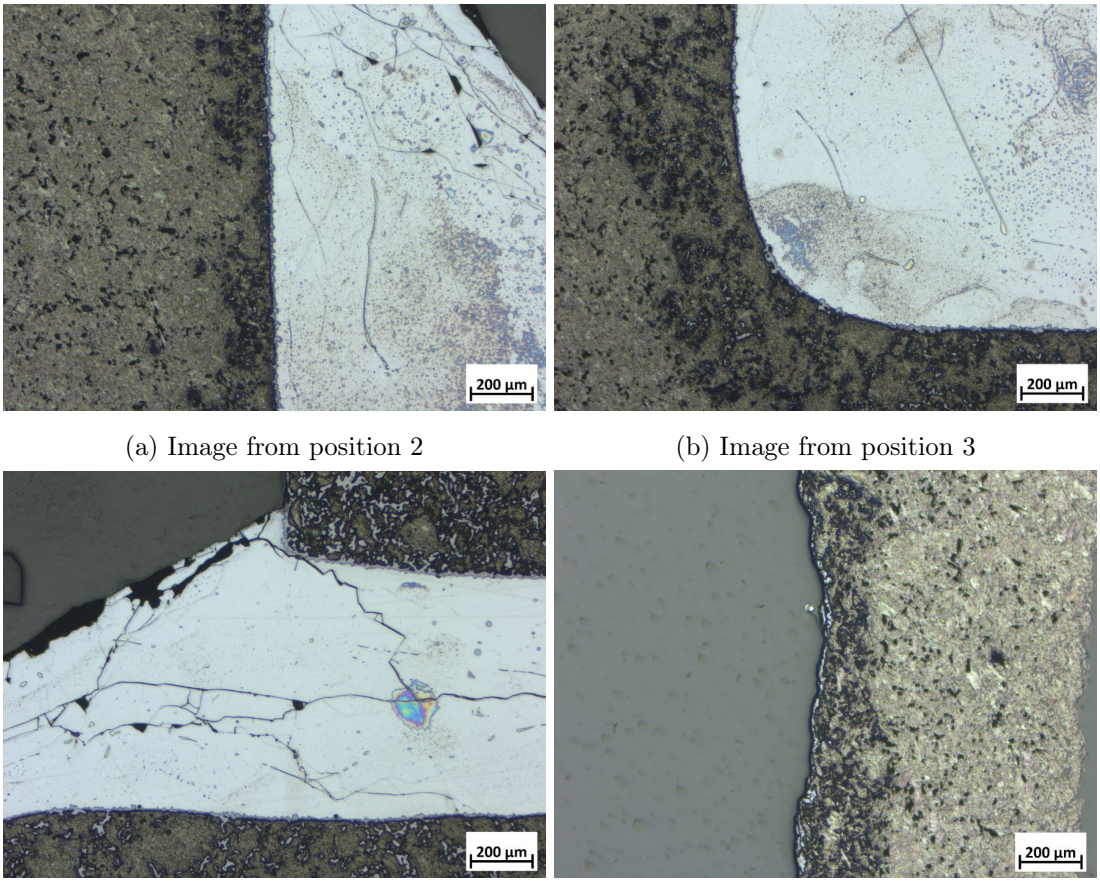

(a) Image from position 2

(b) Image from position 3

(c) Image from position 4

(d) Image from position 5

Figure 104: Image taken by LOM of sample where QZ C was heated at 1650C for 2h, M13.

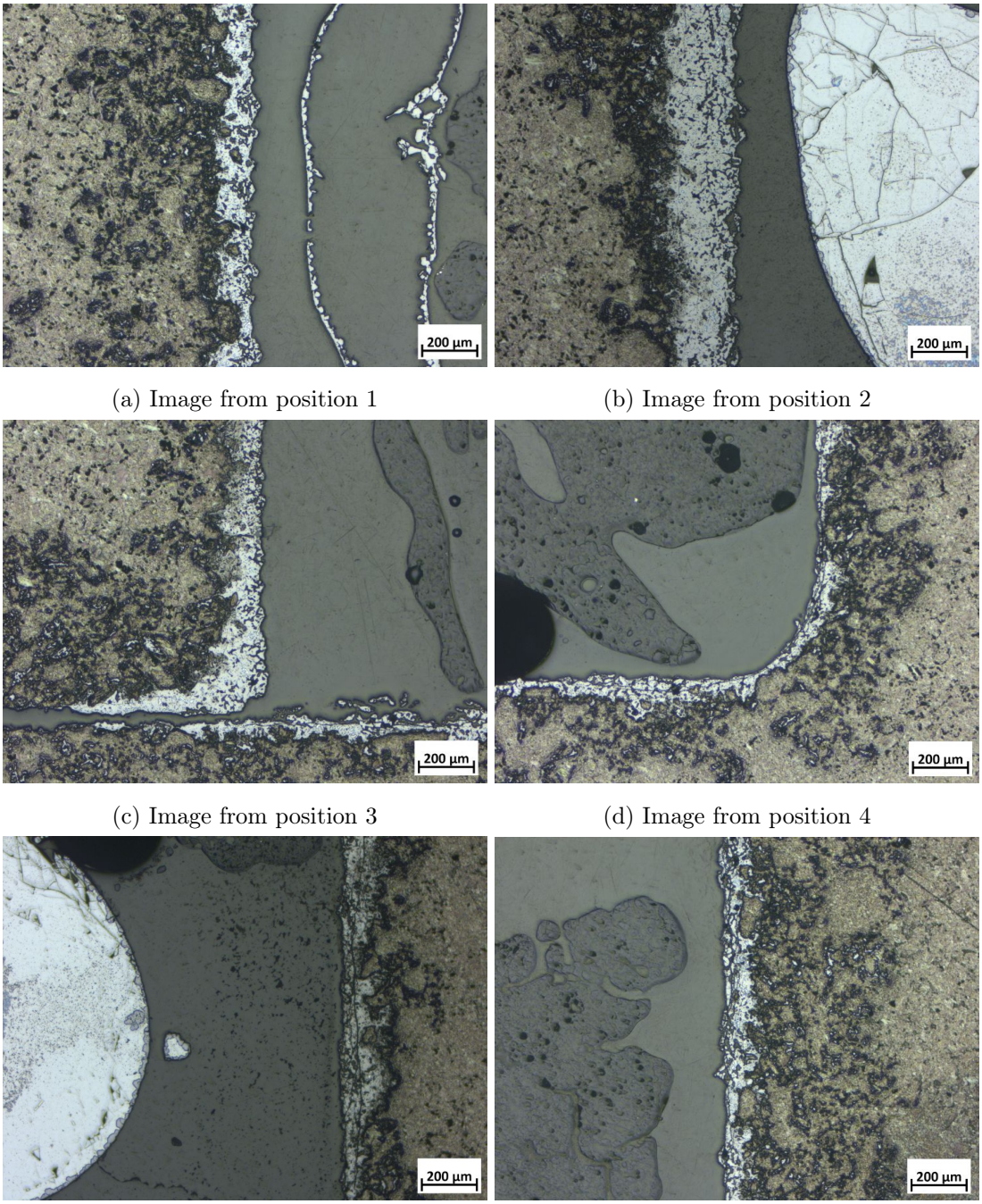

(a) Image from position 1

(b) Image from position 2

(c) Image from position 3

(d) Image from position 4

(e) Image from position 5

(f) Image from position 6

Figure 105: Image taken by LOM of sample where QZ C was heated at 1650C for 2h, M14.

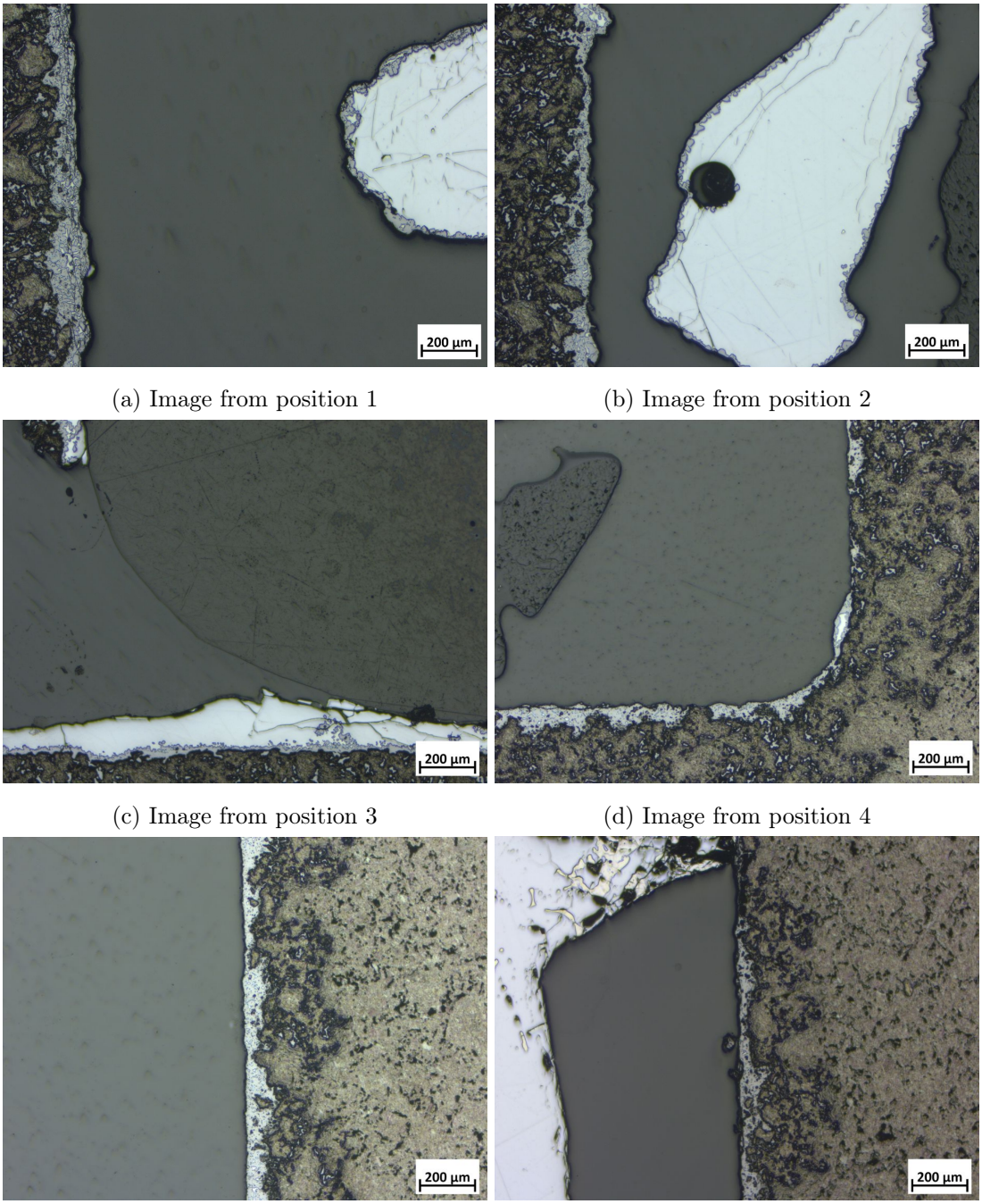

(a) Image from position 1

(b) Image from position 2

(c) Image from position 3

(d) Image from position 4

(e) Image from position 5

(f) Image from position 6

Figure 106: Image taken by LOM of sample where QZ E was heated at 1650C for 2h, M15.

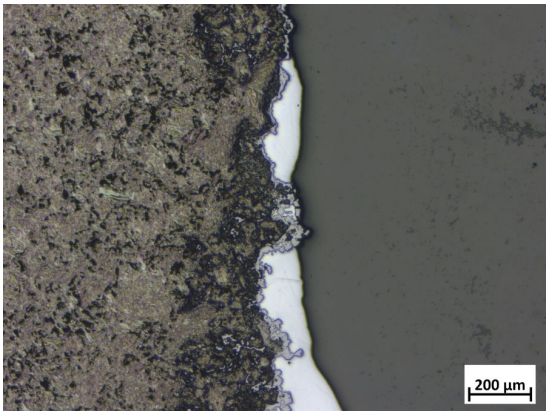

(a) Image from position 2

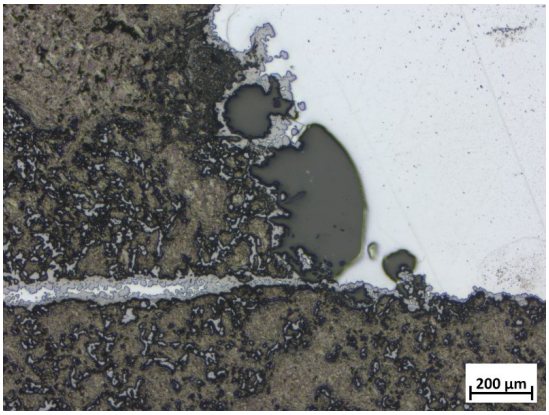

(b) Image from position 3

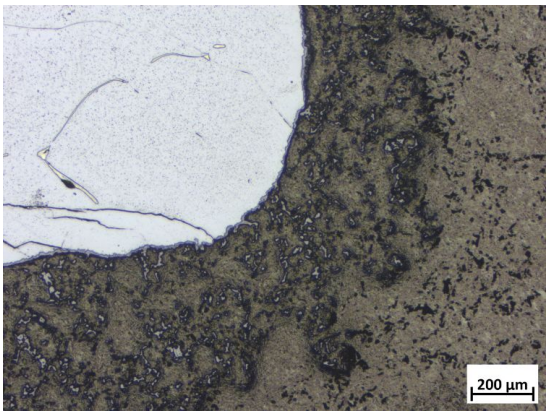

(c) Image from position 4

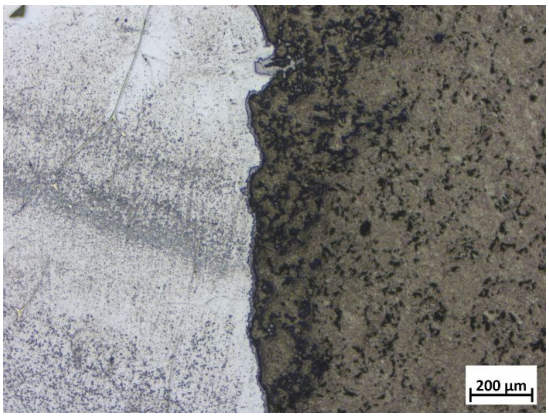

(d) Image from position 5

Figure 107: Image taken by LOM of sample where QZ E was heated at 1850C for 1h, M16.

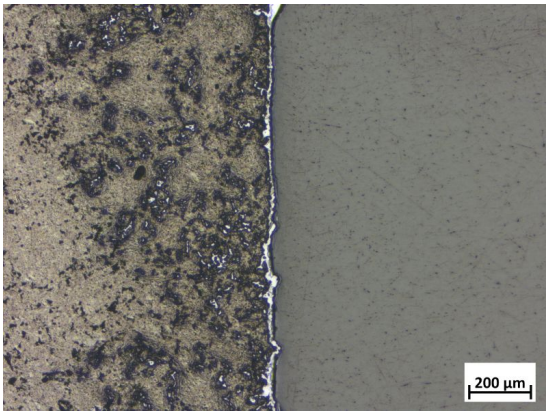

(a) Image from position 1

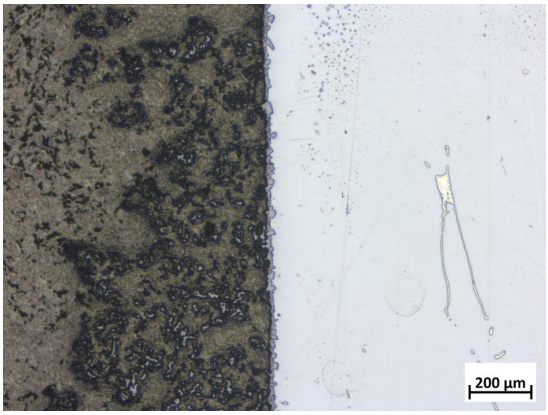

(b) Image from position 2

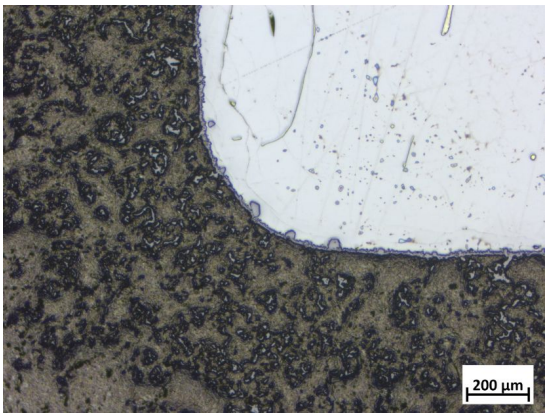

(c) Image from position 3

Figure 108: Image taken by LOM of sample where QZ E was heated at 1850C for 1h, M17.

Caroline Sindland

Production Rate of SiO Gas from Industrial Quartz and Silicon

NTNU
Norwegian University of
Science and Technology